View metadata, citation and similar papers at core.ac.uk

brought to you by CORE

provided by Purdue E-Pubs

Purdue University
Purdue e-Pubs

Open Access Dissertations

Theses and Dissertations

Spring 2015

In pursuit of high resolution radar using pursuit algorithms

Abdur Rahman Maud
Purdue University

Follow this and additional works at: https://docs.lib.purdue.edu/open_access_dissertations

Part of the Electrical and Computer Engineering Commons

Recommended Citation

Rahman Maud, Abdur, "In pursuit of high resolution radar using pursuit algorithms" (2015). *Open Access Dissertations*. 513.
https://docs.lib.purdue.edu/open_access_dissertations/513

This document has been made available through Purdue e-Pubs, a service of the Purdue University Libraries. Please contact epubs@purdue.edu for additional information.

Graduate School Form 30
(Updated 11/20/2014)

PURDUE UNIVERSITY
GRADUATE SCHOOL
Thesis/Dissertation Acceptance

This is to certify that the thesis/dissertation prepared

By Abdur Rahman Mohammad Maud

Entitled
In Pursuit of High Resolution Radar Using Pursuit Algorithms

For the degree of Doctor of Philosophy

Is approved by the final examining committee:

MARK R. BELL

CHARLES A. BOUMAN

DAVID J. LOVE

MICHAEL D. ZOLTOWSKI

To the best of my knowledge and as understood by the student in the Thesis/Dissertation Agreement, Publication Delay, and Certification/Disclaimer (Graduate School Form 32), this thesis/dissertation adheres to the provisions of Purdue University's "Policy on Integrity in Research" and the use of copyrighted material.

Approved by Major Professor(s): MARK R. BELL

Approved by: Michael R Melloch 04/17/2015

Head of the Department Graduate Program Date

IN PURSUIT OF HIGH RESOLUTION RADAR USING PURSUIT ALGORITHMS

A Dissertation

Submitted to the Faculty

of

Purdue University

by

Abdur Rahman Mohammad Maud

In Partial Fulfillment of the

Requirements for the Degree

of

Doctor of Philosophy

May 2015

Purdue University

West Lafayette, Indiana

TABLE OF CONTENTS

LIST OF FIGURES

Figure Page

Dedicated to my parents.

ACKNOWLEDGMENTS

Firstly, I would like to thank my advisor, Professor Bell, for all his help and support during my graduate studies. I feel like his encouragement to think independently and to pursue different research problems is going to serve me well in future. I would also like to thank my advisory committee for their feedback.

I am also indebted to Larry Biehl for his continued support during my graduate studies. I have learnt a lot from him and, most of all, I hope to emulate his incredible work ethic.

I am also grateful for the numerous friendships i was able to make during my stay at Purdue. From the midnight cricket games to the last minute camping trips, I will forever cherish the time i was able to spend with Aurangzeb, Amjad, Sultan, Fazil, Ausaaf, Sulaiman, Adeel, Najaath and other friends.

I would also like to thank my lab mates for helping me during my studies. In particular, i want to thank I-Fan for his help in summer teaching, Joe for the fruitful discussions we have had, Uttam for introducing me to STAP and SAR radar and Wei for proof reading my papers.

Lastly, I want to thank my wife for her love and support the last few years. I know it has been tough for her while I have been busy with studies but I truly appreciate her patience.

ABSTRACT

Maud, Abdur Rahman Mohammad Ph.D., Purdue University, May 2015. In Pursuit of High Resolution Radar Using Pursuit Algorithms. Major Professor: Mark Bell.

Radar receivers typically employ matched filters designed to maximize signal to noise ratio (SNR) in a single target environment. In a multi-target environment, however, matched filter estimates of target environment often consist of spurious targets because of radar signal sidelobes. As a result, matched filters are not suitable for use in high resolution radars operating in multi-target environments. Assuming a point target model, we show that the radar problem can be formulated as a linear underdetermined system with a sparse solution. This suggests that radar can be considered as a sparse signal recovery problem. However, it is shown that the "sensing" matrix obtained using common radar signals does not usually satisfy the mutual coherence condition. This implies that using recovery techniques available in compressed sensing literature may not result in the optimal solution. In this thesis, we focus on the greedy algorithm approach to solve the problem and show that it naturally yields a quantitative measure for radar resolution. In addition, we show that the limitations of the greedy algorithms can be attributed to the close relation between greedy matching pursuit algorithms and the matched filter. This suggests that improvements to the resolution capability of the greedy pursuit algorithms can be made by using a mismatched signal dictionary. In some cases, unlike the mismatched filter, the proposed mismatched pursuit algorithm is shown to offer improved resolution and stability without any noticeable difference in detection performance. Further improvements in resolution are proposed by using greedy algorithms in a radar system using multiple transmit waveforms. It is shown that while using the greedy algorithms together with linear channel combining can yield significant resolution improvement, a greedy

approach using nonlinear channel combining also shows some promise. Finally, a forward-backward greedy algorithm is proposed for target environments comprising of point targets as well as extended targets.

1. INTRODUCTION

Radio detection and ranging, or radar for short, is a device which uses the reflection of radio waves by objects to detect the presence, and estimate the parameters, of an object. The development of radars can be traced back to a patent by Christian Hulsmeyer [1] in 1904. Although the original device patented by Hulsmeyer could only detect the presence of an object, a century of research has resulted in devices capable of estimating multiple target parameters in stringent environments.

Although radars exist for a multitude of applications, this dissertation focuses only on pulse echo measurement systems designed for target range or target range and Doppler. Radars that estimate target azimuth and elevation in addition to range and Doppler can be modeled similarly to the linear redundant dictionary model presented later. Hence, the algorithms proposed in this dissertation may also be utilized in those applications.

Traditionally, radar receivers have utilized matched filters to maximize the signal to noise ratio at the output. This, in turn, maximizes the probability of detection of a target for some fixed probability of false alarm. in a single target environment. Assuming a point target environment, the output of linear receivers can be modeled as a superposition of point spread function or *ambiguity* centered at the target positions. Ideally, for high resolution, it is desirable to have a Dirac delta function as the ambiguity. However, Stutt [2] showed that the total volume under this ambiguity depends on signal energies and is independent of signal design. This led Woodward to remark in [3] “Like slums, ambiguity has a way of appearing In one place as fast as it is made to disappear in another.”. This was, perhaps, the first sign that linear filter receivers were not suitable for resolving point targets. However, the search for a radar signal with suitable ambiguity function has remained a topic of intense research.

Recently, sparse representation of signals in a redundant dictionary has received a lot of attention in the signal processing community. Mathematically, this problem is denoted as

$$\mathbf{y} = \mathbf{A}\mathbf{x},$$

where $x \in \mathbb{R}^N$ is a sparse vector, $A \in \mathbb{R}^{M\times N}$, $M < N$ is the redundant dictionary, and $y \in \mathbb{R}^M$ is the observation. Such representations have been used for signal denoising, signal compression, super resolution, compressed sensing and for other applications with considerable success. At the core of this sparse representation is the problem of finding the optimal sparse representation in an efficient and stable fashion. Unfortunately, this problem is known to be NP hard [4] making the optimal solution computationally unfeasible in most cases. To overcome this problem, iterative greedy *matching pursuit* (MP) [5–7] algorithms have been used and often lead to satisfactory results.

Many recent papers have studied the performance and stability of MP algorithms. In general, it has been observed that under insufficient dictionary incoherence, the inherent greed of the MP algorithms results in non-sparse representation of the signal in redundant dictionary [8]. To overcome this greed, regularizing constraints have been used to improve performance. One example of a regularized algorithm is the *basis pursuit* algorithm [9] which puts an $\ell 1$ constraint on MP algorithm. The improved performance, however, comes at the expense of increased computational complexity.

To obtain high resolution, radar has been formulated as a linear under determined system with a sparse solution in [10, 11]. To guarantee recovery, signals with low coherence dictionaries like the Alltop sequence [12] have been used. Although termed compressed sensing radar, the proposed radars differ from traditional compressed sensing radars proposed in [13, 14]. The focus in [13, 14] is on using fewer samples of received signal to accurately reconstruct the target. In [10, 11], however, all the samples of the received signal are used to achieve higher resolution.

In this dissertation, we study the application of greedy pursuit algorithms on radar systems using signals which do not satisfy the coherence requirement. In particular, we show that for such signals, resolvable and nonresolvable target regions can be computed. This naturally leads to a definition of resolution for radar systems. To resolve targets in the nonresolvable region, we present generalizations of the MP algorithm called the *mismatched pursuit* algorithm and the subspace mismatched pursuit algorithm. The proposed algorithm uses two different dictionaries for improving dictionary incoherence. As will be shown in this thesis, this generalization improves the MP performance and has the same complexity as the MP algorithm. Further improvements in resolution can be obtained by using multiple transmit signals. At the receiver, the channels can be combined either linearly or nonlinearly. Both cases are studied in this thesis. Finally, the greedy target recovery algorithm is modified to recover extended targets.

Rest of this chapter is organized as follows: In section 1.1, atoms, signal dictionaries and their synthesis matrices are introduced. In addition, the mutual coherence of a dictionary is defined and its relation to the sparse signal recovery problem is discussed. In section 1.2, pulsed radar systems are introduced and signal models for pulsed range and pulse-Doppler radar are presented. In particular, it is shown that the pulsed radar systems can be modeled as a sparse recovery problem. Section 1.3 discusses the matched filter detection used in most radar systems. This is used to introduce the ambiguity function and radar uncertainty principle in pulse-Doppler radar. Section 1.4 presents uncertainty principle from the signal dictionary point of view and shows why matched filters are not suitable for systems with redundant signal dictionaries. Commonly used radar waveforms in this thesis are introduced in section 1.5 which is followed by the outline of this thesis in section 1.6.

In this dissertation, vectors will be represented by lowercase boldface letters and matrices will be represented by capital bold face variables. Sets, scalar variables and functions will be represented by non-boldface variables. For any vector $\mathbf{v}$, $[\mathbf{v}]_i$ denotes i^{th} element in the vector. In general, the first element of any vector will be indexed by zero. As a result, the first element of vector $\mathbf{v}$ will be $[\mathbf{v}]_0$. The notation $[\mathbf{A}]_{i,j}$ will be used for the element at row i and column j of the matrix $\mathbf{A}$. The conjugate transpose of any vector or matrix will be denoted as $(\cdot)^H$. The column space of $\mathbf{A}$ will be denoted as $\text{Col}(\mathbf{A})$. For any set $Z \subset M$, $|Z|$ and $\overline{Z}$ will represent the set cardinality and the complement, respectively.

1.1 Atoms, dictionaries and coherence

Let $D = \{\phi_1, \phi_2, \ldots, \phi_P\}$ represent a normalized redundant dictionary of $\mathbb{C}^N$ with *atoms* $\phi_k \in \mathbb{C}^N$. Redundancy means $N < P$. Since D is assumed to be normalized, $\langle \phi_j, \phi_j \rangle = 1$, $\forall j \in \{1, 2, \ldots, P\}$. A subset of dictionary D comprising only linearly independent atoms is called the *sub-dictionary*. The *synthesis matrix* Φ, of a dictionary D, defined as

$$\Phi = \begin{bmatrix} \phi_1 & \phi_2 & \ldots & \phi_P \end{bmatrix},$$

is an $N \times P$ matrix with atoms as its columns. We will use the notation Φ_Γ to refer to the synthesis matrix of the *sub-dictionary* indexed by $\Gamma \subseteq \{1, 2, \ldots, P\}$. The adjoint matrix of Φ, denoted Φ^H, is called the *analysis matrix*.

For any sub-dictionary comprising of linearly independent atoms, $\{\phi_n\}_{n\in\Gamma}$, let $\Phi_\Gamma^\dagger$ denote the *Moore-Penrose pseudoinverse* of synthesis matrix Φ_Γ. Then, $\left(\Phi_\Gamma^\dagger\right)^H$ is a dual synthesis matrix with atoms that are linearly independent and form a *biorthogonal basis* to $\{\phi_n\}_{n\in\Gamma}$ [15]. As a result, if $\left\{\tilde{\phi}_n\right\}_{n\in\Gamma}$ represent the columns of $\left(\Phi_\Gamma^\dagger\right)^H$, then

$$\left\langle \tilde{\phi}_i, \phi_j \right\rangle = \begin{cases} 1, & i = j \\ 0, & i \neq j \end{cases}.$$

The set of atoms $\left\{\tilde{\phi}_n\right\}_{n\in\Gamma}$ is called the *dual basis* of $\text{Col}(\mathbf{\Phi}_\Gamma)$. Hence, for any vector $s \in \text{Col}(\Phi_\Gamma)$, $\exists \alpha, \breve{\alpha} \in \mathbb{C}^{|\Gamma|}$ such that $s = \Phi_\Gamma \alpha = \left(\Phi_\Gamma^\dagger\right)^H \breve{\alpha}$. The coefficients α and their dual basis counterpart $\breve{\alpha}$ can be computed as $\alpha = \Phi_\Gamma^\dagger s$ and $\breve{\alpha} = \Phi_\Gamma^H s$, respectively.

A dictionary, D , is often characterized by its *mutual coherence*, $\mu(D)$, defined as

$$\mu(D) = \sup_{m \neq n} |\langle \phi_m, \phi_n \rangle| \quad m, n \in \{1, 2, \ldots, P\},$$

where $\langle a, b\rangle$ represents the inner product of a and b. For a normalized redundant dictionary D, it can be shown that $0 < \mu(D) \leq 1$. The mutual coherence of a dictionary gives a quantitative measure of the similarity of the atoms in the dictionary. As will be shown later, for robust sparse signal decomposition, it is desirable to have *incoherent dictionary*, that is, $\mu(D) \approx 0$. Dictionaries that *do not* satisfy this condition are the subject of this paper.

The mutual coherence of a dictionary only reflects the extreme correlations between atoms in a dictionary. In most applications, performance bounds based on mutual coherence can be too *"loose"* to be useful. For this purpose, Tropp and Donoho [16, 17] use the *Babel function* defined as

$$\mu_b(m) = \max_{|\Lambda|=m} \max_{l \notin \Lambda} \sum_{k \in \Lambda} |\langle \phi_k, \phi_l \rangle| ,$$

where $\mu_b(0) = 0$.

In general, any N dimensional signal, s, can be represented as a linear combination of atoms in D i.e.

$$s = \sum_{k \in \Lambda} a_k \phi_k = \Phi_\Lambda a, \tag{1.1}$$

where $|\Lambda| \leq P$ and a is a column vector of coefficients a_k. Since $P > N$, there is more than one set Λ satisfying (1.1). The *optimal* sparse signal decomposition finds the set Λ with minimum cardinality. As a result, all atoms in Λ are linearly independent. This is true because if the atoms in Λ were linearly dependent, another Λ^* could be obtained by removing the dependent vectors, resulting in $|\Lambda^*| < |\Lambda|$.The *optimal* sparse signal decomposition problem can be formulated as

$$\min_{a \in \mathbb{C}^p} \left(\|\mathbf{s} - \mathbf{\Phi a}\|^2 + \lambda \|\mathbf{a}\|_0 \right). \tag{1.2}$$

The solution of the optimization problem in 1.2 is known to be NP hard [4]. In [9], the *basis pursuit* algorithm is proposed which computes the sparse decomposition by solving the convex problem

$$\min_{a \in \mathbb{C}^p} \|\mathbf{a}\|_1 , \ s.t. \ \mathbf{s} = \mathbf{\Phi a}, \tag{1.3}$$

where $\|\cdot\|_1$ represents the $l1$ norm.

Further improvement in computations can be achieved by using the greedy *Orthogonal Matching pursuit* (OMP) algorithm [6] or one of its derivatives. Although both OMP and basis pursuit are non-optimal algorithms, in [16] it was shown that both algorithms can recover any optimal sparse set Λ when

$$\mu(D) < \left(\frac{1}{2|\Lambda| - 1}\right). \tag{1.4}$$

The condition in (1.4) shows that when D is sufficiently incoherent and the optimal set, Λ, is sufficiently sparse, both OMP and basis pursuit can recover the optimal sparse set. For robust sparse signal decomposition, it is desirable to have *incoherent dictionary*, that is, $\mu(D) \approx 0$. Dictionaries that *do not* satisfy this condition are the subject of this paper. For rest of the paper, we will use the term *incoherent* for a dictionary when (1.4) is satisfied for the sparsity $|\Lambda|$ of interest.

In most applications, the objective of the sparse signal decomposition is to find an optimal sparse decomposition of the noisy signal, $\mathbf{r}$, in dictionary D,

$$\begin{aligned} \mathbf{r} &= \mathbf{s} + \mathbf{n} \\ &= \Phi_\Lambda \mathbf{a} + \mathbf{n}, \end{aligned} \tag{1.5}$$

where n denotes noise, usually assumed to be white Gaussian noise (WGN). The basis pursuit algorithm is then changed to a Lagrangian problem

$$\hat{a} = \arg\min_{a \in \mathbb{C}^p} \left(\frac{1}{2}\|\mathbf{r} - \Phi\mathbf{a}\|^2 + h\|\mathbf{a}\|_1\right).$$

1.2 Radar

Depending on the positions of the radar transmitter and receiver, radars can be broadly classified as *monostatic* or *multistatic*. In monostatic radars, the transmitter and receiver of the radar are colocated. A multistatic radar consists of either widely separated transmitters and receivers, or multiple monostatic radars focusing on the same area, or a combination of the two. In this thesis, we will only focus on monostatic radars.

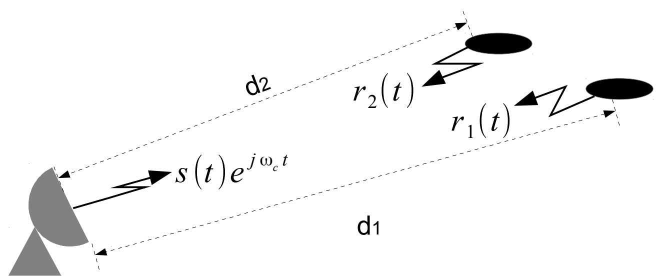

Figure 1.1.: Illustration of a monostatic range radar

Figure 1.1 depicts a monostatic radar looking at two stationary targets. The radar transmits a signal $s(t)$ which modulates a carrier with frequency ω_c radians per second. The use of a high frequency carrier not only shifts the transmitted signal to a suitable frequency band, it also decreases the required antenna size for the radar system. Radar systems can be further classified into *continuous wave radars* and *pulsed radars*. As the name implies, a continuous wave radar transmits a single continuous signal while a pulsed radar periodically transmits short pulses of signal and waits for the target echo in between. While both types of radar have important applications in which they are useful, the signal model used in this dissertation assumes a pulsed radar system. Henceforth, any mention of a radar system will implicitly imply a monostatic pulsed radar system.

1.2.1 Range estimation

Assuming the two targets in figure 1.1 are stationary, the signal echo received from each target can be expressed as

$$r_i(t) = \alpha_i s(t - \tau_i) e^{j\omega_c (t-\tau_i)},\ i \in \{1, 2\},$$

where $\tau_i = \frac{2d_i}{c}$ and c is the speed of electromagnetic wave in free space. The signal amplitude α_i encapsulates signal attenuation factor due to propagation and the radar cross section of the target. Denoting $\beta_i = \alpha_i e^{-j\omega\tau_i}$, the overall received signal $r(t) = r_1(t) + r_2(t)$ after carrier demodulation can be written as

$$r(t) = \sum_{i=1}^{2} \beta_i s(t - \tau_i). \tag{1.6}$$

Theoretically, equation (1.6) shows that high range resolution can be obtained by using the Dirac delta function as the radar transmit waveform. Denoting the Dirac delta function as $\delta(t)$, the received signal can be expressed as $r(t) = \sum_{i=1}^{2} \beta_i \delta(t - \tau_i)$. As a result, the target delay and hence the range may be accurately determined by observing the delays corresponding to the non-zero values in the received signal.

Although a short duration pulse seems like an ideal waveform for range radar, it is not suitable in practice due to three main reasons.

Firstly, the received signal in an actual system can be modeled more accurately as a sum of signal component in equation (1.6) and random noise. Even if interference from other signal sources in the same frequency band and multipath propagation can be ignored, the thermal noise at the output of the receiver antenna and other components used in the receiver still contribute to additive noise. As a result, to make the radar system more robust, it is imperative that the transmitted radar signal has high energy. This, however, requires a radar transmitter designed for high instantaneous power due to the short duration of the transmitted pulse. Depending on the range limits of the radar, such radar systems may often be impractical.

Secondly, a short duration pulse invariably requires a high frequency bandwidth. Even if a frequency band with sufficient bandwidth is available for use in the radar, the atmosphere itself acts as a nonlinear filter over wideband signals. As a result, the received signal is distorted and may no longer be short duration in time. Hence, it may not be possible to achieve high range resolution even if the duration of the transmitted waveform is reduced.

Thirdly, as will be shown later, target Doppler appears as a low frequency carrier on received narrowband signal. As a result, high Doppler resolution requires radar waveforms with sufficiently long time duration. Hence, in a pulse Doppler radar, short duration transmit waveforms are infeasible.

The first two problems can be mitigated by transmitting narrowband waveforms and using matched filters at the receivers. *Narrowband signals* are defined as signals with bandwidth much less than the carrier frequency. Thus, for a sufficiently narrowband signal, the channel attenuation may be assumed constant for all frequencies. As a result, the effect of nonlinear channel behavior can be ignored. In addition, since narrowband signals cannot concurrently be short duration signals in time, this reduces the instantaneous power requirements of the radar.

For the two target scenario depicted in figure 1.1, the received signal model was given in equation (1.6). Denoting the autocorrelation of $s(t)$ as $A_{ss}(\tau)$, the matched filter output for this signal model can be written as

$$\begin{aligned}\Gamma(\tau) &= \int_{-\infty}^{\infty} r(t)\, s^*(t-\tau)\, dt, \\ &= \sum_{i=1}^{2} \beta_i \int_{-\infty}^{\infty} s(t-\tau_i)\, s^*(t-\tau)\, dt, \\ &= \sum_{i=1}^{2} \beta_i A_{ss}(\tau-\tau_i).\end{aligned} \tag{1.7}$$

Denoting the energy in signal $s(t)$ as E_s, the autocorrelation function is known to satisfy two properties: $\forall \tau \in \mathbb{R}$, $A_{ss}(\tau) \leq E_s$ and $A_{ss}(0) = E_s$. As a result, assuming inter-target interference because of sidelobes is negligible, the target positions can be identified by the peaks at the output of the matched filter. Additionally, the matched filter accumulates the energy in the received signal over its complete time duration at the output peak. Intuitively, since no energy is lost at the output of the matched filter, such a receiver is robust in noise.

Equation (1.7) shows that using the matched filter receiver with narrowband transmit waveforms can yield a high resolution radar if the autocorrelation function is similar to $\delta(t)$. In fact, for suitably selected radar waveforms, the first null width of the autocorrelation may be considerably less than the time duration of the signal $s(t)$. This phenomenon is known as *pulse compression*. Figure 1.2 shows an example of pulse compression using a signal $s(t)$ with bandwidth B. In particular, it can be seen that the first null crossing of the autocorrelation function occurs approximately at $1/B$. Defining the ratio of original signal width and the width of the autocorrelation as *pulse compression ratio* (PCR), the PCR for the signal in Figure 1.2 can be expressed as

$$\mathrm{PCR} = \frac{T}{(1/B)} = BT. \tag{1.8}$$

Hence, for high range resolution, the transmit waveform duration and bandwidth should be selected to achieve a high time bandwidth product. Although the result in

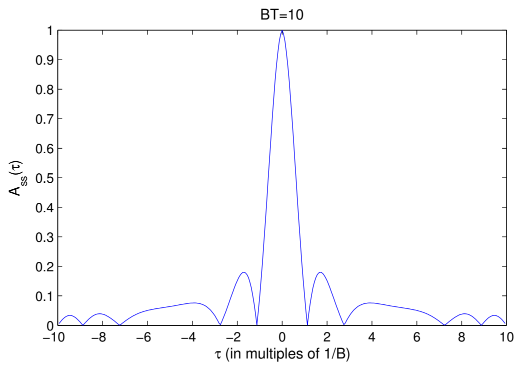

(a) Time bandwidth product 10.

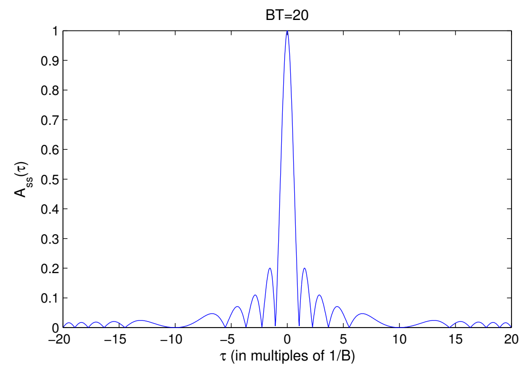

(b) Time bandwidth product 20.

Figure 1.2.: Example of pulse compression at matched filter output for two waveforms of equal length but different bandwidths.

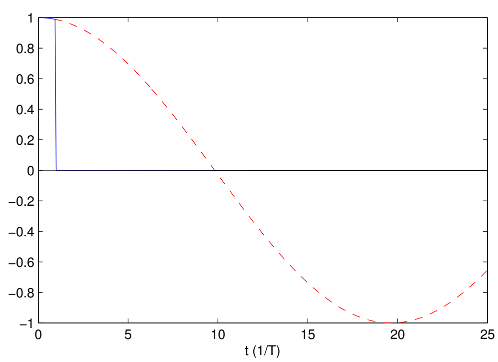

(a) Doppler effect on short pulse.

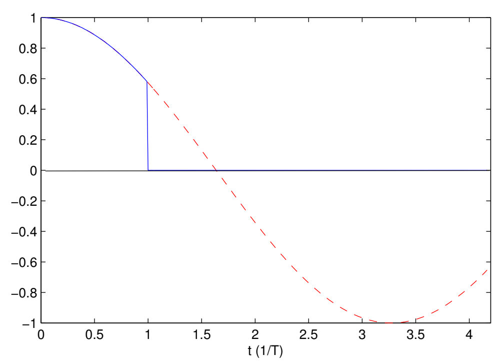

(b) Doppler effect on long pulse.

Figure 1.3.: Effect of Doppler on received signals of different durations.

equation (1.8) was derived for the transmit waveform shown in Figure 1.2, it holds in general for all signals [18]. As a result, in general, improved range resolution can be obtained by increasing time duration or frequency bandwidth or both of the transmit waveform.

1.2.2 Velocity estimation

Going back to Figure 1.1, assume the the two targets are moving at a constant speed. In some radar applications, it is desirable to estimate the target velocity as well as the range. Assuming the two targets have radial velocities v_1 and v_2 relative to the radar, their time varying distances can be written as

$$d_i\left(t\right) = d_i + v_i t,\ i \in \left\{1, 2\right\},$$

where d_i is the distance of the target from radar at time 0. Because of the time varying distance, the time delay between transmit signal and its received echo is also a function of time. Define $\tau_i\left(t\right) = 2d_i\left(t\right)/c$ and $\tau_i = \tau_i\left(0\right)$, the radar signal echo from each target in figure 1.1 can be expressed as

$$\begin{aligned} r_i(t) &= \alpha_i s\left(t - \tau_i\left(t\right)\right) e^{j\omega_c\left(t-\tau_i(t)\right)}, \\ &= \alpha_i s\left(t - \frac{2\left(d_i + v_i t\right)}{c}\right) e^{j\omega_c\left(t-\frac{2\left(d_i+v_i t\right)}{c}\right)}, \\ &= \alpha_i e^{-j\omega_c\tau_i} s\left(\left(1 - \frac{2v_i}{c}\right) t - \tau_i\right) e^{j\omega_c\left(1-\frac{2v_i}{c}\right)t}, \\ &= \beta_i s\left(\left(1 - \frac{2v_i}{c}\right) t - \tau_i\right) e^{j\omega_c\left(1-\frac{2v_i}{c}\right)t}, \end{aligned}$$

for $i \in \{1, 2\}$ and $\beta_i = \alpha_i e^{-j\omega_c\tau_i}$. As a result, after carrier demodulation, the received signal $r\left(t\right) = r_1\left(t\right) + r_2\left(t\right)$ is given as

$$r\left(t\right) = \sum_{i=1}^{2} \beta_i s\left(\left(1 - \frac{2v_i}{c}\right) t - \tau_i\right) e^{-j\omega_D^i t}, \tag{1.9}$$

where $\omega_D^i = \frac{2\omega_c v_i}{c}$ is the Doppler frequency in radians per second. Comparing equation (1.9) with equation (1.6) shows that target motion scales the received signal and shifts it in frequency. The frequency shift ω_D^i is called the *Doppler frequency* and is typically much smaller than the carrier frequency because $\forall i,\ v_i \ll c$.

In this thesis, narrowband signals are used exclusively. As a result, Doppler scaling can be ignored and Doppler manifests itself in terms of Doppler frequency only. The received signal in equation (1.9) can then be approximated as

$$r\left(t\right) = \sum_{i=1}^{2} \beta_i s\left(t - \tau_i\right) e^{-j\omega_D^i t}. \tag{1.10}$$

Now consider a radar system with $f_c = 5GHz$, the Doppler frequency in Hertz for a target moving at a radial velocity of $300m/s$ is $10kHz$. This means that one complete cycle of the Doppler sinusoid will take $T_D = 100\mu s$. From equation (1.10), it can be seen that the Doppler frequency is only visible to the receiver during the pulse duration. Hence, we might expect an accurate Doppler estimate and resolution ability if the signal width $T \gg T_D$. This is shown graphically in Figure 1.3. It can be seen that for the longer duration signal, the Doppler effect is clearly visible and therefore, easier to estimate.

In typical pulsed radar systems, pulse duration is much smaller than the time period of Doppler carrier. As a result, to improve Doppler resolution, it is common for a radar system to coherently process multiple pulses at the same time. This is shown in Figure 1.4. The radar system can be seen to transmit a pulse every $T_r > T$ seconds. T_r is called the *pulse repetition interval* (PRI). At the receiver, the radar listens for echoes for T_c seconds. T_c is called the *coherent processing interval* (CPI). Assuming there are $T_c/T_r = M$ pulses in one CPI, the receiver uses a filter matched to a pulse train of M transmit pulses at the receiver to process the target returns. For a sufficiently large CPI, the radar can accurately estimate and resolve target Doppler.

The selection of PRI itself requires a tradeoff. For long range radar systems, a higher PRI is needed. On the other hand, for fast moving targets, a smaller PRI is preferred. In this thesis, each CPI will be assumed to have only one pulse, that is, $T_c = T_r$. Although practical pulse Doppler radar systems do not use such small CPI, this assumption will simplify simulation results. However, all results presented in this thesis hold for any CPI provided the signal $s(t)$ in the radar model is assumed to represent a complete CPI.

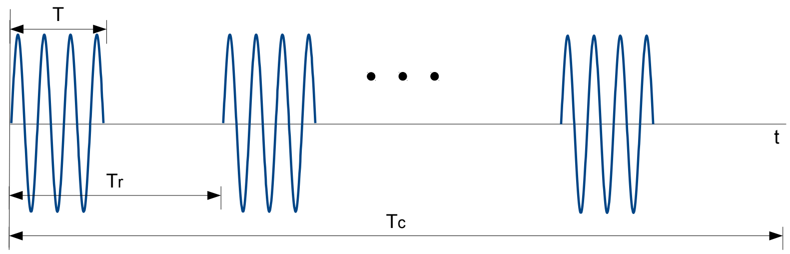

Figure 1.4.: Pulse duration, Pulse repetition interval and Coherent processing interval in a pulsed radar

1.2.3 Range radar

Consider a point target environment with L targets located at a distance of $d_1, d_2, \ldots, d_L$ from the radar transmitter and receiver. Define target delay τ_i as

$$\tau_i = \frac{2d_i}{c}, \tag{1.11}$$

where c denotes the speed of propagation of the electromagnetic wave. Denoting the radar transmit signal as $s(t)$ and the noise in the received signal with $w(t)$, the demodulated signal at the receiver can be modeled as

$$r(t) = \sum_{i=1}^{L} \alpha_i s(t - \tau_i) + w(t), \tag{1.12}$$

where α_i is the complex amplitude of the target return from i^{th} target. α_i depends on the target radar cross section and the signal attenuation due to wave propagation to a distance d_i.

1.2.3.1 Discrete model

Assuming all the target delays are integer multiples of the sampling period T_s, the sampled received signal in a target ranging radar can be written as

$$r[n] = \sum_{i=1}^{L} \alpha_i s[n - k_i] + w[n], \tag{1.13}$$

where $k_i = \tau_i/T_s$. It is assumed that T_S satisfies Nyquist sampling rate. Define vectors $\mathbf{r} = [\ r[1] \quad r[2] \quad \ldots \quad r[N]\ ]^T$ and $\mathbf{w} = [\ w[1] \quad w[2] \quad \ldots \quad w[N]\ ]^T$, (1.13) can be written as

$$\mathbf{r} = \sum_{i=1}^{L} \alpha_i \mathbf{s}_{k_i} + \mathbf{w},$$

where

$$[\mathbf{s}_i]_n = \begin{cases} s\left[n-i-1\right], & 1 \leq i \leq n \leq N, \\ 0 & else \end{cases}.$$

Define the receive signal dictionary as $\mathbf{S} = [\mathbf{s}_1, \ldots, \mathbf{s}_N]$, the receive signal model can be written as

$$\mathbf{r} = \mathbf{S}\boldsymbol{\alpha} + \mathbf{w}, \tag{1.14}$$

where $\boldsymbol{\alpha} \in \mathbb{R}^N$ is the L sparse vector of target amplitudes.

1.2.4 Pulse Doppler radar

Assume a point target environment with L targets present at a distance of $d_1, d_2, \ldots, d_L$ from the radar transmitter/receiver. Furthermore, suppose that the velocity of each point target is denoted by $v_1, v_2, \ldots, v_L$ respectively. Let $s(t)$ be the transmitted signal and $w(t)$ be the receiver noise, the demodulated signal at the receiver can be modeled as

$$r(t) = \sum_{i=1}^{L} \alpha_i s(t-\tau_i) e^{j2\pi v_i t} + w(t), \tag{1.15}$$

where α_i is the complex amplitude of the target return from i^{th} target and τ_i is defined in (1.11).

1.2.4.1 Discrete model

A discretized sampled version of equation (1.15) may be expressed as

$$r[n] = \sum_{i=1}^{L} \alpha_i s[n-k_i] e^{j2\pi\omega_i n/M} + w[n], \tag{1.16}$$

where it is assumed that all target delays are integer multiples of the sampling period T_s and $\forall 1 \leq i \leq L$, $\nu_i T_s$ is an integer multiple of the rational number $1/M$. As a result, for all targets $\nu_i T_s = \omega_i/M$ for some $\omega_i \in \mathbb{Z}$. Define vectors $\mathbf{r} = [\ r[0] \quad r[1] \quad \ldots \quad r[N-1]\ ]^T$, $\mathbf{w} = [\ w[0] \quad w[1] \quad \ldots \quad w[N-1]\ ]^T$, (1.16) can be expressed as

$$\mathbf{r} = \sum_{i=1}^{L} \alpha_i \mathbf{s}_{k_i,\omega_i} + \mathbf{w},$$

where

$$[s_{i,k}]_n = \begin{cases} s[n-i]e^{j2\pi kn/M}, & 0 \leq i \leq n \leq N, \\ 0 & else \end{cases}. \tag{1.17}$$

Define a redundant time-frequency dictionary

$$\mathbf{S} = [\ \mathbf{s}_{0,0} \quad \mathbf{s}_{0,1} \quad \ldots \quad \mathbf{s}_{0,M} \quad \mathbf{s}_{1,0} \quad \ldots \quad \mathbf{s}_{1,M} \quad \ldots \quad \mathbf{s}_{N,M}\ ].$$

The discrete signal model can then be expressed in a form similar to (1.14) as

$$\mathbf{r} = \mathbf{S}\alpha + \mathbf{w}, \tag{1.18}$$

where $\alpha \in \mathbb{C}^{MN}$ is an L-sparse vector of target amplitudes. The dictionary $\mathbf{S}$ has an important *shift invariance* property. Ignoring edge effects, $\forall m, m+i \leq N$ and $\forall n, n+k \leq M$

$$\begin{aligned} \langle s_{m,n}, s_{m+i,n+k} \rangle &= \sum_{l=1}^{N} (s[l-m]e^{j2\pi nl/M} \\ &\quad \times s^*[l-m-i]e^{-j2\pi(n+k)l/M}) \\ &= \sum_{l=1}^{N} s[l]s^*[l-i]e^{-j2\pi kl/M} \\ &= \langle s_{0,0}, s_{i,k} \rangle . \end{aligned} \tag{1.19}$$

As mentioned earlier, the mutual coherence of a dictionary is an important characteristic parameter of a dictionary. For the shift invariant time frequency dictionary S, mutual coherence can be specified as

$$\mu(S) = \max_{i,j} \langle s_{0,0}, s_{i,j} \rangle . \tag{1.20}$$

Typically, in radar applications where the radar clutter can be ignored, $L \ll N$. Hence, the target identification problem in a pulse Doppler radar can be seen to be similar to the problem of finding the optimal sparse signal decomposition discussed earlier.

1.3 Matched filter processing

Traditionally, the receivers used in pulse Doppler radars are designed to maximize the *signal to noise ratio* (SNR). Consider a target environment with a single target at delay τ, with velocity v. Then the received signal can be modeled as

$$r_m(t) = \alpha s(t-\tau)e^{j2\pi vt} + n(t).$$

Assuming the noise,$n(t)$, to be *white Gaussian noise* (WGN), it can be shown that the linear filter maximizing the SNR is the matched filter matched to $s(t-\tau)e^{j2\pi vt}$ [19]. This is equivalent to correlating $r_m(t)$ with $s(t-\tau)e^{j2\pi vt}$ i.e.

$$\begin{aligned} \Gamma &= \int_0^T r_m(t)\overset{*}{s}(t-\tau)e^{-j2\pi vt}dt \\ &= \alpha E_s + N, \end{aligned}$$

where E_s denotes energy in $s(t)$ and N represents the zero mean noise component at the output of the filter. In general, the received signal, $r(t)$, from a multiple point target environment can be modeled as in equation 1.15. To maximize the SNR for each target, pulse Doppler radars typically use a bank of matched filters matched to time delayed and Doppler shifted versions of the transmitted signal $s(t)$. The output, $\Gamma(\tau,\nu)$ is then a function of delay and Doppler,

$$
\begin{aligned}
\Gamma(\tau,\nu) &= \int_0^T r(t)\overset{*}{s}(t-\tau)e^{-j2\pi\nu t}dt \\
&= \sum_{i=1}^{L}\alpha_i\int_0^T s(t-\tau_i)\overset{*}{s}(t-\tau)e^{-j2\pi(\nu-\nu_i)t}dt \\
&= \sum_{i=1}^{L}\alpha_i e^{j2\pi(\nu-\nu_i)\tau_i}\int_0^T s(t)\overset{*}{s}(t-(\tau-\tau_i))e^{-j2\pi(\nu-\nu_i)t}dt \\
&= \sum_{i=1}^{L}\beta_i\chi(\tau-\tau_i,\nu-\nu_i), \qquad (1.21)
\end{aligned}
$$

where $\beta_i = \alpha_i e^{-j2\pi(\nu-\nu_i)\tau_i}$ and

$$\chi(\tau,\nu) = \int s(t)\overset{*}{s}(t-\tau)e^{-j2\pi\nu t}dt, \qquad (1.22)$$

is the well known *asymmetric ambiguity function* [18, 19]. Define the target environment, $P(\tau,\nu)$ as

$$P(\tau,\nu) = \sum_i \beta_i\delta(\tau-\tau_i,\nu-\nu_i), \qquad (1.23)$$

then the output of the matched filter bank can be expressed as

$$\Gamma(\tau,\nu) = \chi(\tau,\nu) * P(\tau,\nu), \qquad (1.24)$$

where $*$ represents the two dimensional convolution. Equation (1.24) shows that the ambiguity function acts as a point spread function in the output of the matched filter. Ideally, we would like to obtain an accurate estimate of $P(\tau,\nu)$ from the output of the matched filter delay Doppler scene, $\Gamma(\tau,\nu)$. This suggests that we use transmit signals $s(t)$ such that the resultant ambiguity function, $\chi(\tau,\nu)$ is as close to a two dimensional Dirac delta function $\delta(\tau,\nu)$ as possible. However, in [2], it was shown that the volume under the cross ambiguity function is constrained by the signal energies and is independent of the waveform design. Consider the Moyal's identity [20](see appendix)

$$\int\int \chi_{sg}(\tau,\nu)\overset{*}{\chi}_{yx}(\tau,\nu)d\tau d\nu = \int f(\tau)\overset{*}{y}(\tau)d\tau\int \overset{*}{g}(\tau)x(\tau)d\tau\,. \qquad (1.25)$$

When $s(t) = y(t)$ and $g(t) = x(t)$, (1.25) simplifies to the Stutts's invariant relation [2]

$$\int_{-\infty}^{\infty}\int_{-\infty}^{\infty} |\chi_{sg}(\tau,\nu)|^2 \, d\tau d\nu = \int_{-\infty}^{\infty} |s(t)|^2 \, dt \int_{-\infty}^{\infty} |g(t)|^2 \, dt \,. \tag{1.26}$$

Since the energy in the receive filter, $g(t)$, does not change the signal to noise ratio, it can be assumed that $\int |g(t)|^2 \, dt = 1$. Furthermore, since $\chi_{sg}(\tau,\nu)$ is continuous if the radar transmit signal $s(t)$ has finite energy, it follows that $\chi_{sg}(\tau,\nu)$ cannot be zero around $\{\tau,\nu\} = \{0,0\}$ unless $s(t) = 0$, $\forall t \in \mathbb{R}$. This result is a form of the radar uncertainty principle and shows that it is not possible to have $\chi_{sg}(\tau,\nu) = \delta(\tau,\nu)$.

For the discrete model in (1.18), the matched filter estimate of the target scene, $\tilde{\alpha}$, is written as

$$\begin{aligned} \tilde{\alpha} &= \mathbf{S}^H \mathbf{r}, \\ &= \mathbf{S}^H \mathbf{S} \alpha + \mathbf{S}^H \mathbf{w}, \\ &= \sum_{(i,j)\in\Lambda} [\alpha]_{iM+j} \, \mathbf{S}^H \mathbf{s}_{(i,j)}, \end{aligned} \tag{1.27}$$

where Λ denotes the set of indexes of the targets. Furthermore, using the notation in equation (1.17) and the structure of the synthesis matrix $\mathbf{S}$, the discrete ambiguity function of the discrete time signal $s[n]$, can be seen to be

$$\chi[\tau,\nu] = \left[\mathbf{S}^H \mathbf{s}_{0,0}\right]_{\tau M+\nu} . \tag{1.28}$$

Because of the shift invariance property (1.19) of the dictionary $\mathbf{S}$, it can be seen that

$$\chi[\tau - i, \nu - j] = \left[\mathbf{S}^H \mathbf{s}_{i,j}\right]_{\tau M+\nu} .$$

Hence, the estimated target scene in (1.27) can be expressed as

$$[\tilde{\alpha}]_{\tau M+\nu} = \sum_{(i,j)\in\Lambda} [\alpha]_{iM+j} \, \chi[\tau - i, \nu - j], \tag{1.29}$$

which is similar to the convolution model of the radar presented in equation (1.24). Using the result in (1.20), the discrete ambiguity function in (1.28) can be seen to be closely related to the mutual coherence of the dictionary $\mathbf{S}$. In particular, they are related as

$$\mu(\mathbf{S}) = \max_{\tau\neq 0, \nu\neq 0} \chi[\tau,\nu] \,. \tag{1.30}$$

1.3.1 Matched filters and detection

Suppose the received signal

$$\mathbf{r} = \sum_{i \in \Lambda} a_i \mathbf{s}_i,$$

consists of *normalized* atoms, $\mathbf{s}_j$, from some dictionary S. In the detection stage, the matched filter approach will compare *likelihood ratio*, $L(j) = \langle r, s_j \rangle$, to some threshold $\gamma \in \mathbb{R}$. If $L(j) = \langle r, s_j \rangle > \gamma$, we say that s_j is a constituent atom or signal of r.

For dictionaries having non-negligible mutual coherence, the matched filter suffers from *false detections*. To explain this, assume $|\Lambda| = M$ and $j \notin \Lambda$. Then ignoring noise,

$$\begin{aligned} L(j) &= \sum_{k \in \Lambda} a_k \langle \mathbf{s}_k, \mathbf{s}_j \rangle \\ &\leq \mu(S) \sum_{k \in \Lambda} a_k \\ &\leq M\mu(S)(\max_{k \in \Lambda}\{a_k\}) \end{aligned} \tag{1.31}$$

which shows that for any $j \notin \Lambda$, as the number of *similar* atoms in Λ increases, the matched filter output, $L(j)$, is more likely to exceed γ. In fact, for dictionaries with $\mu(S) \approx 1$, even $M = 1$ may result in false detections. This example also illustrates why it is desirable to have $\mu(S) \approx 0$. Since $j \notin \Lambda$, we want $L(j) < \gamma$, which can be guaranteed if $\mu(S) \approx 0$.

The problem of false detections makes matched filters unsuitable for sparse signal decomposition. As will be seen later, the iterative matching pursuit algorithm can overcome this problem in certain conditions.

1.4 Uncertainty principle

Redundant dictionaries of practical interest often result in a phenomenon called the uncertainty principle. Consider a dictionary $D = [\ \Phi \quad \Psi\ ]$, which is a concatenation of two orthonormal bases of $\mathbb{C}^N$. In general, any $y \in \mathbb{C}^N$ can be expressed as a linear combination of the columns of Φ or Ψ, that is

$$y = \Phi\alpha = \Psi\beta,$$

where $\alpha = \Phi^H y$ and $\beta = \Psi^H y$ are uniquely defined. The uncertainty principle states that for certain pair of bases Φ and Ψ,

$$\|\alpha\|_0 + \|\beta\|_0 \geq 2/\mu(D), \tag{1.32}$$

that is, either α may be sparse or β may be sparse but not both. Assuming $y = Da$, where $a \in \mathbb{C}^{2N}$ is sparse, 1.32 says that the matched filter estimate, $\hat{a} = D^H y = [\alpha, \beta]$, cannot be sparse. This result shows that the matched filter may not be suitable for determining sparse vectors in a redundant dictionary. The time frequency dictionary is an example of a dictionary which satisfies (1.32).

It was shown earlier in equation (1.26) that the ambiguity function of a pulse Doppler radar has a volume constraint. This volume constraint is commonly used in radar literature to understand the uncertainty principle. In the discrete signal model of radar in equation (1.18), the uncertainty principle can be understood in a slightly different way. Consider a radar system with received signal as given in equation (1.18). The target scene estimate using a linear filter with time frequency dictionary G is then given as

$$\begin{aligned}\hat{\alpha} &= \mathbf{G}^H\mathbf{r} \\ &= \mathbf{G}^H\mathbf{S}\alpha + \mathbf{G}^H\mathbf{w}.\end{aligned}$$

Ignoring noise, the target scene estimate is accurate when $\mathbf{G}^H\mathbf{S} = \mathbf{I}$. Hence, the radar transmit signal and receive filter should be jointly designed to achieve $\mathbf{G}^H\mathbf{S} = \mathbf{I}$. While this is possible in range radar where the receiver filter and receive signal synthesis matrices $\mathbf{G}$ and $\mathbf{S}$ are full column rank, $\mathbf{G}^H\mathbf{S}$ is not even full rank in pulse Doppler radar because of dictionary redundancy. As a result, even if there is no noise, in general, it is not always possible to accurately estimate the target scene in pulse Doppler radar using linear filters because $\mathbf{G}^H\mathbf{S} \neq \mathbf{I}$ for all possible redundant dictionary pairs $\mathbf{G}, \mathbf{S}$. Hence, the uncertainty principle manifests itself in terms of the rank deficiency of the matrix $\mathbf{S}^H\mathbf{S}$.

1.5 Radar waveforms

As mentioned earlier, design of radar signals to improve the ambiguity function and hence improve resolution has remained a topic of intense research for the past six decades. As a result of this effort, there is now a plethora of radar signals and design techniques available for different radar applications [18]. Although theoretically any signal that minimizes ambiguity in some sense may seem suitable for use in a radar, current high-power amplifier technology limits practical radar signals to constant amplitude signals. This limitation further constrains the set of possible ambiguity functions a practical radar signal can have. In general, the complex envelope of a radar signal over a single CPI can be typically modeled as

$$\overline{s}\left(t\right) = a\left(t\right) e^{j\theta(t)},\ 0 \leq t \leq T_c, \tag{1.33}$$

where $\theta\left(t\right)$ represents phase or frequency modulation and $a\left(t\right)$ represents the amplitude modulation of the carrier frequency. Assuming C pulses in one CPI, the amplitude modulation $a\left(t\right)$ in a pulsed radar system can be expressed as

$$a\left(t\right) = \sum_{i=1}^{C} x_i\left(t\right) \operatorname{rect}\left(\frac{t-(i-1)T_r}{T}\right), \tag{1.34}$$

where T_r is the pulse repetition interval, T is pulse duration and

$$\operatorname{rect}\left(t\right) = \begin{cases} 1, & 0 \leq t \leq 1 \\ 0, & \text{otherwise} \end{cases}.$$

Hence, in essence the amplitude modulation in a pulsed radar system acts as a switch turning the radar signal on for time duration T every T_r seconds. Furthermore, since the radar signals of interest in this dissertation are assumed to be constant amplitude, $\forall t \in \mathbb{R}, |x_i(t)|$ will be constant for $i \in \{1, 2, \ldots, C\}$. Using equations (1.34) and (1.33), the radar waveform over one CPI for a pulsed radar system can be expressed as

$$\begin{aligned} \overline{s}(t) &= \sum_{i=1}^{C} x_i(t) e^{j\theta(t)} \text{rect}\left(\frac{t-(i-1)T_r}{T}\right) \\ &= \sum_{i=1}^{C} s_i(t) \text{rect}\left(\frac{t-(i-1)T_r}{T}\right), \end{aligned} \tag{1.35}$$

where $s_i(t) = x_i(t) e^{j\theta(t)}$. In addition, if a pulsed radar system transmits the same pulse in every PRI, $s_i(t) = s(t-(i-1)T_r)$. Although the theory and results presented in this dissertation hold for any waveform that can be expressed as (1.35), for simplicity, the radar waveforms used for simulations will be assumed to have only one pulse in every CPI, that is, $C = 1$. As a result, $T_c = T_r$ and

$$\overline{s}(t) = s(t) \text{rect}\left(\frac{t}{T}\right), \ 0 \leq t \leq T_c.$$

Most of the existing radar signals in literature can be broadly classified as either frequency modulated pulses or phase coded pulses. In this dissertation, both frequency modulated signals and phase coded waveforms will be used for simulation purposes.

The complex envelope of a *phase coded pulse*, $s(t)$ of length T, can be expressed as [18]

$$s(t) = \begin{cases} \sum_{m=1}^{M} u_m \text{rect}\left[\frac{t-(m-1)t_b}{t_b}\right] & 0 \leq t \leq T \\ 0 & \text{else} \end{cases},$$

where $t_b = T/M$ and $u_m = e^{j\phi_m}$, $m \in \{1, 2, \ldots, M\}$ is the *phase code* associated with $s(t)$. Perhaps the most well known phase codes are the Barker codes [18]. The original Barker codes were binary phase coded sequences, that is,

$$\phi_m \in \{0, \pi\}, \forall m \in \{1, 2, ..., M\},$$

and their autocorrelations have a peak to sidelobe ratio (PSL) of $1/M$. Unfortunately, it is known that the Barker codes do not exist for $M > 13$ [18]. Since, practical radar systems employ longer signals to obtain coherent integration gain, minimum PSL binary codes and polyphase generalized Barker codes have been proposed [18]. The phase coded signal used most frequently in this dissertation is a nested (or combined) code [18, 21] obtained using the Kronecker product of length 13 Barker code, $\{b_m^{13}\} = \{1, 1, 1, 1, 1, -1, -1, 1, 1, -1, 1, -1, 1\}$, and the length 4 Barker code $\{b_m^4\} = \{1, 1, -1, 1\}$, that is,

$$b_m^{13} \otimes b_m^4 = \{b_m^4, b_m^4, b_m^4, b_m^4, b_m^4, -b_m^4, -b_m^4, b_m^4, b_m^4, -b_m^4, b_m^4, -b_m^4, b_m^4\}. \tag{1.36}$$

In this dissertation, the code in (1.36) will be referred to as the *combined barker code* or *extended barker code*. Another waveform that will be commonly used in this dissertation is the linear frequency modulated (LFM) chirp given as [18]

$$s(t) = \begin{cases} \frac{1}{\sqrt{T}} e^{j\pi k t^2} & 0 \le t \le T \\ 0 & \text{else} \end{cases}, \tag{1.37}$$

where $k = \pm B/T$ and B is the frequency band sweep in pulse duration T. Depending on whether k is positive or negative, the chirp is said to be an *up-chirp* or *down-chirp* respectively. The LFM chirp is known to provide improved range resolution compared to a constant frequency pulse and good Doppler tolerance. As a result, the LFM chirp is widely used in pulsed range radars. The range-Doppler coupling, however, makes it unsuitable for high resolution pulse Doppler radar.

1.6 Thesis Outline

Sections 1.3 and 1.4 showed why the matched filters are not suitable for target scenes with multiple targets. The primary aim of this thesis is to study detection algorithms for improved target resolution in a multi-target environment. Towards this goal, chapter 2 looks at the optimal detection of multiple targets using the generalized likelihood ratio test. It is shown that the optimal algorithm is computationally impractical and a greedy algorithm is proposed instead. Additionally, it is shown that the matched filter is only suited for multi-target detection when the received signal dictionary is orthogonal. To be able to compare different algorithms, chapter 3, defines radar resolution and proposes a quantitative measure for resolution performance of a radar. The definition of resolution is then used to find conditions for target scene resolution for the greedy algorithm proposed in chapter 2. In chapter 4, two greedy algorithms using mismatched dictionaries at the receiver are used to improve resolution performance. Chapter 5 extends the greedy algorithm from chapter 2 to radar systems with multiple transmit waveforms. It is shown that waveform diversity can help in improving the target resolution performance. Furthermore, it is shown that the use of greedy schemes can help in improving the performance of nonlinear channel combining schemes in radar proposed in [22]. Chapter 6 extends the greedy target detection algorithm of chapter 2 to extended targets. Finally, chapter 7 discusses future work and concludes the thesis.

2. MULTI-TARGET DETECTION IN RADAR

In chapter 1 it was mentioned that radar systems typically utilize matched filters at the receiver for pulse compression. This is due to the fact that the matched filter is the optimal detector for the binary hypothesis of the form

$$\begin{aligned}\mathcal{H}_0 : \mathbf{r} &= \mathbf{w},\\ \mathcal{H}_1 : \mathbf{r} &= \alpha\mathbf{s} + \mathbf{w},\end{aligned}$$

where the noise $\mathbf{w}$ is assumed to be i.i.d. zero mean complex Gaussian and $\mathbf{s}$ is a deterministic signal. Assuming the signal vector $\mathbf{s}$ is unit norm, the expected value at the output of the matched filter under the two hypotheses $\mathcal{H}_0$ and $\mathcal{H}_1$ is given as

$$\begin{aligned}E\left[\mathbf{s}^H\mathbf{r}/\mathcal{H}_0\right] &= 0,\\ E\left[\mathbf{s}^H\mathbf{r}/\mathcal{H}_1\right] &= \alpha.\end{aligned}$$

As a result, the matched filter is suitable for use in radar when the target scene either consists of no target or a single target with known parameters in additive Gaussian noise.

In a multi-target environment, however, the matched filter is not always the optimal detector. Consider a target scene with two targets. Assume the reflected signals from the two targets are $\mathbf{s}_1$ and $\mathbf{s}_2$ with associated target amplitudes α_1 and α_2, respectively. The received signal can then be expressed as

$$\mathbf{r} = \alpha_1\mathbf{s}_1 + \alpha_2\mathbf{s}_2 + \mathbf{w}. \tag{2.1}$$

In section 1.3 it was shown that radar systems typically check for multiple targets by matched filtering with reflected signals from each of the possible targets. Filtering the received signal $\mathbf{r}$ with filters matched to $\mathbf{s}_1$ and $\mathbf{s}_2$ results in

$$\begin{aligned}\mathbf{s}_1^H\mathbf{r} &= \alpha_1 + \alpha_2\mathbf{s}_1^H\mathbf{s}_2 + \mathbf{s}_1^H\mathbf{w},\\ \mathbf{s}_2^H\mathbf{r} &= \alpha_1\mathbf{s}_2^H\mathbf{s}_1 + \alpha_2 + \mathbf{s}_2^H\mathbf{w},\end{aligned}$$

where $\mathbf{s}_1$ and $\mathbf{s}_2$ are assumed to be normalized. Hence, the expected value at the output of each filter is

$$
\begin{aligned}
E\left[\mathbf{s}_1^H\mathbf{r}\right] &= \alpha_1 + \alpha_2\mathbf{s}_1^H\mathbf{s}_2, \\
E\left[\mathbf{s}_2^H\mathbf{r}\right] &= \alpha_1\mathbf{s}_2^H\mathbf{s}_1 + \alpha_2,
\end{aligned}
$$

assuming $\mathbf{w}$ is zero mean i.i.d. Gaussian. It can be seen that if $\mathbf{s}_1$ and $\mathbf{s}_2$ are not orthogonal, the reflected signal from each targets acts as an interference for other targets and can deteriorate detection performance. In fact, if $|\alpha_2| > |\alpha_1|$, then $\mathbf{s}_1^H\mathbf{s}_2 = -\alpha_1/\alpha_2$ can cause $E\left[\mathbf{s}_1^H\mathbf{r}\right] = 0$ and hence the radar system will miss the target 1. This shows that the matched filter is not suitable for multi-target environments unless the reflected signals from all targets can be made orthogonal to one another. Furthermore, since all the reflected signals depend on the radar transmitted signal directly, design of suitable radar waveform is an important part of radar system design.

The nonsuitability of matched filters in the presence of interference has also been observed in other applications. In fact, this is generally true for all binary hypothesis testing problems where the hypothesis $\mathcal{H}_1$ has interference which is not orthogonal to the signal component $\mathbf{s}$. For example, in communication systems using binary phase shift keying, this interference may be present in the form of intersymbol interference when the communication channel has a nonlinear frequency response or consists of multiple paths. Such communication systems typically use equalization at the receiver to counter the effects of intersymbol interference.

Rest of this chapter is organized as follows: In section 2.1, the generalized likelihood ratio test is used to derive the optimal detector for detecting a single target with unknown target parameters. It is shown that the optimal detector in essence compares the maximum output of a bank of matched filters to a detection threshold. Section 2.2 uses the generalized likelihood ratio test to find the optimal detector when multiple targets may be present. It is assumed that the number of targets is not known a priori and an iterative approach is used to derive the optimal detection algorithm. It is further shown that the optimal algorithm is NP-hard in computational complexity unless the dictionary synthesis matrix is orthonormal. For signal dictionaries with orthonormal synthesis matrices, the optimal detector in multi-target environment is observed to be the matched filter. For signal dictionaries that do not satisfy the orthonormal property, section 2.3 presents a greedy algorithm for solving the NP-hard problem. Finally, section 2.4 compares the single target detection performance of the matched filter with the greedy algorithm presented in section 2.3.

2.1 One target case

At the receiver, consider the scenario where we are interested in finding out if there is a target present or not. Using (1.16), this can be written in terms of the following hypotheses,

$$
\begin{aligned}
\mathcal{H}_0 : \mathbf{r} &= \mathbf{w} \\
\mathcal{H}_1 : \mathbf{r} &= \alpha \mathbf{s}_\theta + \mathbf{w},
\end{aligned}
$$

where $\theta \in \mathcal{T}$, $\mathcal{T} = \{(i,k)|0 \leq i \leq N, 0 \leq k \leq M\}$ specifies target range and Doppler, and $\mathbf{w}$ is assumed to be complex Gaussian noise with zero mean and covariance matrix $\mathbf{C}$. In radar terminology, if the detection algorithm at the receiver decides hypothesis $\mathcal{H}_1$ when in fact $\mathcal{H}_0$ is true, it is called a *false alarm*. Conversely, if $\mathcal{H}_1$ is true but the detection algorithm declares hypothesis $\mathcal{H}_0$, it is said to be a *miss*. The goal in radar system design is to minimize both, the probability of false alarm (P_{FA}) and the probability of a miss (P_M). In a simple binary hypothesis testing problem, the detection algorithm that minimizes P_M for some P_{FA} can be found by using the Neyman-Pearson theorem [23]. However, since the target parameters (range and/ or Doppler) are unknown at the receiver, $\mathcal{H}_1$ is a composite hypothesis. Hence, the *Generalized likelihood ratio test* (GLRT) [23] will be used to derive the detection algorithm in this chapter.

Denoting the probability density function (pdf) of received signal as $f_0(\mathbf{r})$ and $f_1(\mathbf{r})$ under hypothesis $\mathcal{H}_0$ and $\mathcal{H}_1$ respectively, the GLRT can be written as

$$L_g(\mathbf{r}) = \frac{\max_\theta f_1(\mathbf{r})}{f_0(\mathbf{r})} \underset{\mathcal{H}_0}{\overset{\mathcal{H}_1}{\gtrless}} \tilde{\gamma}. \tag{2.2}$$

Since $f_0(\mathbf{r}) \sim \mathcal{N}(\mathbf{0}, \mathbf{C})$ and $f_1(\mathbf{r}) \sim \mathcal{N}(\alpha \mathbf{s}_\theta, \mathbf{C})$, $L_g(\mathbf{r})$ can be simplified as

$$\begin{aligned} L_g(\mathbf{r}) &= \max_\theta \left[\exp\left\{ -\frac{1}{2}\Big((\mathbf{r}-\alpha\mathbf{s}_\theta)^H \mathbf{C}^{-1}(\mathbf{r}-\alpha\mathbf{s}_\theta) + \mathbf{r}^H\mathbf{C}^{-1}\mathbf{r} \Big) \right\} \right] \\ &= \max_\theta \left[\exp\left\{ \frac{1}{2}\Big(\overset{*}{\alpha}\mathbf{s}_\theta^H \mathbf{C}^{-1}\mathbf{r} + \alpha\mathbf{r}^H\mathbf{C}^{-1}\mathbf{s}_\theta - |\alpha|^2\, \mathbf{s}_\theta^H\mathbf{C}^{-1}\mathbf{s}_\theta \Big) \right\} \right] \end{aligned} \tag{2.3}$$

The second term in (2.3) is a constant independent of the received signal $\mathbf{r}$. Furthermore, since $\exp(x)$ is a monotonic function, the GLRT in (2.2) can be written as

$$\max_\theta \left(\overset{*}{\alpha}\mathbf{s}_\theta^H\mathbf{C}^{-1}\mathbf{r} + \alpha\mathbf{r}^H\mathbf{C}^{-1}\mathbf{s}_\theta \right) \underset{\mathcal{H}_0}{\overset{\mathcal{H}_1}{\gtrless}} \gamma. \tag{2.4}$$

The detector in (2.4) assumes knowledge of target amplitude $\alpha \in \mathbb{C}$. Since this is usually not known a priori, we can replace it by its maximum likelihood estimate (MLE). Denoting the MLE of α as $\hat{\alpha}$, from [24],

$$\begin{aligned} \hat{\alpha} &= \arg\max_\alpha \exp\left\{ -\frac{1}{2}(\mathbf{r}-\alpha\mathbf{s}_\theta)^H\mathbf{C}^{-1}(\mathbf{r}-\alpha\mathbf{s}_\theta) \right\} \\ &= \arg\max_\alpha \left\{ -\frac{1}{2}(\mathbf{r}-\alpha\mathbf{s}_\theta)^H\mathbf{C}^{-1}(\mathbf{r}-\alpha\mathbf{s}_\theta) \right\} \\ &= \arg\max_\alpha \left\{ \overset{*}{\alpha}\mathbf{s}_\theta^H\mathbf{C}^{-1}\mathbf{r} + \alpha\mathbf{r}^H\mathbf{C}^{-1}\mathbf{s}_\theta - |\alpha|^2\, \mathbf{s}_\theta^H\mathbf{C}^{-1}\mathbf{s}_\theta \right\} \\ &= \frac{\mathbf{s}_\theta^H\mathbf{C}^{-1}\mathbf{r}}{\mathbf{s}_\theta^H\mathbf{C}^{-1}\mathbf{s}_\theta}. \end{aligned} \tag{2.5}$$

Using (2.5) in (2.3), GLRT yields a detector of the form

$$\max_\theta \left(\frac{\left|\mathbf{s}_\theta^H\mathbf{C}^{-1}\mathbf{r}\right|^2}{\mathbf{s}_\theta^H\mathbf{C}^{-1}\mathbf{s}_\theta} \right) \underset{\mathcal{H}_0}{\overset{\mathcal{H}_1}{\gtrless}} \gamma, \tag{2.6}$$

where the threshold γ is selected based on the desired probability of false alarm [23]. Assuming a normalized signal dictionary and i.i.d noise, that is, $\mathbf{s}_\theta^H\mathbf{s}_\theta = 1$, $\forall\theta$ and $\mathbf{C} = \sigma^2\mathbf{I}$, GLRT in (2.6) can be expressed as

$$\max_\theta \left|\mathbf{s}_\theta^H\mathbf{r}\right| \underset{\mathcal{H}_0}{\overset{\mathcal{H}_1}{\gtrless}} \gamma. \tag{2.7}$$

The detector in (2.7) can be implemented using a bank of filters matched to all possible $\mathbf{s}_\theta$, $\theta \in \mathcal{T}$, at the receiver. Then, if $\left|\mathbf{s}_{\widetilde{\theta}}^H \mathbf{r}\right| = \max_\theta \left|\mathbf{s}_\theta^H \mathbf{r}\right|$, there is a target present at parameters specified by $\widetilde{\theta}$ whenever $\left|\mathbf{s}_{\widetilde{\theta}}^H \mathbf{r}\right| > \gamma$. Motivated by the hypothesis test in (2.7), most radar implementations use a bank of matched filters at the receiver. Another reason for its popularity is the straightforward extension of the test in (2.7) to the multiple target scene as discussed next.

2.2 Multiple targets

In a multiple target environment, the number of targets as well as the target parameters has to be estimated. As a result, the hypothesis test is no longer a binary hypothesis test. In this section, an iterative detection algorithm is derived by successively increasing the assumed number of targets in the binary hypotheses. Hence, the algorithm would first decide if there is a target or not in the target environment. Then, if the result of first iteration shows presence of a target, the algorithm will decide if there is only one target or two targets and so on. An advantage of this approach is that it yields a binary hypothesis test in each iteration. In addition, in section 2.3 it will be shown that a greedy algorithm for detecting multiple targets can be easily derived using this iterative approach. Consider a target scene with either K targets or $K+1$ targets. The two hypotheses can be stated as

$$\begin{aligned} \mathcal{H}_0 : \mathbf{r} &= \mathbf{S}\alpha_K + \mathbf{w}, \\ \mathcal{H}_1 : \mathbf{r} &= \mathbf{S}\alpha_{K+1} + \mathbf{w}, \end{aligned} \tag{2.8}$$

where $\alpha_i \in \mathbb{C}^P$ denotes a target scene vector with i targets, that is,$\|\alpha_i\|_0 = i$, and $\mathbf{w} \sim \mathcal{N}(\mathbf{0}, \sigma^2\mathbf{I})$. Because of unknown target parameters, in this case both $\mathcal{H}_0$ and $\mathcal{H}_1$ are composite hypotheses. Let $V_i = \left\{\mathbf{x} \in \mathbb{C}^P \mid \|\mathbf{x}\|_0 = i\right\}$ represent the space of all possible target scenes with i targets. Denoting the pdf of received signal as $f_0(\mathbf{r})$ and $f_1(\mathbf{r})$ under $\mathcal{H}_0$ and $\mathcal{H}_1$, the GLRT for this problem is

$$L_g(\mathbf{r}) = \frac{\max_{V_{K+1}} f_1(\mathbf{r})}{\max_{V_K} f_0(\mathbf{r})} \underset{\mathcal{H}_0}{\overset{\mathcal{H}_1}{\gtrless}} \tilde{\gamma}.$$

Again, using $f_0(\mathbf{r}) \sim \mathcal{N}(\mathbf{S}\alpha_K, \sigma^2\mathbf{I})$ and $f_1(\mathbf{r}) \sim \mathcal{N}(\mathbf{S}\alpha_{K+1}, \sigma^2\mathbf{I})$, the *log likelihood* can be written as

$$\ln L_g(\mathbf{r}) \;=\; \max_{\alpha\in V_{K+1},\beta\in V_K} \left\{ -\frac{1}{2\sigma^2} \left\{ \|\mathbf{r}-\mathbf{S}\alpha\|^2 - \|\mathbf{r}-\mathbf{S}\beta\|^2 \right\} \right\},$$

which results in a hypothesis test of the form

$$\left\{ \min_{\beta\in V_K} \|\mathbf{r}-\mathbf{S}\beta\|^2 \right\} - \left\{ \min_{\alpha\in V_{K+1}} \|\mathbf{r}-\mathbf{S}\alpha\|^2 \right\} \underset{\mathcal{H}_0}{\overset{\mathcal{H}_1}{\gtrless}} \gamma. \tag{2.9}$$

The test in (2.9) searches over all possible target parameters as well as target amplitudes. The computational complexity can be partially reduced by making the test independent of the target amplitudes. Define the index set of signal dictionary, $I = \{1, 2, \ldots, P\}$. Then, the MLE of β, denoted $\hat{\beta}$ is given as

$$\begin{aligned} \hat{\beta} &= \arg\max_{\beta\in V_K} f_0(\mathbf{r}) \\ &= \arg\min_{\beta\in V_K} \|\mathbf{r}-\mathbf{S}\beta\|^2 . \end{aligned}$$

Let $\Lambda_j = \{x \subset I \mid |x| = j\}$ denote the set of all subsets of I with j elements. Denoting the K non-zero elements in β as β^K, the ML estimate of β^K can be written as

$$\begin{aligned} \hat{\beta}^K &= \arg\min_{\mathcal{L}\in\Lambda_K,\beta_{\mathcal{L}}} \|\mathbf{r}-\mathbf{S}_{\mathcal{L}}\beta_{\mathcal{L}}\|^2 \\ &= \arg\min_{\mathcal{L}\in\Lambda_K} \left(\mathbf{S}_{\mathcal{L}}^{\dagger} r\right) \end{aligned} \tag{2.10}$$

A similar approach can be used to show that the ML estimate of α is $\hat{\alpha} = \arg\min_{\mathcal{L}\in\Lambda_{K+1}} \left(\mathbf{S}_{\mathcal{L}}^{\dagger} r\right)$. Using (2.10) in (2.9), the hypothesis test can be written as

$$\min_{\mathcal{L}\in\Lambda_K} \left\|\mathbf{r}-\mathbf{S}_{\mathcal{L}}\mathbf{S}_{\mathcal{L}}^{\dagger} r\right\|^2 - \min_{\mathcal{L}\in\Lambda_{K+1}} \left\|\mathbf{r}-\mathbf{S}_{\mathcal{L}}\mathbf{S}_{\mathcal{L}}^{\dagger}\mathbf{r}\right\|^2 \underset{\mathcal{H}_0}{\overset{\mathcal{H}_1}{\gtrless}} \gamma, \tag{2.11}$$

where the test only searches over the unknown target parameters. To obtain a test for the presence of a single target, as in section 2.1, set $K = 0$ in equation (2.11). The hypothesis test in (2.1) then simplifies to

$$\begin{aligned}
\|\mathbf{r}\|^2 - \|\mathbf{r}\|^2 \min_{\mathcal{L}\in\Lambda_1} \left\|\mathbf{r} - \mathbf{S}_{\mathcal{L}}\mathbf{S}_{\mathcal{L}}^{\dagger}\mathbf{r}\right\|^2 &= \|\mathbf{r}\|^2 - \min_{\mathcal{L}\in\Lambda_1} \left\{\|\mathbf{r}\|^2 + \left\|\mathbf{S}_{\mathcal{L}}\mathbf{S}_{\mathcal{L}}^{\dagger}\mathbf{r}\right\|^2 - 2\mathbf{r}^H\mathbf{S}_{\mathcal{L}}\mathbf{S}_{\mathcal{L}}^{\dagger}\mathbf{r}\right\}, \\
&= \max_{\mathcal{L}\in\Lambda_1} \left\{2\mathbf{r}^H\mathbf{S}_{\mathcal{L}}\mathbf{S}_{\mathcal{L}}^{\dagger}\mathbf{r} - \left\|\mathbf{S}_{\mathcal{L}}\mathbf{S}_{\mathcal{L}}^{\dagger}\mathbf{r}\right\|^2\right\}, \\
&= \max_{\mathcal{L}\in\Lambda_1} \left\{2\mathbf{r}^H\mathbf{S}_{\mathcal{L}}\mathbf{S}_{\mathcal{L}}^{\dagger}\mathbf{r} - \mathbf{r}^H\left(\mathbf{S}_{\mathcal{L}}^{\dagger}\right)^H\mathbf{S}_{\mathcal{L}}^H\mathbf{S}_{\mathcal{L}}\mathbf{S}_{\mathcal{L}}^{\dagger}\mathbf{r}\right\}, \\
&= \max_{\mathcal{L}\in\Lambda_1} \left\{2\mathbf{r}^H\mathbf{S}_{\mathcal{L}}\mathbf{S}_{\mathcal{L}}^{\dagger}\mathbf{r} - \mathbf{r}^H\mathbf{S}_{\mathcal{L}}\mathbf{S}_{\mathcal{L}}^{\dagger}\mathbf{r}\right\}, \\
&= \max_{\mathcal{L}\in\Lambda_1} \left\{\mathbf{r}^H\mathbf{S}_{\mathcal{L}}\mathbf{S}_{\mathcal{L}}^{\dagger}\mathbf{r}\right\}, \qquad (2.12)
\end{aligned}$$

where the definition of Moore-Penrose pseudo inverse $\mathbf{S}_{\mathcal{L}}^{\dagger} = \left(\mathbf{S}_{\mathcal{L}}^H\mathbf{S}_{\mathcal{L}}\right)^{-1}\mathbf{S}_{\mathcal{L}}^H$ was used. Furthermore, since all the sets $\mathcal{L} \in \Lambda_1$ consist of only one element, $\mathbf{S}_{\mathcal{L}}$ denotes a column of the synthesis matrix $\mathbf{S}$. Hence, using the fact that the dictionary is assumed to be normalized, that is $\mathbf{S}_{\mathcal{L}}^H\mathbf{S}_{\mathcal{L}} = 1$, the expression to be maximized in equation can be further simplified to $\left\{\mathbf{r}^H\mathbf{S}_{\mathcal{L}}\mathbf{S}_{\mathcal{L}}^H\mathbf{r}\right\} = \left|\mathbf{S}_{\mathcal{L}}^H\mathbf{r}\right|^2$. The simplified detector for a single target case is then given as

$$\max_{\mathcal{L}\in\Lambda_1} = \left|\mathbf{S}_{\mathcal{L}}^H\mathbf{r}\right|^2,$$

which is equivalent to the matched filter test in (2.7).

When the number of targets in a target scene is unknown *a priori*, the hypothesis test in (2.11) suggests that an iterative algorithm can be used to estimate the number and position of targets. This is shown as algorithm (2.1). Appendix B shows that algorithm (2.1) is an iterative implementation of the optimal sparse problem (1.2) when $\lambda = \gamma$. Therefore, application of algorithm (2.1) to radar problems is computationally infeasible in general. However, recently a number of computationally tractable algorithms have been proposed to find the solution of the sparse recovery problem in (1.2). Most of these algorithms assume that the dictionary is incoherent. This is discussed in more detail in the next section. For now, assume that the normalized signal dictionary, S, is perfectly non coherent, that is

$$\mu(\mathbf{S}) = 0.$$

This means that the synthesis matrix is orthonormal. Now suppose the iterative application of the test in (2.11) shows that there are at least K targets in the target scene. Let $\hat{\mathcal{L}} = \arg\min_{\mathcal{L}\in\Lambda_K} \left\|\mathbf{r} - \mathbf{S}_{\mathcal{L}}\mathbf{S}_{\mathcal{L}}^H\mathbf{r}\right\|^2$. Then, appendix C shows that the GLRT for hypothesis $\mathcal{H}_0$ and $\mathcal{H}_1$ in (2.8) can be written as

$$\max_{\theta\in\Lambda_1/\hat{\mathcal{L}}} \left\|\mathbf{s}_\theta^H\mathbf{r}\right\|^2 \underset{\mathcal{H}_0}{\overset{\mathcal{H}_1}{\gtrless}} \gamma. \tag{2.13}$$

Comparing (2.13) with (2.7), (2.13) can be seen to be an extension of matched filters to the multiple target case. In addition, the decision in any iteration of the matched filter detector in (2.13) can be seen to be independent of all other iterations. Hence, for a perfectly non-coherent dictionary S, the test in (2.13) can be modified to estimate the set of all unknown target positions at once as

$$\mathcal{L} = \left\{\theta \mid \left\|\mathbf{s}_\theta^H\mathbf{r}\right\| \underset{\mathcal{H}_0}{\overset{\mathcal{H}_1}{\gtrless}} \gamma,\ \theta\in\mathcal{T}\right\}. \tag{2.14}$$

The target amplitude, a_θ, corresponding to each target position θ can then be estimated using the MLE

$$\hat{a}_\theta = \mathbf{s}_\theta^H\mathbf{r}.$$

Although a receiver implementing the hypothesis test in (2.14) can be implemented using the same hardware used in one target case, non-coherent dictionaries rarely arise in practice. This is especially true when the signal dictionary is redundant as in pulse Doppler radar. Nevertheless, because of its simplicity, the hypothesis test in (2.14) is widely used in radar systems.

The limitations of the matched filter hypothesis test (2.14) in a system with non-coherent dictionary can be seen by considering a range radar using the combined barker sequence. Figure 2.1a shows the matched filter output when the target scene consists of a target at delay 0 and a second target at delay $6t_b$. The presence of

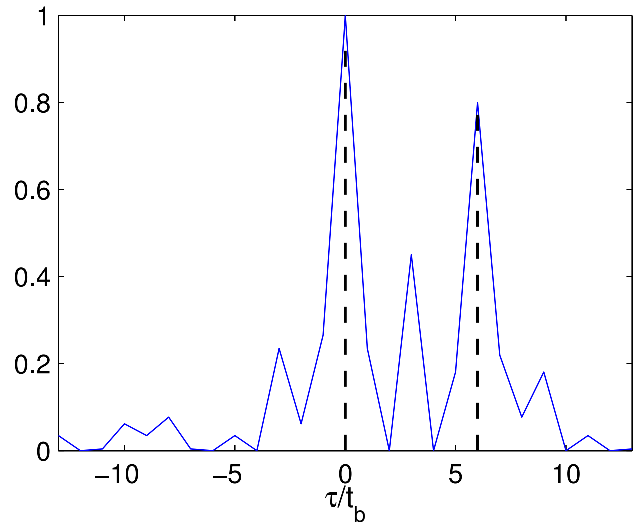

(a) Targets at 0 and $6t_b$ with normalized amplitudes 1 and 0.8 respectively.

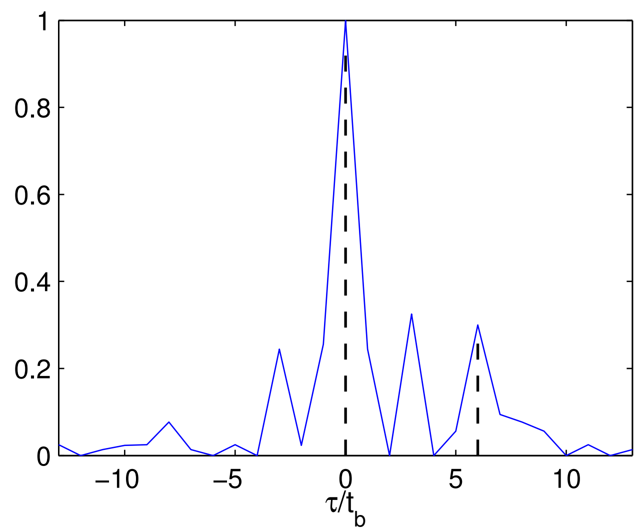

(b) Targets at 0 and $6t_b$ with normalized amplitudes 1 and 0.3 respectively.

Figure 2.1.: Matched filter output for two targets located at delays of 0 and $6t_b$.

significant sidelobes at $-3t_b$ and $3t_b$ can cause a false alarm if the threshold γ is not chosen appropriately. Conversely, Figure 2.1b shows that choosing a higher value of threshold γ can cause the weaker targets to remain invisible from the radar system. Linear filters designed to reduce sidelobe levels have been proposed to overcome this problem in matched filters [25–27]. Such filters are commonly called *mismatch filters*. Figure 2.2 shows the output of a radar system using a length $52t_b$ mismatched filter designed using the least squares technique proposed in [25]. It can be seen that the reduced sidelobe level makes it easier to resolve targets with small radar cross sections close to stronger targets. It is, however, important to point out that Figures 2.1 and 2.2 were obtained by ignoring noise in the received signal. In chapter 3 it will be shown that although mismatched filter performs better in high signal to noise ratio (SNR), the detection performance can suffer in low SNR. This trade-off between algorithmic performance and performance in noise will be discussed in detail in chapter 3. Compared to the mismatched filter, the greedy detector presented in section 2.3 can overcome the sidelobe problem of the matched filter detector (2.14) without losing detection performance in noise.

2.3 Greedy Iterative detection

The hypothesis tests in (2.9) and (2.11), though optimal, are impractical because of their computational complexity. Computationally tractable, but suboptimal algorithms can be obtained by imposing constraints on α_K and α_{K+1} in (2.8). In this section, we assume the target coefficient vectors, α_K and α_{K+1} under the two hypotheses are related as

$$\alpha_{K+1} = \alpha_K + \alpha_1, \tag{2.15}$$

where $\|\alpha_1\|_0 = 1$. In the $(K+1)^{th}$ iteration, the two hypothesis can be written as

$$\begin{aligned} \mathcal{H}_0 : \mathbf{r} &= \mathbf{S}\alpha_K + \mathbf{w}, \\ \mathcal{H}_1 : \mathbf{r} &= \mathbf{S}\alpha_K + a\mathbf{s}_\theta + \mathbf{w}, \end{aligned}$$

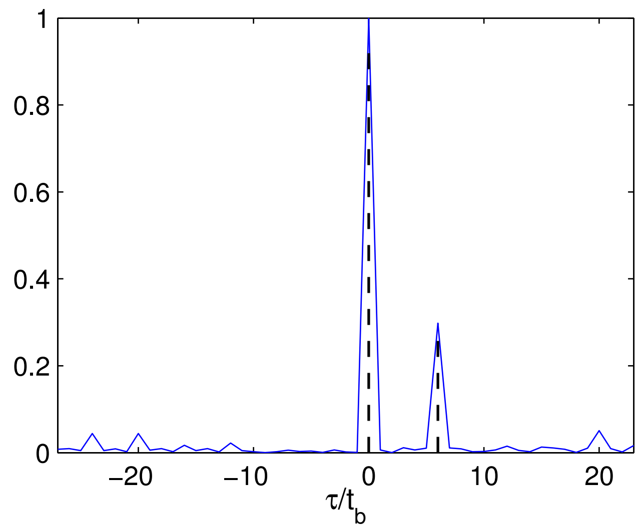

Figure 2.2.: Mismatched filter output for targets located at delays of 0 and $6t_b$ with normalized amplitudes 1 and 0.3 respectively.

Algorithm 2.1 Optimal algorithm for sparse signal decomposition of $r = \sum_{i \in \Lambda} s_i \alpha_i + n,\ s_i \in S$. The position of the non-zero coefficients is specified by $\hat{\Lambda}$ and the corresponding coefficient values are given by $\hat{\alpha}$.

- Initialize $\hat{\Lambda} = \emptyset,\ k = 1,\ \epsilon = \|r\|^2$.
- $\hat{\mathcal{L}}_k = \arg\min_{\mathcal{L} \in \Lambda_k} \left\| r - S_{\mathcal{L}} S_{\mathcal{L}}^{\dagger} r \right\|^2$.
- $\beta = \left\| r - S_{\hat{\mathcal{L}}_k} S_{\hat{\mathcal{L}}_k}^{\dagger} r \right\|^2$.
- while $(\epsilon - \beta) > \gamma$
  - $\hat{\Lambda} = \hat{\mathcal{L}}_k$.
  - $k = k + 1$.
  - $\epsilon = \beta$.
  - $\hat{\mathcal{L}}_k = \arg\min_{\mathcal{L} \in \Lambda_k} \left\| r - S_{\mathcal{L}} S_{\mathcal{L}}^{\dagger} r \right\|^2$.
  - $\beta = \left\| r - S_{\hat{\mathcal{L}}_k} S_{\hat{\mathcal{L}}_k}^{\dagger} r \right\|^2$.
- $\hat{\alpha} = S_{\hat{\Lambda}}^{\dagger} r$.

where α_K is assumed to be known from the previous K iterations. The *log likelihood* ratio can be written as

$$\begin{aligned} \ln L_g(\mathbf{r}) &= \min_{\theta \in \mathcal{T}} \left\{ \|\mathbf{r} - \mathbf{S}\alpha_K - a\mathbf{s}_\theta\|^2 - \|\mathbf{r} - \mathbf{S}\alpha_K\|^2 \right\}, \\ &= \min_{a \in \mathbb{R}, \theta \in \mathcal{T}} \left\{ \|\bar{\mathbf{r}} - a\mathbf{s}_\theta\|^2 - \|\bar{\mathbf{r}}\|^2 \right\}, \end{aligned} \tag{2.16}$$

where $\bar{\mathbf{r}} = \mathbf{r} - \mathbf{S}\alpha_K$ is called the *residual* vector. From (2.10), the MLE of a is given as $\hat{a} = \mathbf{s}_\theta^H \bar{\mathbf{r}}$. Using this in (2.16), the hypothesis test can be written as

$$\max_\theta \left| \mathbf{s}_\theta^H \left(\mathbf{r} - \mathbf{S}\alpha_K \right) \right| \underset{\mathcal{H}_0}{\overset{\mathcal{H}_1}{\gtrless}} \gamma. \tag{2.17}$$

In a general radar application, the number of targets and their locations are unknown *a priori*. Algorithm (2.2) shows an iterative implementation of the hypothesis test in (2.17). In each iteration, the MLE of the target vector from the previous iteration is canceled from the received signal vector to obtain the residual vector. This approach to multiple target detection was first proposed by Hogbom [28] for deconvolution of images with point sources. More recently, this algorithm was rediscovered [6, 7] as an effective way to solve the sparse problem in (1.2). In sparse signal processing community, this algorithm is commonly known as the Orthogonal Matching Pursuit (OMP) algorithm. As a result, we will refer to algorithm (2.2) as OMP for the rest of the paper.

If the greedy assumption in equation (2.15) is not valid in any iteration of the OMP algorithm, the selected target may not be in the optimal sparse set Λ. When this happens, the targets selected in successive iterations may also be wrong. Hence, while greedy approach may yield good results in some cases, a wrong target selection in one iteration may throw the algorithm off track. The conditions for correct target recovery are analyzed in more detail in chapter 3.

2.3.1 Matched filters vs Matching Pursuit

Although not apparent, there is an inherent similarity between the the OMP algorithm and the matched filter. Consider for example, the sparse representation of

Algorithm 2.2 Matching pursuit solution for signal decomposition of $r = \sum_k a_k \phi_k + n$

- Initialize $\hat{\Lambda} = \emptyset$, $\bar{r} = r$, γ
- $\sigma = \max_\theta \left| s_\theta^H r \right|$
- while $\sigma > \gamma$
  - $\hat{\theta} = \arg\max_\theta \left| s_\theta^H \bar{r} \right|$
  - $\hat{\Lambda} = \hat{\Lambda} \cup \hat{\theta}$
  - $\hat{\alpha} = \arg\min_\alpha \left\| r - S_{\hat{\Lambda}} \alpha \right\|^2$
  - $\bar{r} = r - S_{\hat{\Lambda}} \hat{\alpha}$
  - $\sigma = \max_\theta \left| s_\theta^H \bar{r} \right|$

$\mathbf{r} = \sum_{k\in\Lambda} \mathbf{a}_k \mathbf{s}_k$, where Λ is the optimal sparse set and $\mathbf{s}_k \in S,\ k \in \{1, 2, \ldots, P\}$. Furthermore, assume the greedy assumption in equation (2.15) is satisfied in all iterations of OMP algorithm. The likelihood ratio is then related to the atom, $\mathbf{s}_{k_1} \in S$, chosen by the first iteration of the OMP algorithm as

$$\mathbf{s}_{k_1} = \arg\max_k L(k),$$

where $L(j) = \langle \mathbf{r}, \mathbf{s}_j \rangle$, $j \in \{1, 2, \ldots, P\}$ denotes the likelihood ratio. The residue, $\bar{\mathbf{r}}$, is then calculated by subtracting the estimated targets from $\mathbf{r}$. In general, in the j^{th} iteration, the OMP algorithm selects $\mathbf{s}_{k_j} = \arg\max_k L^j(k)$, where $L^j(k) = \langle \bar{\mathbf{r}}, \mathbf{s}_k \rangle$, $k \in \{1, 2, \ldots, P\}$. Assuming the iterations are continued until $L^j(k) < \gamma, \forall k \in \{1, 2, \ldots, P\}$, the OMP algorithm is seen to be an iterative implementation of the matched filter if γ is the matched filter threshold.

The iterative nature of the OMP algorithm makes it more robust to false detections compared to the matched filter. To explain this, consider the j^{th} iteration of the OMP algorithm. Assuming condition in (2.15) is satisfied in all iterations, let $\mathbf{s}_{k_m} \in S$, $m \in \{1, \ldots, j\}$ denote the atoms selected by OMP algorithm. Ignoring noise, the assumption implies $k_m \in \Lambda$, $m \in \{1, 2, \ldots, j\}$. Define $\Lambda_j = \{k_m | m \in \{1, 2, \ldots, j\}\}$ as the set of indexes of all atoms selected by the OMP algorithm in j iterations. Then $\forall l \notin \Lambda$, an upper bound on the likelihood $L^j(l)$ is

$$\begin{aligned} L^j(l) &= \sum_{k\in\Lambda\setminus\Lambda_j} \mathbf{a}_k \langle \mathbf{s}_k, \mathbf{s}_l \rangle \\ &\leq (|\Lambda| - j)\mu(S) \max_{k\in\Lambda\setminus\Lambda_j} \{\mathbf{a}_k\}. \end{aligned} \tag{2.18}$$

A comparison of the upper bounds in (2.18) and (1.31) shows how false detections decrease in OMP algorithms with iterations. In fact, if the algorithm correctly selects target from the optimal sparse set Λ in all iterations, after $|\Lambda|$ iterations,

$$L^M(l) = 0,$$

which implies there are no false detections.

2.4 Detection threshold and probability of false alarm

One important aspect of both the matched filter detector and the greedy algorithm in 2.2 is their dependence on the *detection threshold* γ. The detection threshold, in turn, directly affects the probability of false alarm (P_{FA}) and the probability of miss (P_M). Typically, the maximum tolerable P_{FA} in a radar is a known system design parameter. The goal of detection algorithms is to minimize P_M while keeping false alarm rate tolerable.

Consider the following binary hypothesis

$$\begin{aligned}\mathcal{H}_0 : \mathbf{r} &= \mathbf{w} \\ \mathcal{H}_1 : \mathbf{r} &= \alpha\mathbf{s} + \mathbf{w},\end{aligned} \tag{2.19}$$

where $\mathbf{s}$ is a known signal and $\mathbf{w} \sim C\mathcal{N}\left(\mathbf{0}, \sigma^2\mathbf{I}\right)$. Since the signal $\mathbf{s}$ is known at the receiver, the optimal detector for this problem is a simplified version of the one target matched filter given in equation (2.7). In particular, hypothesis $\mathcal{H}_1$ is no longer a composite hypothesis and the Neyman Pearson detector in this case can be written as

$$\left|\mathbf{s}^H\mathbf{r}\right| \underset{\mathcal{H}_0}{\overset{\mathcal{H}_1}{\gtrless}} \gamma. \tag{2.20}$$

By definition, if $\left|\mathbf{s}^H\mathbf{r}\right| > \gamma$ when in fact hypothesis $\mathcal{H}_0$ is true, it is said to be a false alarm. Hence, for the detector in (2.20), P_{FA} can be stated as

$$P_{FA} = P\left(\left|\mathbf{s}^H\mathbf{r}\right| > \gamma | \mathcal{H}_0\right). \tag{2.21}$$

Define $z = \mathbf{s}^H\mathbf{r}$, the mean and variance of the random variable under $\mathcal{H}_0$ is given as

$$\begin{aligned}\mathbf{E}\left(z|\mathcal{H}_0\right) &= 0, \\ \mathbf{E}\left(zz^*|\mathcal{H}_0\right) &= \sigma^2,\end{aligned}$$

where it is assumed that $\|\mathbf{s}\|^2 = 1$. Additionally, since z is a weighted sum of zero mean normal random variables, $z \sim \mathcal{CN}(0, \sigma^2)$ under $\mathcal{H}_0$. Hence, $x = |z|$ is a Rayleigh random variable with probability density function

$$p(x) = \frac{x}{\sigma^2} e^{-x^2/2\sigma^2},$$

when hypothesis $\mathcal{H}_0$ is true. As a result, the probability of false alarm P_{FA} is given as

$$P_{FA} = e^{-\gamma^2/2\sigma^2}.$$

Thus, if ρ is the maximum tolerable false alarm rate in a system, the detection threshold should be selected as

$$\gamma = \sqrt{2\sigma^2 \ln\left(\frac{1}{\rho}\right)}. \tag{2.22}$$

Similarly, the probability of a miss can be computed as

$$P_M = P\left(\left|\mathbf{s}^H \mathbf{r}\right| < \gamma | \mathcal{H}_1\right),$$

where $z = \mathbf{s}^H \mathbf{r}$ is a complex Gaussian random variable with mean and variance

$$\begin{aligned} \mathbf{E}(z|\mathcal{H}_1) &= \alpha, \\ \mathbf{E}\left((z-\alpha)(z-\alpha)^* |\mathcal{H}_1\right) &= \sigma^2. \end{aligned}$$

Hence, $|z|$ is a random variable following the Rician distribution with parameters $|\alpha|$, σ. Denoting the *Marcum Q-function* as Q_1, the probability of miss is given as

$$P_M = 1 - Q_1\left(\frac{|\alpha|}{\sigma}, \frac{\gamma}{\sigma}\right).$$

In radar literature, instead of probability of a miss (P_M), it is more common to use probability of detection (P_d) for comparing radar system performance. Since probability of detection is defined as the probability that hypothesis $\mathcal{H}_1$ is correctly selected at the receiver, it is related to P_M as

$$P_d = 1 - P_M.$$

Another important parameter affecting the radar system performance is the signal to noise ratio (SNR). For the simple hypothesis in equation (2.19), SNR is defined as the ratio of signal power to noise power under hypothesis $\mathcal{H}_1$, that is

$$\mathrm{SNR} = \frac{|\alpha|^2}{\sigma^2}. \tag{2.23}$$

As a result, the probability of single target detection is given as

$$P_d = Q_1\left(\sqrt{\mathrm{SNR}}, \sqrt{2\ln\left(\frac{1}{\rho}\right)}\right), \tag{2.24}$$

where ρ is the maximum tolerable probability of false alarm. Equation (2.24) shows that the radar system detection performance can be completely determined by SNR and the probability of false alarm. Because of this, detection algorithms in radar are frequently compared by fixing one of these parameters while varying the other.

Figure 2.3 shows the *receiver operating characteristics* (ROC) of the matched filter designed for single target. The ROC is frequently used to study the relation between P_d and P_{FA} of a radar system for some fixed SNR. From figure 2.3, it can be seen that improving the probability of false alarm requires a tradeoff with probability of detection. The ROC can provide a visual guide to selecting an appropriate probability of false alarm for the system.

Unlike the ROC, figure 2.4 shows the relation between probability of detection and SNR for a fixed probability of false alarm. This will be referred to as the *detection performance* graph in this dissertation. As can be seen in figure 2.4, for a fixed false alarm rate, the detection performance is improved as SNR increases. This shows that a radar system will perform better for “strong” targets compared to “weaker” targets. This aspect of radar performance dependence on targets will be looked into in more detail in Chapter 3.

Till now, all the results for single target detection in this section have been obtained assuming matched filter processing. Similarly, if the OMP algorithm is used to detect a known signal as in hypothesis (2.19), the number of iterations can be constrained to a maximum of one. Then, the algorithm 2.2 gives a false alarm under $\mathcal{H}_0$

when $\left|\mathbf{s}^H\mathbf{r}\right| > \gamma$. Comparing this condition with (2.21), it can be seen that matched filter and OMP have the same false alarm rate for the same γ. Hence, the formula for detection threshold in equation (2.22) can also be used for OMP algorithms. Furthermore, because the OMP algorithm is essentially doing matched filtering ($\left|s^H\bar{r}\right| > \gamma$) of the received signal in the first iteration, the detection probability for both will also be the same.

Before ending this section, it is important to mention that the detection threshold in equation (2.22) was derived assuming a constraint on P_{FA} in a single target environment. In a multi-target environment, the target sidelobes can increase the false alarm rate at some range and Doppler bins. The false alarm rate and hence the detection threshold in this case depends on the location of the targets as well as their amplitudes. For simplicity, however, detection thresholds are commonly designed assuming a hypothesis of the form (2.19).

In a multi-target environment with unknown number of targets, the ROC and detection performance graphs obtained for a single target are not sufficient to study a radar system. This is due to the fact that the matched filters for single target and multi-target environment are very different filters. In Chapter 3, modified ROC and detection performance graphs will be proposed for comparing radar systems in multi-target environments. These will be used to show that unlike the single target case, performance of OMP algorithm and matched filters in a multi-target environment is different.

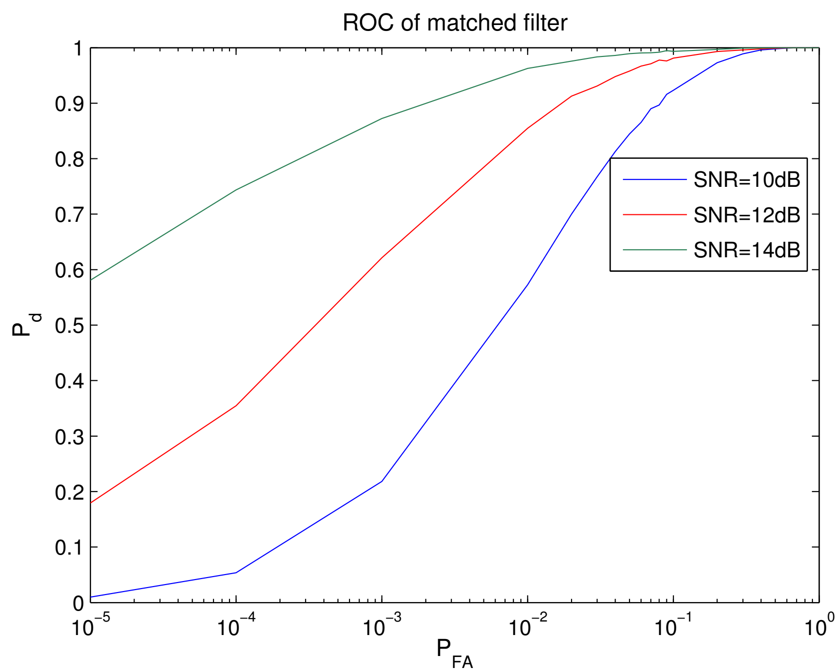

Figure 2.3.: Receiver operating characteristic of the matched filter and the OMP algorithm.

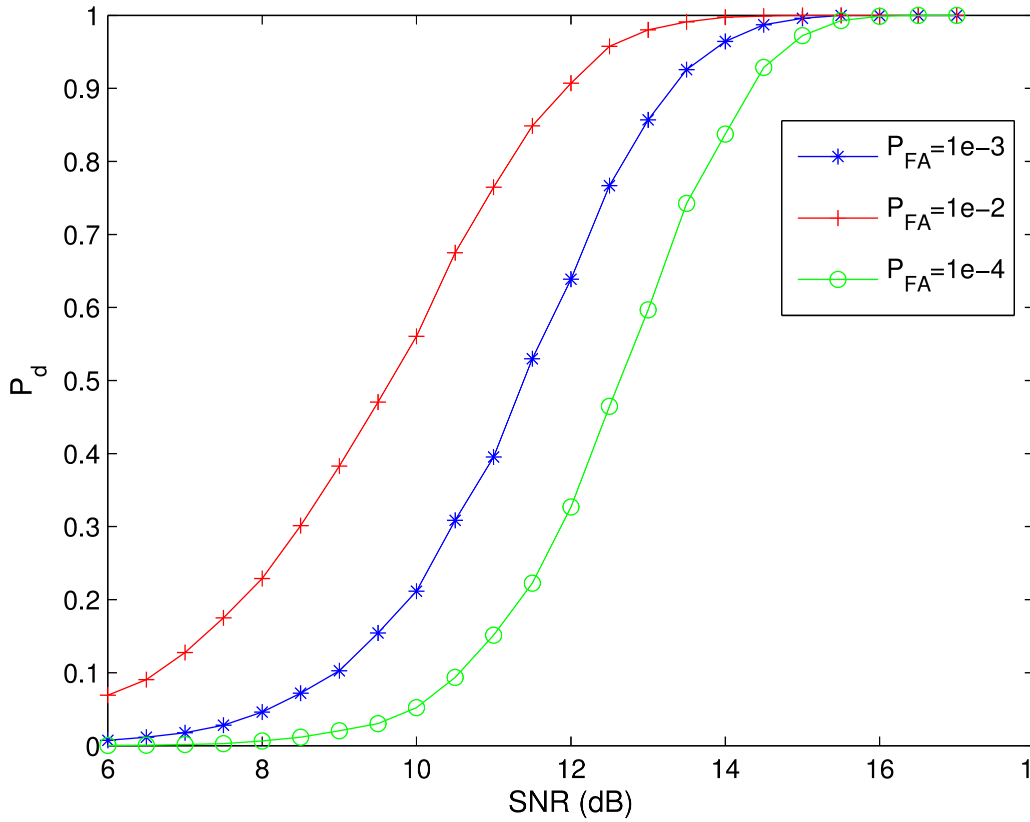

Figure 2.4.: Single target detection performance of matched filter and OMP algorithm.

3. RADAR RESOLUTION

Radar system performance is typically measured in terms of *detection* and *resolution*. *Detection* performance of a radar refers to the ability of a radar system to detect targets in noise. This has been extensively studied and it is well known that the matched filter yields optimal detection performance in additive white Gaussian noise when the target scene consists of a single target only or no target at all.

The *resolution* of a radar refers to its ability to separate multiple targets. Depending on the problem of interest, resolution depends on two main ambiguity function characteristics. For example, the ability of a radar to separate two closely spaced targets is often called resolution. This definition of resolution depends on the mainlobe of the ambiguity function and is usually measured using the same measures as the single target case. Another common use of resolution in multiple target scene refers to the ability of the radar to resolve a weak target in presence of a strong target. Total sidelobe energy, peak sidelobe level (PSL) and variance of the ambiguity function are a few measures that are used to compare this type of resolution. Unlike the previous definitions of resolution, this definition of resolution takes into account the sidelobe behavior of the ambiguity function.

In the rest of this chapter, we discuss some of these commonly used definitions of radar resolution in more detail. We discuss examples of target scenarios where each one of these definitions is unsuitable for use in general, and with iterative algorithms in particular. This is due to the fact that most definitions of resolution either focus on the mainlobe behavior of the ambiguity function or just account for the sidelobes. A good radar resolution measure should be a balance of both of these in some way. For the case of iterative algorithms in radar, we intuitively discuss what resolution means. From the discussion, we will naturally obtain a definition of resolution suitable for iterative algorithms. We then generalize this resolution definition and use it to propose a single metric which can be used to quantitatively compare the resolution performance of different radar systems. Finally, the resolution performance of the OMP algorithm is analyzed using the proposed framework.

3.1 Signal model

The complex envelope of a phase coded pulse, $s(t)$ of length T, can be expressed as [18]

$$s(t) = \sum_{m=1}^{M} u_m rect\left[\frac{t-(m-1)t_b}{t_b}\right],$$

where $t_b = T/M$ and $u_m = e^{j\phi_m}$, $m \in \{1, 2, \ldots, M\}$ is the *phase code* associated with $s(t)$. In this chapter, we will use phase coded pulses to compare different resolution definitions. For simplicity, we will limit ourselves to $M = 7$ binary phase coded sequences, that is,

$$\phi_m \in \{0, \pi\}, \forall m \in \{1, 2, ..., 7\}.$$

The two binary phase coded pulses used in this chapter have phase codes $\{u_m^1\} = \{-1, 1, -1, 1, -1, 1, -1\}$ and $\{u_m^2\} = \{1, 1, 1, 1, -1, -1, 1\}$ and will be referred to as *sequence 1* and *sequence 2* from now on. The absolute value of the autocorrelation for these two sequences is shown in figure 3.1. It can be seen that sequence 1 has higher sidelobes but a narrower mainlobe compared to sequence 2.

3.2 Resolution based on mainlobe

In radar literature, resolution is most commonly associated with the ability of the radar system to separate and identify closely spaced targets. Figure 3.2 shows the matched filter output corresponding to two nearby targets when sequence 1 and sequence 2 are used. In each case, the two targets are located at $8.125\tau/t_b$ and $9.25\tau/t_b$. We observe that the presence of the two targets results in two distinct peaks in figure 3.2a, but the two peaks in figure 3.2b are not as easily distinguishable. This will be specially true in practice when noise is present. This shows that sequence 1

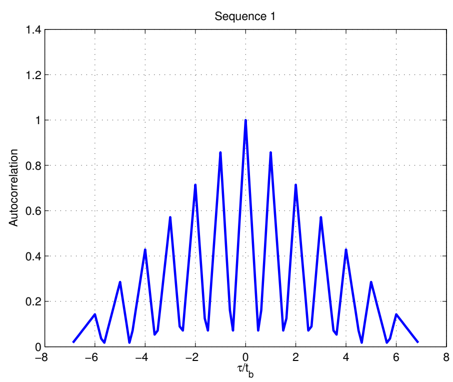

(a) Absolute value of the autocorrelation of sequence 1

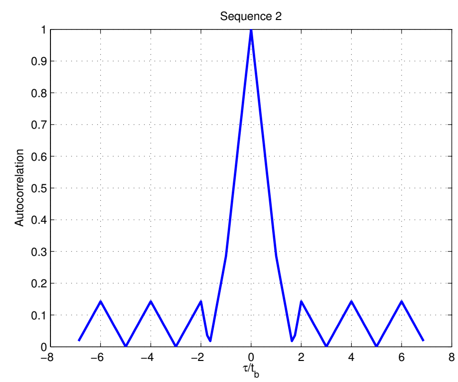

(b) Absolute value of the autocorrelation of sequence 2

Figure 3.1.: Phase coded sequences used as examples

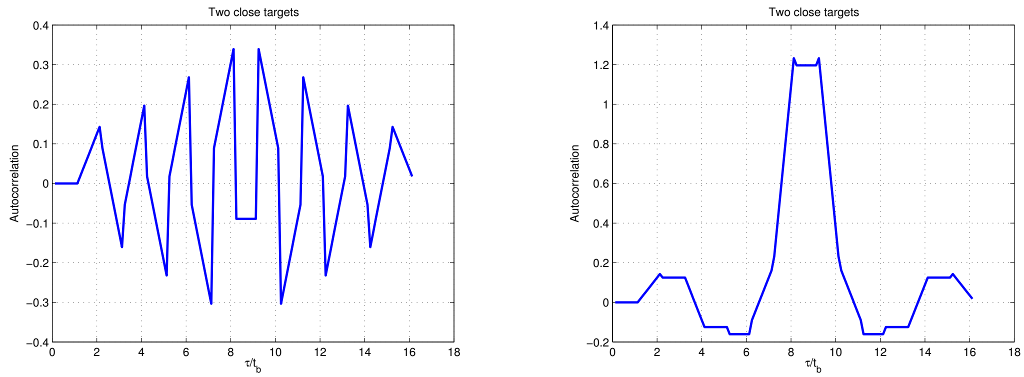

(a) Sequence 1 (b) Sequence 2

Figure 3.2.: Matched filter output, $A(\tau)$, for two targets separated by $1.125\tau/t_b$

should be preferred over sequence 2 for separating nearby targets. In radar literature, sequence 1 would be said to have a higher *resolution* compared to sequence 2.

This difference in resolution between sequence 1 and sequence 2, when using matched filters, can be traced to the mainlobe width of their autocorrelation functions. Suppose a radar pulse has a continuous autocorrelation function $A(\tau)$. Assuming the pulse has been normalized to have unit energy, $A(\tau)$ satisfies [29]

$$\forall \tau \in \mathbb{R},\ |A(\tau)| \leq 1.$$

Furthermore, it can be shown that $A(\tau) = 1$ if and only if $\tau = 0$. Assume $\tau_r \in \mathbb{R},\ \tau_r > 0$ is the smallest delay at which $A(\tau_r) = \gamma, 0 < \gamma < 1$. Then by symmetry of the autocorrelation function and the continuity assumption, $A(\tau) \geq \gamma,\ |\tau| < \tau_r$. Now assume we have a target environment with two targets located at $\tau = \tau_0$ and $\tau = \tau_0 + 2\tau_m$. By linearity of the matched filter, the output $\Gamma(\tau)$, can be expressed as

$$\Gamma(\tau) = A(\tau - \tau_0) + A(\tau - (\tau_0 + 2\tau_m)).$$

Ideally, to be able to separate and distinguish the two targets, $\Gamma(\tau)$ must have two distinct peaks at $\tau = \tau_0$ and $\tau = \tau_0 + 2\tau_m$. This in turn depends on the transmit

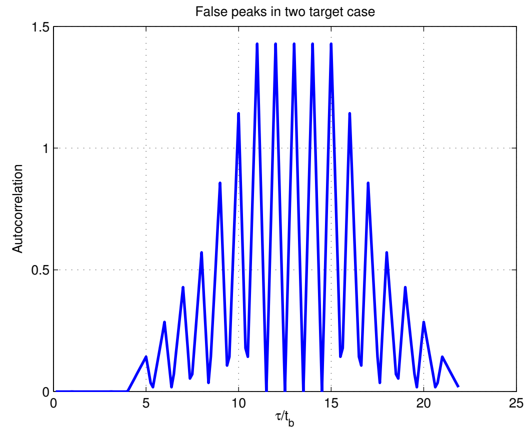

Figure 3.3.: False target peaks example

pulse used by the radar system. However, for the two target case and $\gamma = 0.5$, we observe that

$$\Gamma(\tau - (\tau_0 + \tau_m)) \geq 1,\ \forall \tau_m < \tau_r,$$

which guarantees detection of a false target at $\tau = \tau_0 + \tau_m$, irrespective of the transmit waveform, when the matched filter processing is used. Because of this, $2\tau_r$ is often used as a measure of resolution in radar literature. In pulse-Doppler radars where targets may be close in delay and Doppler, $\gamma < 0.5$ may be more suitable when more than two close targets are of interest.

Before ending this section, it is important to note that there may be other points, $\tau_k \notin \{\tau_0, \tau_0 + \tau_m, \tau_0 + 2\tau_m\}$, such that $\Gamma(\tau_k) \geq 1$ depending on the radar pulse used. In fact, depending on the transmit pulse used, there may be points $\tau_k \notin \{\tau_0, \tau_0 + 2\tau_m\}$ such that $\Gamma(\tau_k) \geq 1$ for some $\tau_m > \tau_r$. Figure 3.3 shows the magnitude of the matched filter output for two targets located at $11\tau/t_b$ and $15\tau/t_b$, when sequence 1 ($2\tau_r < 1$) is used. In this example, $\forall \tau \in \{10\tau/t_b, 12\tau/t_b, 13\tau/t_b, 14\tau/t_b, 16\tau/t_b\}$, $\Gamma(\tau) > 1$. For such pulses, a different resolution measure would be more suitable. In section 3.4, we propose such a resolution measure which accounts for the intricacies of transmit pulse.

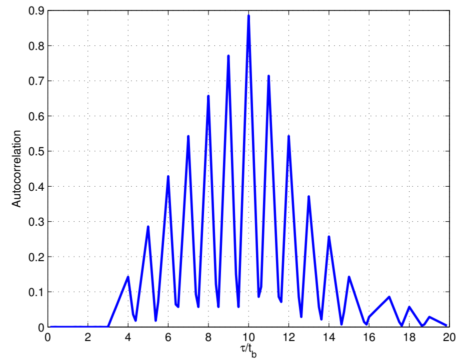

(a) Sequence 1

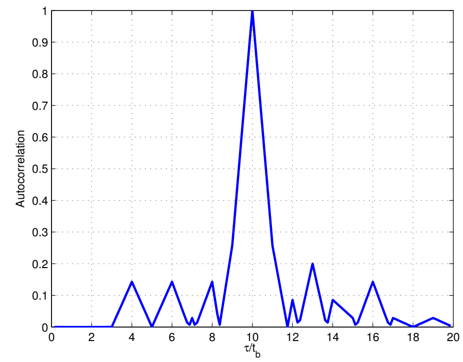

(b) Sequence 2

Figure 3.4.: Matched filter output, $A(\tau)$, for a strong target at $10\tau/t_b$ and a weak target located at $13\tau/t_b$

3.3 Resolution based on sidelobes

The last section showed the importance of using pulses having narrow autocorrelation mainlobes for separately identifying nearby targets. In radar community, resolution is sometimes also used to refer to the ability of a radar to detect a weak target in the presence of a strong nearby target. Figure 3.4 shows the matched filter output when the target scene consists of a strong target at $10\tau/t_b$ and a weak target at $13\tau/t_b$. The magnitude of the weak target is $-7dB$ relative to the strong target.

A comparison of matched filter outputs for sequence 1 and sequence 2 shows that sequence 2 should be preferred when identification of weak targets close to strong targets is important. This result can be attributed to the sidelobe levels relative to the mainlobe. As figure 3.1 shows, the PSL of sequence 1 is $-0.7dB$ relative to the mainlobe making it difficult to distinguish weak targets from the sidelobes. The PSL level in sequence 2, however, is approximately $-8dB$ relative to the mainlobe. This makes sequence 2 much more suitable for identifying targets with magnitudes greater than $-8dB$ relative to the strong target.

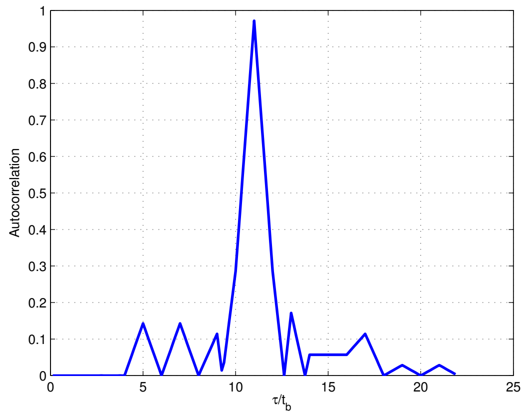

Figure 3.5.: Matched filter output for strong target at $11\tau/t_b$ and weak target at $15\tau/t_b$.

It is important to note that the results in figure 3.4 show the difficulty in identifying weak targets even in the absence of noise. In this case, the sidelobe levels are unwanted signal components interfering with nearby targets. Because of this, sidelobes are often called *waveform self-clutter* in radar literature. Designing waveforms with low sidelobe levels has been an active area of research for the past few decades. Apart from PSL, the total sidelobe energy is another measure often used to compare self-clutter.

Although PSL has been discussed as a measure for resolution in this section, it should be noted that identification of weak targets close to strong targets is dependent on the relative position of the targets. For example, figure 3.5 shows the matched filter output when the target scene consists of a strong target at $11\tau/t_b$ and a weak target at $15\tau/t_b$.The relative magnitudes of the targets are same as in figure 3.4. It can be seen that identification of the weak target is now more difficult.

3.4 Proposed radar resolution

The resolution of a radar is its ability to correctly detect all the targets in the target scene without detecting false targets. Consider a target scene with $L < N$

targets. Let $\Lambda = \{\theta_1, \ldots, \theta_L\}$, $\theta_i \in \mathcal{T}, \forall 1 \leq i \leq L$ represent the set of all targets. The received signal can be written as

$$\mathbf{r} = \sum_{i=1}^{L} \alpha_i \mathbf{s}_{\theta_i} + \mathbf{w}. \tag{3.1}$$

Let $\hat{\Lambda}$ denote the set of target parameters recovered by the radar system. The target scene is called *resolvable* if $\hat{\Lambda} = \Lambda$. Hence, the resolution of a target scene is equivalent to the target recovery performance of the radar system. One factor affecting resolution of a target scene is the received signal noise (3.1). This is commonly characterized by the probability of detection (P_d) of a target for the received signal to noise ratio (SNR). In this paper, it will be assumed that the SNR of each target is sufficiently large, that is,

$$\frac{\|\alpha_i \mathbf{s}_{\theta_i}\|^2}{\|\mathbf{w}\|^2} = \frac{|\alpha_i|^2}{\|\mathbf{w}\|^2} \gg 1, \ \forall 1 \leq i \leq L, \tag{3.2}$$

and as a result, the effect of noise on resolution will be ignored.

The second factor influencing resolution of a target scene is the recovery algorithm used at the receiver. Assuming the noise in the received signal can be ignored, solution of the optimal sparse recovery problem (1.2) or algorithm (2.1) will perfectly reconstruct the target scene. However, as mentioned before, radar systems typically use suboptimal algorithms for target scene recovery because of the computational complexity of the optimal algorithms. Hence, even when the received signal has no noise, not all target scenes are correctly recovered by the radar system. For example, Figure 2.1 shows that using the matched filter at the receiver to detect multiple targets can result in false alarms due to signal dictionary coherence. This phenomenon is usually called *self clutter* in radar literature.

It should be mentioned here that when noise in the receive signal cannot be ignored, it is important to consider probability of detection along with the resolution of the radar. For example, Figure 2.2 shows that radar systems using mismatched filters may have a better resolution than the systems using matched filter (see Figure 2.1b). However, in this particular example, this comes at the expense of 1.83dB loss in signal to noise ratio. While the effect of this loss in SNR on probability of detection may be negligible in low noise, it may severely reduce the probability of detection when there is significant noise present. This trade off between detection performance in noise and algorithmic resolution is a common theme in many high resolution radar schemes [22, 25]. Unless explicitly mentioned, resolution in this paper will refer to the algorithmic resolution assuming noise can be ignored.

In general, the resolution of a radar system will depend on the radar transmit signal and the detection algorithm used. In this paper, this will be termed *absolute resolution* of a radar system. A framework is now proposed to compare the absolute resolution of different recovery algorithms as well as different radar transmit signals.

Definition 3.4.1 *Let $\Lambda = \{\theta_1, \ldots, \theta_L\}$, $\theta_i \in \mathcal{T}, \forall 1 \leq i \leq L$ represent the set of all L target parameters in a target scene. Assume the radar cross sections associated with the targets in Λ are $\boldsymbol{\alpha} = [\alpha_1, \ldots, \alpha_L]$, respectively. Let $\hat{\Lambda} = \{\eta_1, \ldots, \eta_L\}$ be the set of target parameters recovered by a radar system. The target scene with target parameter set Λ is called* absolutely resolvable *by the radar system if and only if $\hat{\Lambda} = \Lambda$, $\forall \boldsymbol{\alpha} \in \mathbb{C}^L$.*

The definition of absolute resolution of a target scene does not assume any constraints on the radar cross section (RCS) of each individual target. Hence, if the detection of a target scene Λ with a radar system results in an $\tilde{\boldsymbol{\alpha}} \in \mathbb{R}^L$ such that $\Lambda \neq \hat{\Lambda}$, the target scene is not absolutely resolvable. In some radar applications, the target amplitudes may be known to satisfy some constraints *a priori*. In such cases, the definition of absolute resolution may be too stringent to be useful.

Definition 3.4.2 *Let $\Lambda = \{\theta_1, \ldots, \theta_L\}$, $\theta_i \in \mathcal{T}, \forall 1 \leq i \leq L$ represent the set of all L target parameters in a target scene. Assume the amplitudes associated with the targets in Λ are $\boldsymbol{\alpha} = [\alpha_1, \ldots, \alpha_L]$, respectively. Furthermore, assume $\boldsymbol{\alpha} \in \mathcal{H}$, where $\mathcal{H} \subset \mathbb{C}^L$ is known* a priori. *Let $\hat{\Lambda} = \{\eta_1, \ldots, \eta_L\}$ be the set of target parameters recovered by a radar system. The target scene with target parameter set Λ is called* partially resolvable *by the radar system if and only if $\hat{\Lambda} = \Lambda$, $\forall \boldsymbol{\alpha} \in \mathcal{H}$.*

Resolution of weak targets located close to strong targets is an important example of constrained target amplitudes. In this case, the ability of the radar to correctly detect the target scene, given prior constraints on the receiver filter output for each target, is of particular interest. Consider a radar system with transmit signal dictionary $\mathbf{S}$ and receive filter dictionary $\tilde{\mathbf{S}}$. For the received signal model in (3.1), the filter output corresponding to target parameters can be written as $\check{\boldsymbol{\alpha}}_\Lambda = \left|\tilde{\mathbf{S}}_\Lambda^H \mathbf{S}\boldsymbol{\alpha}\right|$, where $\Lambda = \{\theta_1, \ldots, \theta_L\}$. Denoting $\check{\alpha}^* = \max_i \left[\check{\boldsymbol{\alpha}}_\Lambda\right]_i, \forall 1 \leq i \leq L$, assume all the receiver filter outputs corresponding to actual targets are constrained as $\left[\check{\boldsymbol{\alpha}}_\Lambda\right]_i \leq \rho_i \check{\alpha}^*$, $0 < \rho_i \leq 1, \forall 1 \leq i \leq L$. Targets for which $\rho_i \approx 1$ are known as *strong targets*. Conversely, targets satisfying $\rho_i \ll 1$ are called the *weak targets*. The set of constrained target amplitudes is given as

$$\mathcal{H} = \left\{\boldsymbol{\alpha} \in \mathbb{C}^L \mid \left[\check{\boldsymbol{\alpha}}_\Lambda\right]_i \leq \rho_i \check{\alpha}^*, \forall 1 \leq i \leq L\right\}, \tag{3.3}$$

where $\boldsymbol{\alpha} = [\alpha_1, \ldots, \alpha_L]$, $\check{\boldsymbol{\alpha}}_\Lambda = \left|\tilde{\mathbf{S}}_\Lambda^H \mathbf{S}\boldsymbol{\alpha}\right|$ and $\check{\alpha}^* = \max_i \left[\check{\boldsymbol{\alpha}}_\Lambda\right]_i, \forall 1 \leq i \leq L$. When the radar uses a matched filter, that is $\tilde{\mathbf{S}} = \mathbf{S}$, the filter output at the target parameters $\check{\boldsymbol{\alpha}}_\Lambda$ are the coefficients of the received signal in the dual basis of $\mathbf{S}_\Lambda$. Hence, the weak target constraints can be considered as constraints on the coefficients of the dual basis of the target scene dictionary. Finally, it should be observed that since $\mathcal{H} \subseteq \mathbb{C}^L$, by definition, absolute resolution of a target scene guarantees partial resolution. The converse, however, is not true.

The absolute resolution and the partial resolution of a target scene convey little information about the resolution capabilities of a radar system in general. To be able to compare two radar systems or radar transmit signals, it will be more useful to define a quantitative measure that is independent of the target positions.

Definition 3.4.3 *Let $I = \{1, 2, \ldots, P\}$ represent the set of indexes of the atoms in signal dictionary S, and let $P(I)$ denote the* power set *of I. The* absolute (partial) resolution *of any radar system is defined as the ratio of the number of $\chi \in P(I)$ which are absolutely (partially) resolvable, and the total number of elements in $P(I)$. More* *formally, define $G(I)$ as the set of all $\chi \in P(I)$ that can be absolutely (partially) recovered by the radar system. Then,*

$$\begin{aligned} \textit{resolution} &= \frac{|G(I)|}{|P(I)|} \\ &= \frac{|G(I)|}{2^P - 1}, \end{aligned} \tag{3.4}$$

where $|S|$ denotes the cardinality of set S.

For large dictionaries, calculation of total performance can be unfeasible. Since the number of targets in the target scene is usually small, it may be more reasonable to consider a subset of $P(I)$ as a performance metric. In this paper, a subset $P_2(I) \subseteq P(I)$ consisting of all sets in $P(I)$ with 2 elements will be used. Denoting the set of all $\chi \in P_2(I)$ that can be recovered as $G_2(I)$, *resolution* of dictionary S can be formally defined as

$$\begin{aligned} \text{resolution} &= \frac{|G_{2,Z}(I)|}{|P_2(I)|} \\ &= \frac{|G_{2,Z}(I)|}{C(P,2)}, \end{aligned} \tag{3.5}$$

where $C(P,2) = \frac{P!}{2 \times (P-2)!}$.

Let $\Lambda_1 = \{\theta_1, \theta_2\} \subset P_2(I)$ and $\Lambda_2 = \{\theta_1 + \epsilon, \theta_2 + \epsilon\} \subset P_2(I)$ be two target scenes consisting of two targets each. The detection algorithms discussed in this paper are shift invariant with respect to resolution, that is, if $\Lambda_1$is absolutely (partially) resolvable, then so is Λ_2 and vice versa. For such algorithms, it may be unnecessary to compute the *resolution* measure for target scenes which are shifted versions of each other. Let $m \in I$ and let $I_c = I/\{m\}$. Define the set $P_{SI}(I) = \{\{m,k\}, \forall k \in I_c\}$, $P_{SI}(I) \subseteq P_2(I)$. For detection algorithms with shift invariant resolution, *resolution* can be defined as

$$\text{resolution} = \frac{|G_{SI}(I)|}{P - 1} \tag{3.6}$$

where $G_{SI}(I)$ is the set of all $\chi \in P_{SI}(I)$ that are resolvable. Practical radar systems are designed for a finite range of target scene. Hence, to overcome boundary effects, it is desirable to choose the fixed target index, $m \in I$, which is approximately in the centre of the target scene.

A close inspection of (3.6) shows that all *resolvable* sets of the form $\{m, k\} \in P_{SI}(I)$, for some $m \in I$ and $k \in I_c$, have equal weight in the performance measure. In radar applications, sometimes it may be more desirable to emphasize some region of the target scene relative to a fixed target. For example, to separately identify targets in a convoy of vehicles using a pulse Doppler radar, it may be more useful to focus on the targets in the same Doppler bin but different nearby range bins. In such an application, range bins may be more heavily weighted to accentuate the difference in *resolution* measure for resolving convoys of vehicles.

Consider a target scene with *a priori* known conditional probabilities p_i, $i \in I_c$. p_i represents the probability of second target being located at index i given that the first target is located at index m. Define an indicator function

$$\Im_i = \begin{cases} 1, & r_{\{i,m\}} < 1 \\ 0, & otherwise \end{cases}$$

where $r_{\{i,m\}} < 1$ implies that the two targets at index i and m are resolvable. A generalized resolution performance which takes into account the *a priori* probabilities can be defined as

$$\text{resolution} = \sum_{i \in I_c} \Im_i p_i. \tag{3.7}$$

3.5 Multi-target receiver operating characteristics

The receiver operating characteristic (ROC) was introduced in Chapter 2 as a tool to compare radar detection performance. The ROC compared the probability of detection (P_d) of a known single target in noise for different probability of false alarms. For any target scene consisting of more than one target, the performance of different radar systems can be compared by using the probability of resolution (P_r) instead of P_d.

Consider any target scene with target parameter set Λ. By definition, the target scene is *resolvable* using a radar system if the recovered target parameter set $\hat{\Lambda} = \Lambda$. This means that the radar system correctly detects all the targets without any false alarm. The probability of resolution (P_r) is defined as the probability that the target parameter set is correctly recovered in noise. In a multi-target environment, it is more useful to compare P_r for different P_{FA} and signal to noise ratio. Henceforth, this will be called the multi-target ROC and will be an important tool for comparing different algorithms.

Before ending this section, it should be pointed out that no assumptions were made regarding target amplitudes. Hence, the multi-target ROC for target scenes with same parameter set but different amplitudes will be different. As a result, when comparing multi-target ROC curves, it is important to clearly mention the relative amplitudes of the targets in the target environment.

3.6 Resolution of OMP algorithm

The fundamental difference between OMP algorithm (2.2) and algorithm (2.1) is that OMP assumes greedy selection (2.15) in each iteration. Hence, if for any target scene the greedy assumption in (2.15) is not true, OMP will not be able to correctly detect all the targets. Consider a target scene with target parameter set $\Lambda = \{\theta_1, \ldots, \theta_L\}, \theta_i \in \mathcal{T}, \forall 1 \leq i \leq L$. The OMP algorithm (2.2) correctly detects all the targets if, in each iteration of the algorithm, $\hat{\theta} \in \Lambda$ and hence,

$$\max_{\theta \in \Lambda} \left| \mathbf{s}_\theta^H \bar{\mathbf{r}} \right| > \max_{\theta \in \overline{\Lambda}} \left| \mathbf{s}_\theta^H \bar{\mathbf{r}} \right|. \tag{3.8}$$

where $\bar{\mathbf{r}}$ is the residual vector at each iteration. The condition for target scene recovery in equation (3.8) can be rewritten as

$$\frac{\left\| \mathbf{S}_{\overline{\Lambda}}^H \bar{\mathbf{r}} \right\|_\infty}{\left\| \mathbf{S}_\Lambda^H \bar{\mathbf{r}} \right\|_\infty} < 1. \tag{3.9}$$

Assuming the first $j < L$ iterations of the OMP algorithm correctly detect targets, the set of partially recovered targets, $\hat{\Lambda}$ satisfies $\left| \hat{\Lambda} \right| = j$ and $\hat{\Lambda} \subset \Lambda$. Furthermore,

$\mathbf{r} \in \mathrm{Col}\left(\mathbf{S}_\Lambda\right)$, since received signal noise is assumed to be negligible (3.2). Hence, from the definition of residue vector, $\bar{\mathbf{r}}$, in algorithm (2.2), $\bar{\mathbf{r}} \in \mathrm{Col}\left(\mathbf{S}_\Lambda\right)$. As a result, the condition for absolute resolution of a target scene with target parameter set Λ can be restated as

$$\sup_{\mathbf{h} \in \mathrm{Col}(\mathbf{S}_\Lambda)} \frac{\left\|\mathbf{S}_{\overline{\Lambda}}^H \mathbf{h}\right\|_\infty}{\left\|\mathbf{S}_\Lambda^H \mathbf{h}\right\|_\infty} < 1. \tag{3.10}$$

The condition in (3.10) was first proposed by Tropp [16] for sparse signal decomposition using OMP. It is commonly known as the *exact recovery condition* (ERC) of a sparse basis set Λ [15, 16]. In general, ERC is difficult to compute because of nonlinear optimization over a column space. This can, however, be overcome using the result in [16],

$$\sup_{\mathbf{h} \in \mathrm{Col}(\mathbf{S}_\Lambda)} \frac{\left\|\mathbf{S}_{\overline{\Lambda}}^H \mathbf{h}\right\|_\infty}{\left\|\mathbf{S}_\Lambda^H \mathbf{h}\right\|_\infty} = \max_{\theta \in \overline{\Lambda}} \left\|\mathbf{S}_\Lambda^\dagger \mathbf{s}_\theta\right\|_1. \tag{3.11}$$

It was also shown in [16] that an upper bound to ERC, that depends only on $|\Lambda|$, is given as

$$\mathrm{ERC} \;\leq \frac{|\Lambda|\, \mu(\mathbf{S})}{1 - (|\Lambda| - 1)\, \mu(\mathbf{S})},$$

where $\mu(\mathbf{S})$ is the mutual coherence of the radar received signal dictionary. Hence, any target scene with $|\Lambda|$ targets is guaranteed to be absolutely resolved by OMP if

$$\mu(\mathbf{S}) < \frac{1}{2\,|\Lambda| - 1}. \tag{3.12}$$

When equation (3.12) is not satisfied for a radar signal, there may exist some target scenes with $|\Lambda|$ targets which are not absolutely resolvable using the OMP algorithm. Hence, it may be useful in this case to consider the resolvability of all the target scenes of interest. The following theorem shows the condition for absolute resolvability of a target scene Λ.

Theorem 3.6.1 *Let $\Lambda = \{\theta_1, \ldots, \theta_L\}, \theta_i \in \mathcal{T}, \forall 1 \leq i \leq L$ denote the set of target parameters in an L target scene with associated amplitudes $\alpha = \{a_1, \ldots, a_L\}$, respectively. Let $\mathbf{S}$ denote the synthesis matrix of the receive signal dictionary. Then, the target scene is absolutely resolvable using OMP if*

$$\max_{\theta \in \overline{\Lambda}} \left\|\mathbf{S}_\Lambda^\dagger \mathbf{s}_\theta\right\|_1 < 1.$$

If $\max_{\theta\in\overline{\Lambda}} \left\|\mathbf{S}_{\Lambda}^{\dagger}\mathbf{s}_{\theta}\right\|_1 > 1$*, then there is at least one target amplitude vector* α*, for which OMP will not correctly detect all the targets.*

Proof From (3.11), if $\max_{\theta\in\overline{\Lambda}} \left\|\mathbf{S}_{\Lambda}^{\dagger}\mathbf{s}_{\theta}\right\|_1 < 1$, then the condition in (3.10) is satisfied. Hence a target scene with target parameter set Λ is absolutely resolvable if $\max_{\theta\in\overline{\Lambda}} \left\|\mathbf{S}_{\Lambda}^{\dagger}\mathbf{s}_{\theta}\right\|_1 < 1$.

Conversely, from (3.11), when $\max_{\theta\in\overline{\Lambda}} \left\|\mathbf{S}_{\Lambda}^{\dagger}\mathbf{s}_{\theta}\right\|_1 > 1$, there is some $\mathbf{h} \in \mathrm{Col}\left(\mathbf{S}_{\Lambda}\right)$ for which the condition in (3.10) is not satisfied. ■

The result in (3.11) is based on the inequality

$$\left\|\mathbf{S}_{\overline{\Lambda}}^{H}\mathbf{h}\right\|_{\infty} \leq \left\|\mathbf{S}_{\Lambda}^{H}\mathbf{h}\right\|_{\infty} \max_{\theta\in\overline{\Lambda}} \left\|\mathbf{S}_{\Lambda}^{\dagger}\mathbf{s}_{\theta}\right\|_1 . \tag{3.13}$$

The inequality in (3.13) is tight when

$$\left[\mathbf{S}_{\Lambda}^{H}\mathbf{h}\right]_i = \left\|\mathbf{S}_{\Lambda}^{H}\mathbf{h}\right\|_{\infty}, \forall 1 \leq i \leq |\Lambda| . \tag{3.14}$$

From section 1.1, the dual basis target amplitude vector is given as $\check{\boldsymbol{\alpha}} = \mathbf{S}_{\Lambda}^{H}\mathbf{h}$. Hence, the condition in (3.14) is satisfied when all the targets in the target scene have equal amplitudes in the dual basis, that is , $[\check{\boldsymbol{\alpha}}]_i \approx \|\check{\boldsymbol{\alpha}}\|_{\infty}$, $\forall 1 \leq i \leq |\Lambda|$. As a result, the condition in Theorem 3.6.1 for absolute resolution may be unsuitable for finding the partial resolution of a target scene containing weak targets.

Theorem 3.6.2 *Assume* $\Lambda = \{\theta_1, \ldots, \theta_L\}, \theta_i \in \mathcal{T}$, $\forall 1 \leq i \leq L$ *denotes the set of target parameters in a target scene. Let* $\{\check{\mathbf{s}}_i\}_{i\in\Lambda}$ *be the dual basis of* $\{\mathbf{s}_i\}_{i\in\Lambda}$ *in Col*$(\mathbf{S}_{\Lambda})$*, with associated synthesis matrices* $\check{\mathbf{S}}_{\Lambda}$ *and* $\mathbf{S}_{\Lambda}$ *respectively. Furthermore, suppose the residue vector in the* j^{th} *iteration of the OMP algorithm is given as* $\bar{\mathbf{r}} = \mathbf{S}_{\Lambda}\alpha = \check{\mathbf{S}}_{\Lambda}\check{\alpha}$*. Then, the OMP correctly selects a target in* Λ *in the* j^{th} *iteration if*

$$\max_{\theta\in\overline{\Lambda}} \left\|\mathbf{D}\mathbf{S}_{\Lambda}^{\dagger}\mathbf{s}_{\theta}\right\|_1 < 1,$$

where $\mathbf{D}$ *is a diagonal matrix with* $[\mathbf{D}]_{i,i} = \left|[\check{\alpha}]_i\right| / \max_k \left|[\check{\alpha}]_k\right|$.

Proof The OMP algorithm correctly selects a target in an iteration when (3.8) is satisfied. It can be restated as

$$\frac{\max_{q\in\overline{\Lambda}} |\langle \bar{\mathbf{r}}, \mathbf{s}_q \rangle|}{\max_{p\in\Lambda} |\langle \bar{\mathbf{r}}, \mathbf{s}_p \rangle|} < 1.$$

Since $\bar{\mathbf{r}} \in \mathrm{Col}\,(\mathbf{S}_\Lambda)$,

$$\begin{aligned} \frac{\max_{q\in\overline{\Lambda}} |\langle \bar{\mathbf{r}}, \mathbf{s}_q \rangle|}{\max_{p\in\Lambda} |\langle \bar{\mathbf{r}}, \mathbf{s}_p \rangle|} &= \frac{\max_{q\in\overline{\Lambda}} \left|\left\langle \mathbf{S}_\Lambda^H \bar{\mathbf{r}}, \mathbf{S}_\Lambda^\dagger \mathbf{s}_q \right\rangle\right|}{\max_{p\in\Lambda} |\langle \bar{\mathbf{r}}, \mathbf{s}_p \rangle|} \\ &= \frac{\max_{q\in\overline{\Lambda}} \left|\left\langle \breve{\alpha}, \mathbf{S}_\Lambda^\dagger \mathbf{s}_q \right\rangle\right|}{\max_i |[\breve{\alpha}]_i|} \\ &\leq \max_{q\in\overline{\Lambda}} \left\|\mathbf{D}\mathbf{S}_\Lambda^\dagger \mathbf{s}_q\right\|_1 . \end{aligned}$$

Hence, the selected target in this iteration belongs to Λ if $\max_{q\in\overline{\Lambda}} \left\|\mathbf{D}\mathbf{S}_\Lambda^\dagger \mathbf{s}_q\right\|_1 < 1$. ■

Observation 3.6.1 *Let* $\check{\mathbf{S}}_\Lambda$ *represent the synthesis matrix of the dual basis of the radar signal sub-dictionary for a target parameter set* Λ. *In some iteration of the OMP algorithm, let* $\bar{\mathbf{r}}_1 = \check{\mathbf{S}}_\Lambda \breve{\alpha}_1$ *and* $\bar{\mathbf{r}}_2 = \check{\mathbf{S}}_\Lambda \breve{\alpha}_2$ *be two possible residue vectors with the constraint* $\arg\max_i |[\breve{\alpha}_1]_i| = \arg\max_i |[\breve{\alpha}_2]_i|$. *Assume* $|\breve{\alpha}_1| / \max_i |[\breve{\alpha}_1]_i| = \left[a_1, \ldots, a_{|\Lambda|}\right], 0 \leq a_i \leq 1 \forall i \in \{1, 2, \ldots, |\Lambda|\}$ *and* $|\breve{\alpha}_2| / \max_i |[\breve{\alpha}_2]_i| = \left[b_1, \ldots, b_{|\Lambda|}\right], 0 \leq b_i \leq a_i \; \forall i \in \{1, 2, \ldots, |\Lambda|\}$. *If OMP algorithm correctly selects a target in* Λ *in this iteration from* $\bar{\mathbf{r}}_1$, *then the target selected from* $\bar{\mathbf{r}}_2$ *will also be from* Λ.

Proof Define diagonal matrices $\mathbf{D}_1$ and $\mathbf{D}_2$ with diagonal values $[\mathbf{D}_1]_{i,i} = |\breve{\alpha}_1| / \max_i |[\breve{\alpha}_1]_i|$ and $[\mathbf{D}_2]_{i,i} = |\breve{\alpha}_2| / \max_i |[\breve{\alpha}_2]_i|$. Then, because of the constraints on $\breve{\alpha}_1$ and $\breve{\alpha}_2$,

$$\max_{\theta\in\overline{\Lambda}} \left\|\mathbf{D}_2\mathbf{S}_\Lambda^\dagger \mathbf{s}_\theta\right\|_1 \leq \max_{\theta\in\overline{\Lambda}} \left\|\mathbf{D}_1\mathbf{S}_\Lambda^\dagger \mathbf{s}_\theta\right\|_1 .$$

Hence, if $\max_{\theta\in\overline{\Lambda}} \left\|\mathbf{D}_1\mathbf{S}_\Lambda^\dagger \mathbf{s}_\theta\right\|_1 < 1$, then $\max_{\theta\in\overline{\Lambda}} \left\|\mathbf{D}_2\mathbf{S}_\Lambda^\dagger \mathbf{s}_\theta\right\|_1 < 1$. ■

This corollary shows an important difference in weak target resolution between matched filter and the OMP algorithm. In a matched filter receiver, weak targets can be difficult to differentiate from the sidelobes caused by the strong target. Hence, if the matched filter can resolve two strong targets at θ_1 and θ_2, it does not guarantee resolvability of a target scene with a strong target and weak target at θ_1 and θ_2 respectively. On the contrary, in any iteration, the greedy target selection step in OMP algorithm performs better if the residue also contains weak targets. For example, for the target scene $\Lambda = \{0, 6T\}$, shown in Figure 2.1, $\max_{\theta \in \overline{\Lambda}} \left\| S_\Lambda^\dagger s_\theta \right\|_1 = 0.5$. Hence, Λ is absolutely resolvable using the OMP algorithm.

3.6.1 Resolution of two targets

As mentioned in section 3.4, the resolution of two target scenes is of particular interest in this paper. This is due to the simple resolution metric that can be defined for comparing radar algorithms and signals. Two such metrics were proposed in equations (**??**) and (**??**). Furthermore, in section 3.6.2, it will be shown that the resolution of two target scenes can also be visualized using *resolution plots.* A condition for resolution of a target scene comprising of a weak target and a strong target is now presented based on Theorem 3.6.2.

Theorem 3.6.3 *Suppose the OMP algorithm is used to recover a two target target scene from the received signal* $\mathbf{r} = \breve{\alpha}_1 \breve{\mathbf{s}}_{\theta_1} + \breve{\alpha}_2 \breve{\mathbf{s}}_{\theta_2}$, *where* $\{\breve{\mathbf{s}}_{\theta_1}, \breve{\mathbf{s}}_{\theta_2}\}$ *is the dual basis of* $\{\mathbf{s}_{\theta_1}, \mathbf{s}_{\theta_2}\}$ *and* $|\breve{\alpha}_1| > |\breve{\alpha}_2|$. *Furthermore, assume it is known that* $|\breve{\alpha}_2| / |\breve{\alpha}_1| \leq \rho$. *Denoting the target parameter set as* $\Lambda = \{\theta_1, \theta_2\}$, *the target scene is partially resolvable if* $\left\| \mathbf{S}_{\overline{\Lambda}}^H \breve{\mathbf{s}}_{\theta_2} \right\|_\infty < 1$ *and*

$$\max_{\theta \in \overline{\Lambda}} \left\| \begin{bmatrix} 1 & 0 \\ 0 & \rho \end{bmatrix} \mathbf{S}_\Lambda^\dagger \mathbf{s}_\theta \right\|_1 < 1.$$

Proof From Theorem 3.6.2, the first iteration of OMP algorithm will select a target in Λ if $\max_{\theta \in \overline{\Lambda}} \left\| \begin{bmatrix} 1 & 0 \\ 0 & \rho \end{bmatrix} \mathbf{S}_\Lambda^\dagger \mathbf{s}_\theta \right\|_1 < 1$. Furthermore, since $\left| \mathbf{s}_{\theta_1}^H \mathbf{r} \right| = |\breve{\alpha}_1| > \left| \mathbf{s}_{\theta_2}^H \mathbf{r} \right|$, the target selected in the first iteration is θ_1. In the second iteration, the test for resolvability in Theorem 3.6.2 becomes $\max_{\theta \in \overline{\Lambda}} \left\| \breve{\mathbf{s}}_{\theta_2}^H \mathbf{s}_\theta \right\|_1 < 1$, which is equivalent to $\left\| \mathbf{S}_{\overline{\Lambda}}^H \breve{\mathbf{s}}_{\theta_2} \right\|_\infty < 1$. ∎

Theorems 3.6.1 and 3.6.2 provide conditions for resolvability of target scenes with known target parameter set Λ. In section (3.4), a generalized resolution measure (3.7) was proposed to compare resolution performance of different algorithms independent of the target scene. In a target scene with two targets, however, the resolution performance of a radar system can be visualized graphically. For example, a useful tool for resolution analysis of two targets in a pulse-Doppler radar is the *resolution plot*. In these plots for pulse-Doppler radar, one target is fixed at $\tau/T = 0$ and $\nu T = 0$ and the second target is moved. A binary color scheme can then be used to differentiate the resolvable and non-resolvable range Doppler bins. In this dissertation, white color will be used to show the position of the second target for which the target scene is not absolutely resolvable and black color will signify resolvable bins.

3.6.2 Simulation results

Barker codes were introduced in Chapter 1. It was mentioned there that the longest known binary Barker code is length 13 with phase code

$$\{b_m^{13}\} = \{1, 1, 1, 1, 1, -1, -1, 1, 1, -1, 1, -1, 1\}.$$

Figure 3.6 shows the ambiguity function and the resolution diagram of the length 13 barker sequence when matched filters and OMP algorithm are used at the receiver.

Since long Barker codes do not exist, in section 1.5 it was shown that longer codes can be obtained by combining known Barker codes. In particular, a length 52 extended barker code was shown in equation (1.36).

Figure 3.8a shows the ambiguity function of a chirp which was defined in equation (1.37). It can be seen that most of the volume of the ambiguity function is concentrated on a ridge. Intuitively, it should be expected that the radar would have difficulty in resolving multiple targets on the same ridge. This is evident in the resolution diagram for this signal in figure 3.8b obtained when matched filter is used at the receiver. The resolution diagram and the ambiguity function show that the LFM is suitable for resolving targets in the same range with different Doppler or vice versa.

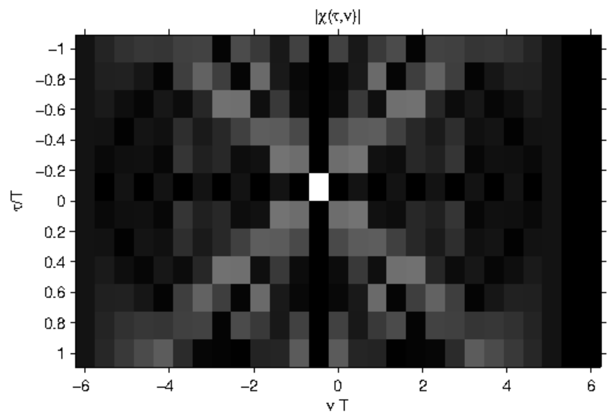

(a) Ambiguity function of a length 13 barker sequence

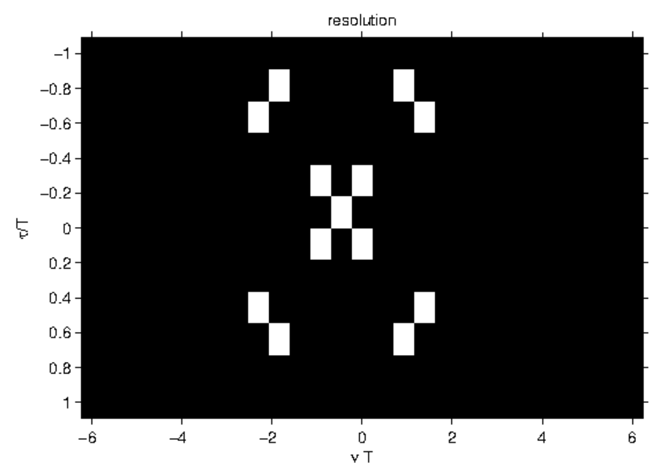

(b) Resolution of a length 13 barker sequence with matched filter receiver

Figure 3.6.: Ambiguity function and resolution diagram of length 13 barker sequence

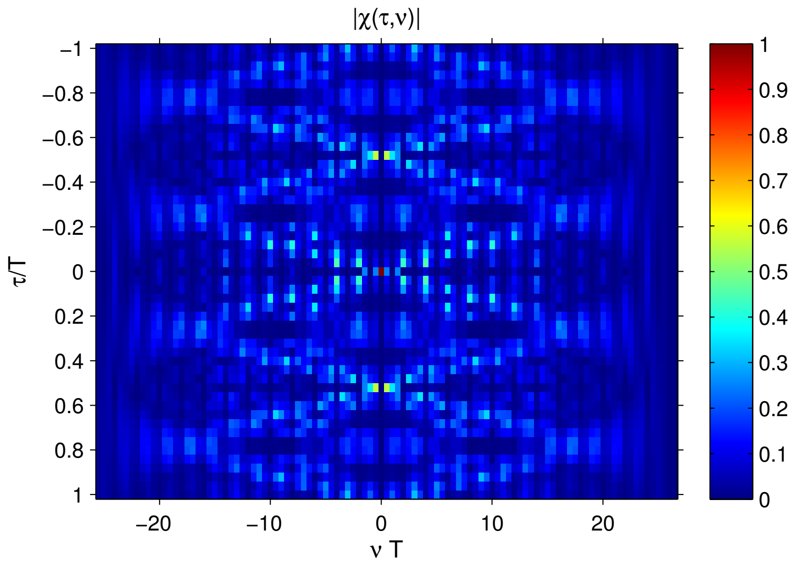

(a) Ambiguity function.

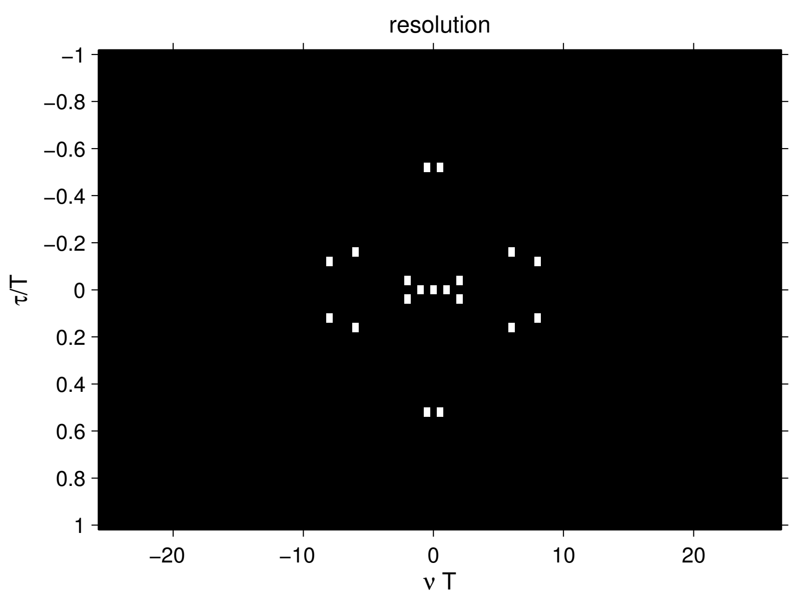

(b) Resolution plot.

Figure 3.7.: Resolution plot of extended barker code defined in (1.36).

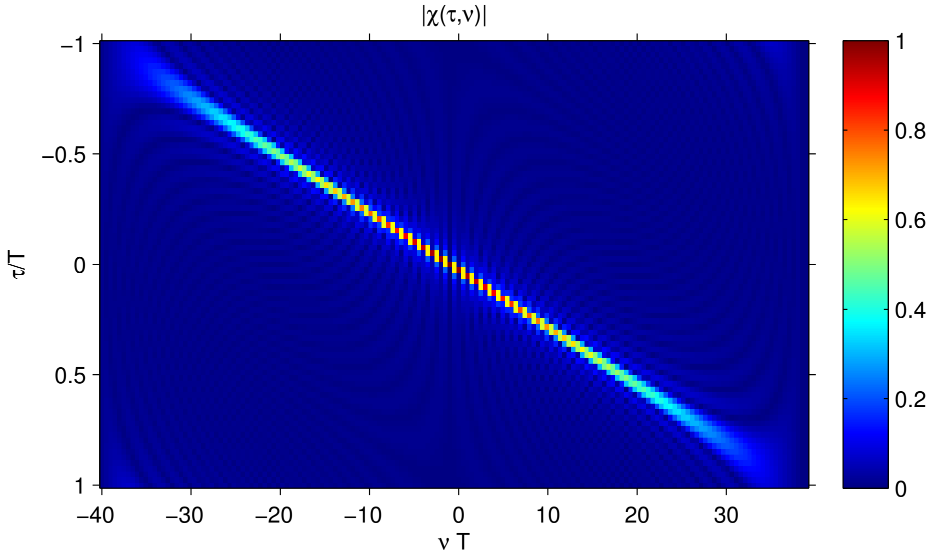

(a) Normalized ambiguity function of LFM chirp with $BT = 40$

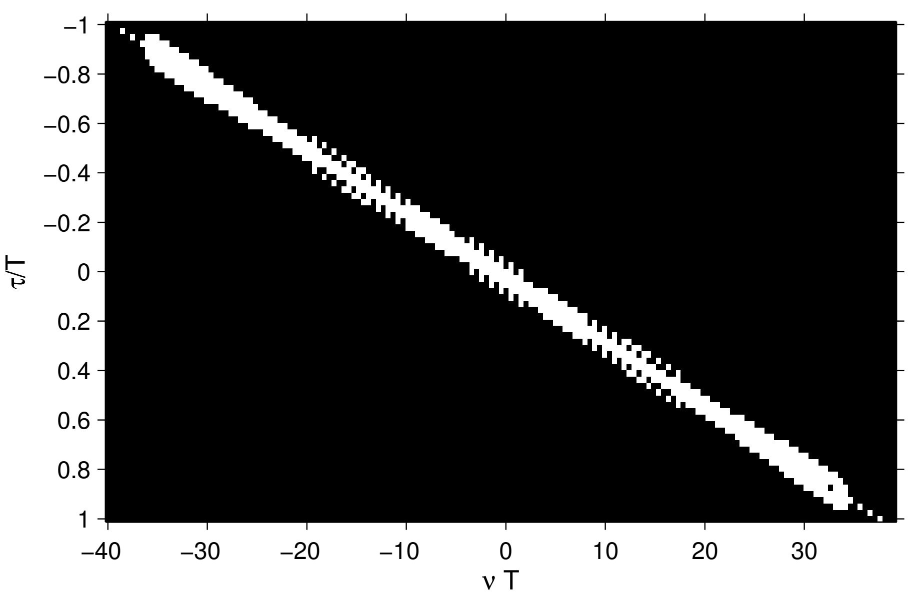

(b) Resolution of LFM chirp with $BT = 40$. All delay-Doppler bins in black are resolvable

Figure 3.8.: Ambiguity function and the resolution diagram of an LFM chirp

It is important to note that the condition for resolution in Theorem 3.6.1 is necessary for absolute resolution of the target scene. Hence, even when the condition in Theorem 3.6.1 is not satisfied, it may still be possible to recover the target scene for some target amplitudes. Figure 3.9 shows a target scene with 7 targets. All targets are assumed to have the same amplitude and phase. The recovery condition, $\max_{\theta \in \overline{\Lambda}} \left\| \mathbf{S}_{\Lambda}^{\dagger} \mathbf{s}_{\theta} \right\|_1 = 2.99$ for this particular target scene. Assuming the combined barker code as the radar transmit signal, the matched filter output after applying a threshold of 0.1 is shown in Figure 3.10a. The output of the OMP algorithm is shown in Figure 3.10b. It can be seen that the OMP exactly recovers the target scene even though it is not absolutely resolvable using the OMP algorithm.

In section 2.2 it was mentioned that the threshold selection in a matched filter receiver is a trade-off between the ability to resolve weak targets and false alarm. The ability of OMP algorithm to overcome this limitation of the matched filter is shown in Figure 3.11 for two different target scenes. In Figure 3.11, for each SNR, the threshold was selected using the result in equation (2.22) for a probability of false alarm of 10^{-4}. As a result, the value of the detection threshold decreases as SNR is increased. This results in decreased probability of resolution of the matched filter output because of the false alarms caused by the sidelobes. Furthermore, since the recovery condition of the target scene is indicative of the peak sidelobe to mainlobe ratio, Figure 3.11 shows that a target scene with a higher value of ERC is liable to be unresolvable at a lower SNR.

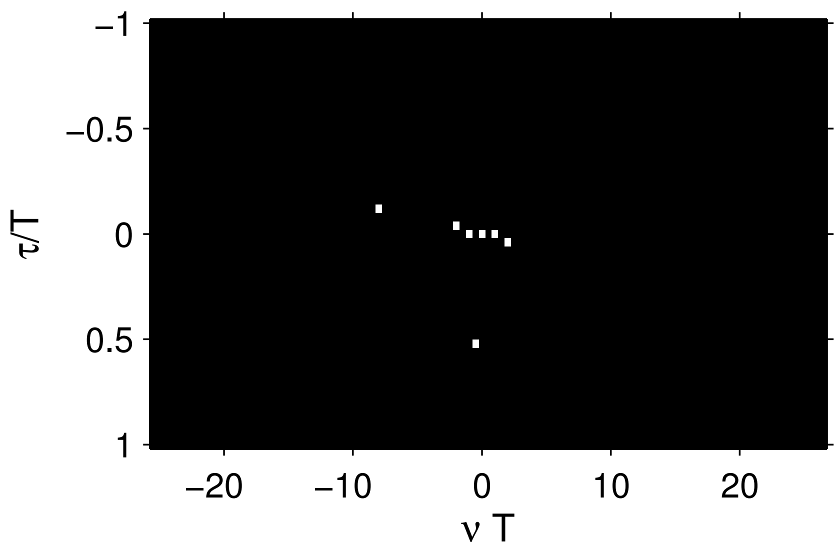

Figure 3.9.: Target scene with $\max_{\theta \in \overline{\Lambda}} \left\| \mathbf{S}_{\Lambda}^{\dagger} \mathbf{s}_{\theta} \right\|_1 = 2.99$.

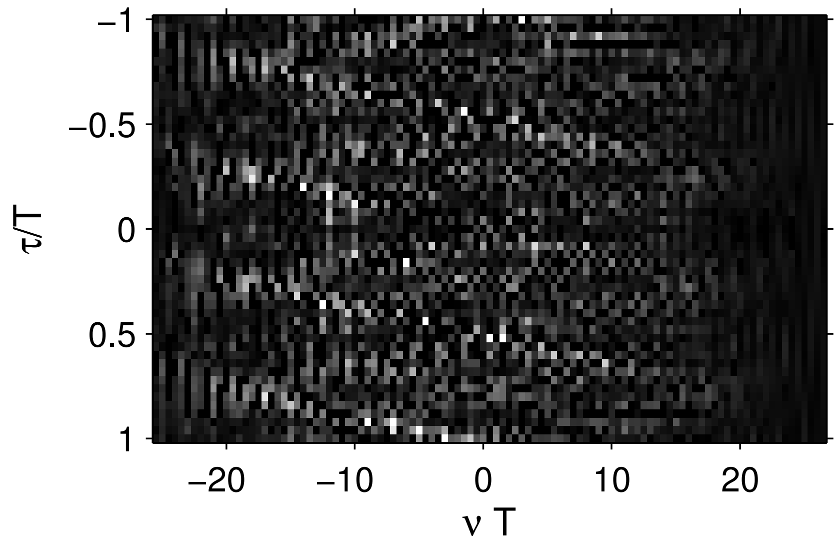

(a) Normalized matched filter output with a threshold of 0.1.

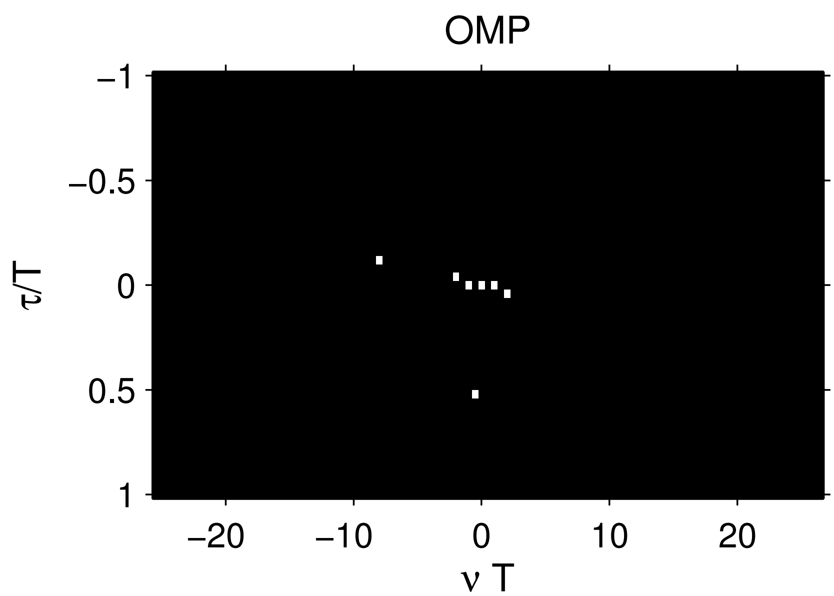

(b) Target scene recovered using OMP algorithm.

Figure 3.10.: Estimation of target scene in (3.9) with a radar using the combined barker sequence. Matched filter output is shown in (3.10a) and OMP output is shown in figure (3.10b).

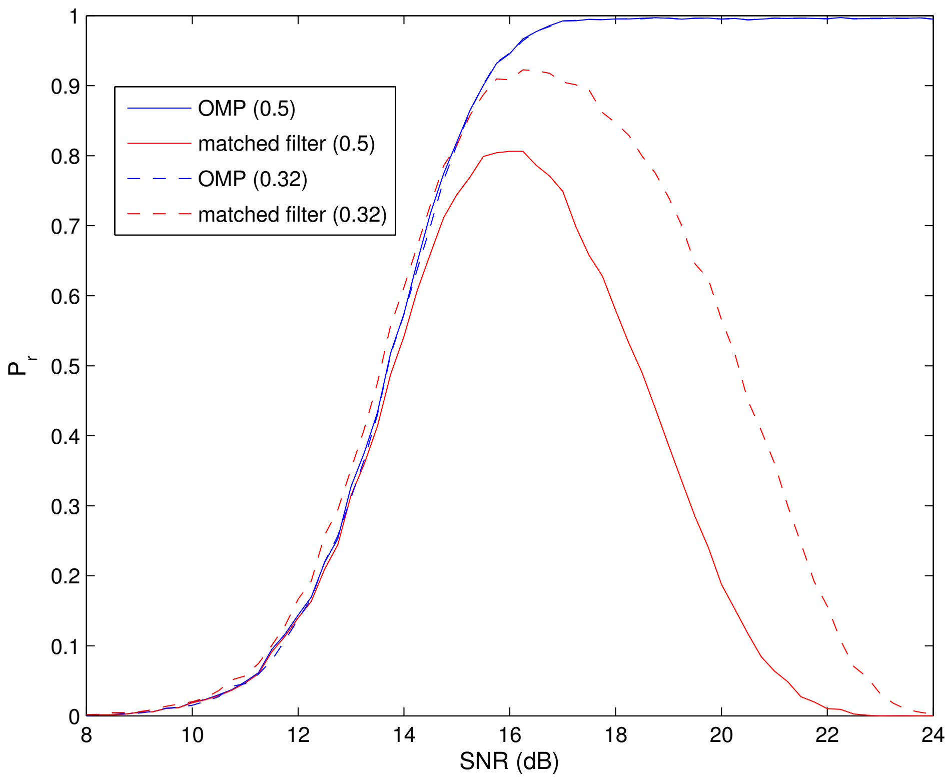

Figure 3.11.: Probability of resolution of Matched filter and OMP for two different target scenes: ERC $= 0.5$ and ERC $= 0.32$. Probability of false alarm was set at 10^{-4}.

4. PURSUIT USING MISMATCHED DICTIONARIES

The key to resolution performance of the OMP algorithm is the greedy hypothesis test (2.17) in every iteration. Since $\bar{\mathbf{r}} \in \mathrm{Col}\left(\mathbf{S}_\Lambda\right)$, the greedy hypothesis test in equation (2.17) can be written as

$$\max_{\theta} \left|\mathbf{s}_\theta^H \mathbf{h}\right| \underset{\mathcal{H}_0}{\overset{\mathcal{H}_1}{\gtrless}} \gamma, \tag{4.1}$$

where $\mathbf{h} \in \mathrm{Col}\left(\mathbf{S}_\Lambda\right)$. The hypothesis test in equation (4.1) has the same form as the matched filter test for one target shown in equation (2.7). Hence, the resolution of the OMP algorithm might be expected to be closely related to the resolution of matched filter. Suppose $\mathbf{h} = \mathbf{S}\mathbf{x}$ where $\mathbf{x} \in \mathbb{C}^N$ is a sparse target amplitude vector such that $\forall i \notin \Lambda$, $[\mathbf{x}]_i = 0$. The OMP algorithm can absolutely resolve the target scene if,

$$\hat{\theta} = \arg\max_{\theta} \left|\mathbf{s}_\theta^H \mathbf{S}\mathbf{x}\right| \in \Lambda.$$

Thus a target scene is resolvable using OMP if the application of one target matched filter test always selects a target in Λ. If the signal dictionary is perfectly incoherent, that is, $\mathbf{S}^H\mathbf{S} = \mathbf{I}$, correct selection of target is guaranteed. Hence, all target scenes are absolutely resolvable if the signal dictionary is incoherent. In section 1.2 it was shown that the signal dictionaries satisfy a structure that depends on the type of radar. Because of this structure and other practical considerations, it is usually hard to design a radar signal with incoherent dictionaries. Mismatched filters have been proposed to achieve this incoherence while trading off performance in noise. In mismatched linear filters, a receive signal dictionary with synthesis matrix $\tilde{\mathbf{S}}$ is designed such that $\tilde{\mathbf{S}}^{\mathbf{H}}\mathbf{S} \approx \mathbf{I}$. In this dissertation, we will focus on mismatch filters which reduce the *mismatched mutual coherence*, $\mu(S, \tilde{S})$, defined as

$$\mu(S, \tilde{S}) = \sup_{m \neq n} \left|\langle s_m, \tilde{s}_n \rangle\right| \quad m, n \in \{1, 2, \ldots, P\} \tag{4.2}$$

where $\tilde{\mathbf{s}}_k \in \tilde{S}$, $k \in \{1, 2, \ldots, P\}$ are the atoms belonging to the mismatched dictionary $\tilde{S}$. Here, we assume $\tilde{S}$ satisfies the following two conditions

$$\begin{aligned} \langle \mathbf{s}_k, \tilde{\mathbf{s}}_k \rangle &= 1,\ k \in \{1, 2, \ldots, P\} \\ \tilde{\mathbf{S}}_I^H \mathbf{S}_I &> 0,\ \forall I \subset \{1, 2, \ldots, P\}, |I| \le N \\ \mu(S, \tilde{S}) &< \mu(S). \end{aligned} \tag{4.3}$$

We start by looking at the use of mismatched dictionaries in non redundant dictionaries in section 4.1. The algorithms and results in this section hold for all dictionaries not constrained by the uncertainty principle. In addition, an iterative algorithm for designing mismatched dictionaries is also introduced. In section 4.2, we extend the mismatched pursuit algorithm to redundant dictionaries with uncertainty constraints. In particular, we propose a subspace mismatching pursuit algorithm to improve the resolution performance of the standard pursuit algorithms.

4.1 Nonredundant dictionaries

The key to resolution performance of the OMP algorithm is the greedy hypothesis test (2.17) in every iteration. Since $\bar{\mathbf{r}} \in \mathrm{Col}\,(\mathbf{S}_\Lambda)$, the greedy hypothesis test in (2.17) can be written as

$$\max_\theta \left| \mathbf{s}_\theta^H \mathbf{h} \right| \underset{\mathcal{H}_0}{\overset{\mathcal{H}_1}{\gtrless}} \gamma, \tag{4.4}$$

where $\mathbf{h} \in \mathrm{Col}\,(\mathbf{S}_\Lambda)$. The hypothesis test in (4.4) has the same form as the matched filter test for one target (2.7). Hence, the resolution of the OMP algorithm might be expected to be closely related to the resolution of matched filter. Suppose $\mathbf{h} = \mathbf{S}\mathbf{x}$ where $\mathbf{x} \in \mathbb{C}^N$ is a sparse target amplitude vector such that $\forall i \notin \Lambda$, $[\mathbf{x}]_i = 0$. The OMP algorithm can absolutely resolve the target scene if,

$$\hat{\theta} = \arg\max_\theta \left| \mathbf{s}_\theta^H \mathbf{S}\mathbf{x} \right| \in \Lambda.$$

Thus a target scene is resolvable using OMP if the application of one target matched filter test always selects a target in Λ. If the signal dictionary is perfectly incoherent, that is, $\mathbf{S}^H\mathbf{S} = \mathbf{I}$, correct selection of target is guaranteed. Hence, all target scenes are absolutely resolvable if the signal dictionary is incoherent. In section 1.2 it was shown that the signal dictionaries satisfy a structure that depends on the type of radar. Because of this structure and other practical considerations, it is usually hard to design a radar signal with incoherent dictionaries.

Mismatched filters have been proposed to achieve dictionary incoherence while trading off performance in noise. In mismatched linear filters, a receive signal dictionary with synthesis matrix $\tilde{\mathbf{S}}$ is designed such that $\tilde{\mathbf{S}}^{\mathbf{H}}\mathbf{S} \approx \mathbf{I}$. Algorithm 4.1 shows a modified OMP algorithm in which the greedy target selection is done using a mismatched receive dictionary. The atoms in the mismatched dictionary are denoted $\tilde{s}_\theta$. For rest of the paper, algorithm 4.1 will be called *mismatched* OMP (MOMP) algorithm. A similar algorithm called oblique matching pursuit has been proposed before in [30, 31]. However, oblique matching pursuit differs from algorithm 4.1 in two key ways. Firstly, unlike oblique matching pursuit, the mismatched dictionary is only used during the greedy selection step and not during the projection step to compute the residue vector. This makes the resolution analysis of MOMP in terms of Tropp's exact recovery condition [16] relatively simple. Secondly, in every iteration, the MOMP algorithm uses matched filter output to decide if another target is present or not. The advantage of this will be studied in section 4.1.2.

4.1.1 Pursuit Recovery

Consider a radar system with transmit signal dictionary $\mathbf{S}$ and receive filter dictionary $\tilde{\mathbf{S}}$. Let $\Lambda = \{\theta_1, \ldots, \theta_L\}, \theta_i \in \mathcal{T}, \forall 1 \le i \le L$ represent the target parameters of a target scene. Similar to the development in section 3.6, the MOMP algorithm correctly recovers the target set if, in every iteration

$$\frac{\left\|\tilde{\mathbf{S}}_{\bar{\Lambda}}^H \bar{\mathbf{r}}\right\|_\infty}{\left\|\tilde{\mathbf{S}}_{\Lambda}^H \bar{\mathbf{r}}\right\|_\infty} < 1.$$

Algorithm 4.1 Mismatching pursuit solution for signal decomposition of $r = \sum_k a_k s_k + n$

- Initialize $\hat{\Lambda} = \emptyset$, $\bar{r} = r$, γ
- $\sigma = \max_\theta \left| s_\theta^H r \right|$
- while $\sigma > \gamma$
  - $\hat{\theta} = \arg\max_{\theta \notin \hat{\Lambda}} \left| \tilde{s}_\theta^H \bar{r} \right|$
  - $\hat{\Lambda} = \hat{\Lambda} \cup \hat{\theta}$
  - $\hat{\alpha} = \arg\min_\alpha \left\| r - S_{\hat{\Lambda}} \alpha \right\|^2$
  - $\bar{r} = r - S_{\hat{\Lambda}} \hat{\alpha}$
  - $\sigma = \max_\theta \left| s_\theta^H \bar{r} \right|$

Once again, the definition of residue signal, $\bar{\mathbf{r}}$, in algorithm 4.1 ensures that $\bar{\mathbf{r}} \in \mathrm{Col}\left(\mathbf{S}_\Lambda\right)$. Hence, in general, the target scene with parameter set Λ is resolvable if

$$\sup_{h \in \Gamma} \frac{\left\|\tilde{\mathbf{S}}_{\overline{\Lambda}}^H \mathbf{h}\right\|_\infty}{\left\|\tilde{\mathbf{S}}_{\Lambda}^H \mathbf{h}\right\|_\infty} < 1, \tag{4.5}$$

where $\Gamma = \mathrm{Col}\left(\mathbf{S}_\Lambda\right)$ for absolute resolution and $\Gamma = \mathcal{H}$ for weak target resolution. The set $\mathcal{H}$ was previously defined in (3.3).

Theorem 4.1.1 *Let $\Lambda = \{\theta_1, \ldots, \theta_L\}, \theta_i \in \mathcal{T}, \forall 1 \leq i \leq L$ denote the set of target parameters in an L target scene with associated target amplitudes $\alpha = \{a_1, \ldots, a_L\}$, respectively. Let $\mathbf{S}$ denote the synthesis matrix of the receive signal dictionary and $\tilde{\mathbf{S}}$ represent the synthesis matrix of the receive filter dictionary. Then, the target scene is absolutely resolvable using MOMP if*

$$\max_{\theta \in \overline{\Lambda}} \left\| \left(\mathbf{S}_\Lambda^H \tilde{\mathbf{S}}_\Lambda\right)^{-1} \mathbf{S}_\Lambda^H \tilde{\mathbf{s}}_\theta \right\|_1 < 1.$$

If $\max_{\theta \in \overline{\Lambda}} \left\| \left(\mathbf{S}_\Lambda^H \tilde{\mathbf{S}}_\Lambda\right)^{-1} \mathbf{S}_\Lambda^H \tilde{\mathbf{s}}_\theta \right\|_1 > 1$, then there is at least one target amplitude vector α, for which MOMP will not correctly detect all the targets.

Proof Using definition of matrix norm, the numerator in (4.5) can be simplified as

$$\begin{aligned}
\left\|\tilde{\mathbf{S}}_{\overline{\Lambda}}^H \mathbf{h}\right\|_\infty &= \max_{q \in \overline{\Lambda}} \left|\langle \mathbf{h}, \tilde{\mathbf{s}}_q \rangle\right| = \max_{q \in \overline{\Lambda}} \left|\langle \mathbf{S}_\Lambda \alpha, \tilde{\mathbf{s}}_q \rangle\right| \\
&= \max_{q \in \overline{\Lambda}} \left| \left\langle \mathbf{S}_\Lambda \left(\tilde{\mathbf{S}}_\Lambda^H \mathbf{S}_\Lambda\right)^{-1} \tilde{\mathbf{S}}_\Lambda^H \mathbf{S}_\Lambda \alpha, \tilde{\mathbf{s}}_q \right\rangle \right| \\
&= \max_{q \in \overline{\Lambda}} \left| \left\langle \tilde{\mathbf{S}}_\Lambda^H \mathbf{S}_\Lambda \alpha, \left(\mathbf{S}_\Lambda^H \tilde{\mathbf{S}}_\Lambda\right)^{-1} \mathbf{S}_\Lambda^H \tilde{\mathbf{s}}_q \right\rangle \right| \\
&\leq \left\|\tilde{\mathbf{S}}_\Lambda^H \mathbf{S}_\Lambda \alpha\right\|_\infty \max_{q \in \overline{\Lambda}} \left\| \left(\mathbf{S}_\Lambda^H \tilde{\mathbf{S}}_\Lambda\right)^{-1} \mathbf{S}_\Lambda^H \tilde{\mathbf{s}}_q \right\|_1,
\end{aligned} \tag{4.6}$$

where $\mathbf{S}_\Lambda^H \tilde{\mathbf{S}}_\Lambda$ is invertible because of the assumptions in (4.3). Since $\mathbf{h} = \mathbf{S}_\Lambda \alpha$, using (4.6) in (4.5) yields

$$\sup_{h \in \Gamma} \frac{\left\|\tilde{\mathbf{S}}_{\overline{\Lambda}}^H \mathbf{h}\right\|_\infty}{\left\|\tilde{\mathbf{S}}_{\Lambda}^H \mathbf{h}\right\|_\infty} \leq \max_{q \in \overline{\Lambda}} \left\| \left(\mathbf{S}_\Lambda^H \tilde{\mathbf{S}}_\Lambda\right)^{-1} \mathbf{S}_\Lambda^H \tilde{\mathbf{s}}_q \right\|_1.$$

Let $q^* = \arg\max_{q\in\overline{\Lambda}} \left\| \left(\mathbf{S}_\Lambda^H \tilde{\mathbf{S}}_\Lambda\right)^{-1} \mathbf{S}_\Lambda^H \tilde{\mathbf{s}}_q \right\|_1$. Denote $\mathbf{G}_\Lambda = \mathbf{S}_\Lambda \left(\tilde{\mathbf{S}}_\Lambda^H \mathbf{S}_\Lambda\right)^{-1}$, and the i^{th} column of $\mathbf{G}_\Lambda$ as $\mathbf{g}_i$. Then equality is achieved if $\mathbf{h} = \sum_{i=1}^{|\Lambda|} \operatorname{sgn}\left(\langle \mathbf{g}_i, \mathbf{s}_{q^*}\rangle\right) \mathbf{g}_i$, where sgn represents the complex signum function, $\max_{q\in\overline{\Lambda}} \left\| \left(\mathbf{S}_\Lambda^H \tilde{\mathbf{S}}_\Lambda\right)^{-1} \mathbf{S}_\Lambda^H \tilde{\mathbf{s}}_q \right\|_1 = |\langle \mathbf{h}, \mathbf{s}_{q^*}\rangle|$. Hence, $\sup_{\mathbf{h}\in\Gamma} \frac{\left\|\tilde{\mathbf{S}}_{\overline{\Lambda}}^H \mathbf{h}\right\|_\infty}{\left\|\tilde{\mathbf{S}}_\Lambda^H \mathbf{h}\right\|_\infty} = \max_{q\in\overline{\Lambda}} \left\| \left(\mathbf{S}_\Lambda^H \tilde{\mathbf{S}}_\Lambda\right)^{-1} \mathbf{S}_\Lambda^H \tilde{\mathbf{s}}_q \right\|_1$. ■

For target scenes containing weak targets, a tighter condition for resolution similar to Theorem 3.6.2 can be obtained. The following theorem presents this condition.

Theorem 4.1.2 *Assume $\Lambda = \{\theta_1, \ldots, \theta_L\}, \theta_i \in \mathcal{T}$, $\forall 1 \le i \le L$ denotes the set of target parameters in a target scene. Suppose the residue vector in the j^{th} iteration of the MOMP algorithm is given as $\bar{r} = S_\Lambda \alpha$. Let $\check{\boldsymbol{\alpha}}_\Lambda = \left|\tilde{\mathbf{S}}_\Lambda^H \bar{\mathbf{r}}\right|$ denote the receive filter output corresponding to the target parameters. Then, the MOMP correctly selects a target in Λ in the j^{th} iteration if*

$$\max_{\theta\in\overline{\Lambda}} \left\| \mathbf{D} \left(\mathbf{S}_\Lambda^H \tilde{\mathbf{S}}_\Lambda\right)^{-1} \mathbf{S}_\Lambda^H \tilde{\mathbf{s}}_\theta \right\|_1 < 1,$$

where $\mathbf{D}$ is a diagonal matrix with $[\mathbf{D}]_{i,i} = |[\check{\boldsymbol{\alpha}}_\Lambda]_i| / \max_k |[\check{\boldsymbol{\alpha}}_\Lambda]_k|$.

Proof The proof of this theorem is very similar to that of Theorem 3.6.2. The MOMP algorithm correctly selects a target in an iteration when (4.5) is satisfied. Since $\bar{\mathbf{r}} \in \operatorname{Col}(\mathbf{S}_\Lambda)$,

$$\begin{aligned}
\frac{\max_{q\in\overline{\Lambda}} |\langle \bar{\mathbf{r}}, \tilde{\mathbf{s}}_q\rangle|}{\max_{p\in\Lambda} |\langle \bar{\mathbf{r}}, \tilde{\mathbf{s}}_p\rangle|} &= \frac{\max_{q\in\overline{\Lambda}} \left| \left\langle \tilde{\mathbf{S}}_\Lambda^H \mathbf{S}_\Lambda \alpha, \left(\mathbf{S}_\Lambda^H \tilde{\mathbf{S}}_\Lambda\right)^{-1} \mathbf{S}_\Lambda^H \tilde{\mathbf{s}}_q \right\rangle \right|}{\max_{p\in\Lambda} |\langle \bar{\mathbf{r}}, \tilde{\mathbf{s}}_p\rangle|} \\
&= \frac{\max_{q\in\overline{\Lambda}} \left| \left\langle \check{\alpha}_\Lambda, \left(\mathbf{S}_\Lambda^H \tilde{\mathbf{S}}_\Lambda\right)^{-1} \mathbf{S}_\Lambda^H \tilde{\mathbf{s}}_q \right\rangle \right|}{\max_i |[\check{\alpha}_\Lambda]_i|} \\
&\le \max_{q\in\overline{\Lambda}} \left\| \mathbf{D} \left(\mathbf{S}_\Lambda^H \tilde{\mathbf{S}}_\Lambda\right)^{-1} \mathbf{S}_\Lambda^H \tilde{\mathbf{s}}_q \right\|_1 .
\end{aligned}$$

Hence, the selected target in this iteration belongs to Λ if $\max_{q\in\overline{\Lambda}} \left\| \mathbf{D} \left(\mathbf{S}_\Lambda^H \tilde{\mathbf{S}}_\Lambda\right)^{-1} \mathbf{S}_\Lambda^H \tilde{\mathbf{s}}_q \right\|_1 < 1$. ■

Theorems 4.1.1 and 4.1.2 are useful for checking the resolvability of target scenes with known target locations. However, for radar waveform and filter design, it is more useful to have a resolution condition independent of the target location. For OMP algorithm, such a condition (1.4) was presented by Tropp [16] in terms of mutual coherence of the receive signal dictionary. An equivalent condition in terms of the mismatched mutual coherence defined in (4.2) is presented in the following theorem.

Theorem 4.1.3 *Consider a radar system with received signal dictionary S and receiver filter dictionary $\tilde{S}$. Let $\mathbf{S}$ and $\tilde{\mathbf{S}}$ denote the synthesis matrices of the two dictionaries. Then, any target scene with $|\Lambda|$ targets is absolutely resolvable using MOMP algorithm if*

$$\frac{|\Lambda|\,\mu(S,\tilde{S})}{1-(|\Lambda|-1)\,\mu\left(S,\tilde{S}\right)}<1.$$

Proof In equation (4.5), since $\mathbf{h}\in \mathrm{Col}\left(\mathbf{S}_\Lambda\right)$, the recovery condition can be rewritten as

$$\sup_{\alpha\in\mathbb{C}^{|\Lambda|}}\frac{\left\|\tilde{\mathbf{S}}_{\overline{\Lambda}}^H\mathbf{S}_\Lambda\alpha\right\|_\infty}{\left\|\tilde{\mathbf{S}}_{\Lambda}^H\mathbf{S}_\Lambda\alpha\right\|_\infty}<1.$$

For any $\alpha\in\mathbb{C}^{|\Lambda|}$, the numerator in the recovery condition can be bounded as

$$\begin{aligned}\left\|\tilde{\mathbf{S}}_{\overline{\Lambda}}^H\mathbf{S}_\Lambda\alpha\right\|_\infty &= \max_{i\in\overline{\Lambda}}\left|\tilde{\mathbf{s}}_i^H\mathbf{S}_\Lambda\alpha\right| \\ &\leq \mu\left(S,\tilde{S}\right)\|\alpha\|_1 .\end{aligned}$$

Similarly, the denominator in the recovery condition can be bounded as

$$\begin{aligned}\left\|\tilde{\mathbf{S}}_{\Lambda}^H\mathbf{S}_\Lambda\alpha\right\|_\infty &= \max_{i\in\Lambda}\left|\tilde{\mathbf{s}}_i^H\mathbf{S}_\Lambda\alpha\right| \\ &= \max_{i\in\Lambda}\left|\tilde{\mathbf{s}}_i^H\mathbf{s}_i\alpha_i+\tilde{\mathbf{s}}_i^H\mathbf{S}_{\Lambda/i}\alpha_{\Lambda/i}\right| \\ &\geq \max_{i\in\Lambda}\left\{\left|\tilde{\mathbf{s}}_i^H\mathbf{s}_i\alpha_i\right|-\left|\tilde{\mathbf{s}}_i^H\mathbf{S}_{\Lambda/i}\alpha_{\Lambda/i}\right|\right\} \\ &\geq \max_{i\in\Lambda}\left\{|\alpha_i|-\left|\tilde{\mathbf{s}}_i^H\mathbf{S}_{\Lambda/i}\alpha_{\Lambda/i}\right|\right\} \\ &\geq \max_{i\in\Lambda}\left\{|\alpha_i|-\left(\|\alpha\|_1-|\alpha_i|\right)\mu\left(S,\tilde{S}\right)\right\} \\ &\geq \max_{i\in\Lambda}\left\{\|\alpha\|_\infty-\left(\|\alpha\|_1-\|\alpha\|_\infty\right)\mu\left(S,\tilde{S}\right)\right\}.\end{aligned}$$

Combining the two bounds, the recovery condition can be bounded as

$$\begin{aligned}\sup_{\alpha\in\mathbb{C}^{|\Lambda|}} \frac{\left\|\tilde{\mathbf{S}}_{\bar{\Lambda}}^{H}\mathbf{S}_{\Lambda}\alpha\right\|_{\infty}}{\left\|\tilde{\mathbf{S}}_{\Lambda}^{H}\mathbf{S}_{\Lambda}\alpha\right\|_{\infty}} &\leq \frac{\mu\left(S,\tilde{S}\right)}{\left(1+\mu\left(S,\tilde{S}\right)\right)\frac{\|\alpha\|_{\infty}}{\|\alpha\|_{1}}-\mu\left(S,\tilde{S}\right)} \\ &\leq \frac{|\Lambda|\,\mu(S,\tilde{S})}{1-(|\Lambda|-1)\,\mu\left(S,\tilde{S}\right)}.\end{aligned}$$

Hence, whenever the condition in Theorem 4.1.3 is satisfied, any target scene consisting of $|\Lambda|$ or less targets is absolutely resolvable using MOMP algorithm. ■

Theorem 4.1.3 can be written in a slightly different form,

$$\mu\left(S,\tilde{S}\right) < \frac{1}{2\,|\Lambda|-1},$$

which is more similar to equation (1.4). Hence, if a target scene is expected to consist of a maximum of L targets, the mismatched mutual coherence should satisfy $\mu\left(S,\tilde{S}\right) < (2L-1)^{-1}$.

4.1.2 Detection threshold and probability of detection

Consider the simple binary hypothesis problem in equation (2.19). The mismatched filter detector for this hypothesis can be written as

$$\left|\tilde{\mathbf{s}}^{H}\mathbf{r}\right| \underset{\mathcal{H}_0}{\overset{\mathcal{H}_1}{\gtrless}} \tilde{\gamma},$$

where $\tilde{\mathbf{s}}$ is the mismatched signal corresponding to signal $\mathbf{s}$ and satisfies conditions in (4.3). A direct consequence of the mismatched signal conditions is that $\|\tilde{\mathbf{s}}\|^2 \geq 1$. Assuming the noise is i.i.d. zero mean Gaussian, the mean and variance of $z = \tilde{\mathbf{s}}^{H}\mathbf{r}$ under hypothesis $\mathcal{H}_0$ can be written as

$$\begin{aligned}\mathbf{E}\left(z/\mathcal{H}_0\right) &= 0, \\ \mathbf{E}\left(zz^{*}/\mathcal{H}_0\right) &= \sigma^2 E_{\tilde{\mathbf{s}}},\end{aligned}$$

where $E_{\tilde{\mathbf{s}}} = \|\tilde{\mathbf{s}}\|^2$. Compared to the matched filter output in section 2.4, it can be seen that the mismatched filter has higher noise power at the output. In addition, since

$|z|$ is a Rayleigh random variable under $\mathcal{H}_0$, the detection threshold can be written as

$$\tilde{\gamma} = \sqrt{2\sigma^2 E_{\tilde{\mathbf{s}}} \ln\left(\frac{1}{\rho}\right)}, \tag{4.7}$$

where ρ is the desired false alarm rate. The detection threshold $\tilde{\gamma}$ for mismatched filters can be seen to be greater than the corresponding threshold for matched filters given in equation (2.22).

Under hypothesis $\mathcal{H}_1$, the mean and variance of the random variable $z = \tilde{\mathbf{s}}^H \mathbf{r}$ is given as

$$\begin{aligned} \mathbf{E}\left(z/\mathcal{H}_1\right) &= \alpha, \\ \mathbf{E}\left(\left(z-\alpha\right)\left(z-\alpha\right)^* / \mathcal{H}_1\right) &= \sigma^2 E_{\tilde{\mathbf{s}}}. \end{aligned}$$

Also, since z is a complex Gaussian random variable with nonzero mean, $|z|$ is a Rician random variable. Hence, the probability of detection using the mismatched filter can be expressed as

$$P_d = Q_1\left(\sqrt{\frac{\mathrm{SNR}}{E_{\tilde{\mathbf{s}}}}}, \sqrt{2\ln\left(\frac{1}{\rho}\right)}\right), \tag{4.8}$$

where SNR is defined in equation (2.23). Comparing equation (4.8) with (2.24), it can be seen that the mismatched filter has reduce probability of detection for the same SNR and false alarm rate. This loss is sometimes called the *mismatching loss* and is completely determined by $E_{\tilde{\mathbf{s}}}$. Figure 4.1 compares the probability of detecting a single target using matched filter and a mismatched filter in a range radar using the combined Barker code. The mismatched dictionary with a mismatching loss of 1.83dB was designed using the algorithm presented in the next section. It can be seen that unless the SNR is sufficiently high, the matched filter outperforms the mismatched filter in noise.

Figure 4.1 also shows the single target detection performance of the MOMP algorithm. It can be seen that even though MOMP essentially uses mismatched filtering to decide the position of the target, the detection performance is very similar to the matched filter. While this may seem surprising initially, a close inspection of the while-loop condition in MOMP algorithm shows why this is true. As alluded to earlier, MOMP differs from some other modifications of OMP algorithm in that it uses the matched filter threshold test to decide if a target is present or not. This means that for some known false alarm rate, the detection threshold in MOMP should be calculated using equation (2.22) instead of the threshold in (4.7). Furthermore, in a single target case with known target parameters, once the while-loop condition decides a target is present, we are guaranteed to select the correct target. Hence, the probability of detection of MOMP is similar to that of the matched filter.

In general, the threshold γ should always be calculated using equation (2.22) to achieve a given false alarm rate. Furthermore, this "trick" of using the matched filter to decide on the presence of a target and then using a different algorithm to select the target parameters will be used throughout this dissertation. As will be seen later, this will improve the resolution performance of these modified algorithms.

4.1.3 Design of mismatched dictionary

To improve the resolution performance as defined in equation (3.7), theorem 4.1.3 shows that it is sufficient to reduce the mismatched mutual coherence $\mu\left(S, \tilde{S}\right)$. This is equivalent to reducing the peak sidelobe level at the output of the receiver filter bank. Design of mismatched filters to reduce sidelobes has remained a topic of interest to radar engineers [25–27,32]. The design approach presented in this thesis is adapted from [32] and is equivalent to iterative re-weighted least squares technique.

While it is possible to design the complete mismatched synthesis matrix $\tilde{\mathbf{S}}$ without imposing any constraints, the resulting filter output will not be shift invariant. This makes it harder to analyze the resolution performance of the MOMP algorithm in general. Among existing techniques for designing mismatched filters, it is more common to design a signal $g\left(t\right)$ corresponding to the radar transmit waveform $s\left(t\right)$.

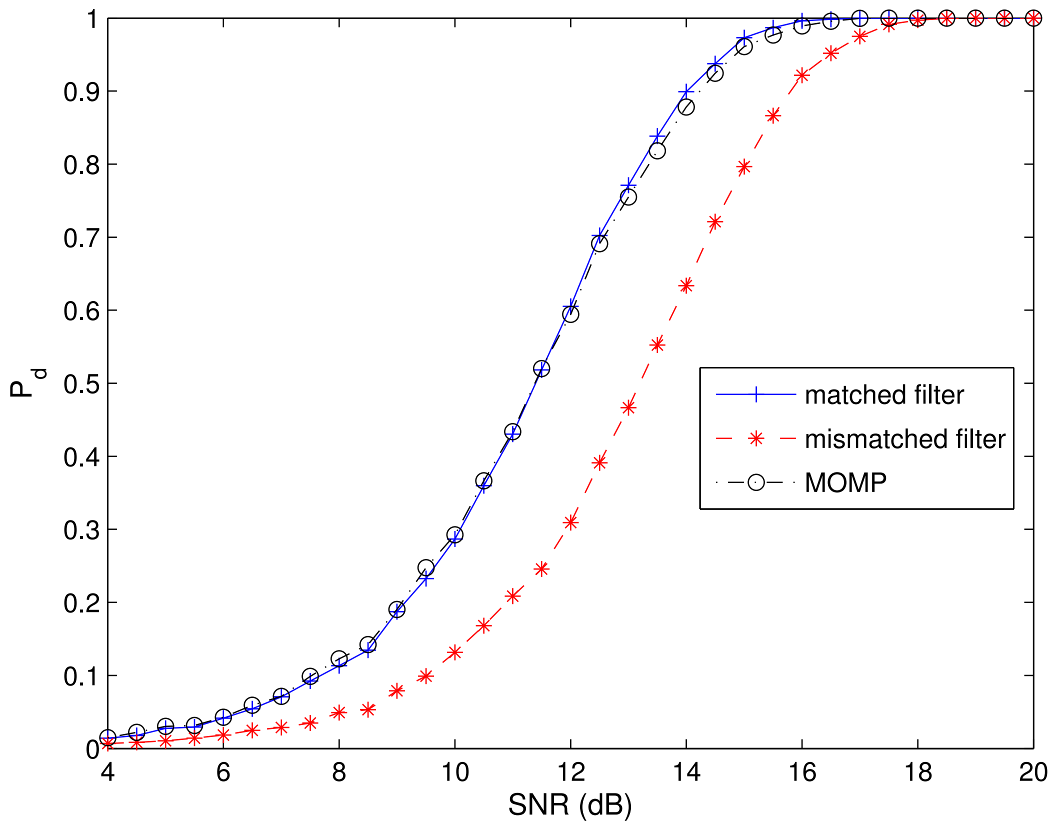

Figure 4.1.: Single target probability of detection of matched filter, mismatched filter and MOMP algorithm for $P_{FA} = 10^{-3}$. Both MOMP and mismatched filter use the same filter at the receiver. However, the mismatch loss of 1.83dB using mismatched filter can be avoided by using MOMP algorithm.

The mismatched synthesis matrix is then assumed to have a structure similar to that of $\mathbf{S}$ in section 1.2.4.1.

Assuming sampling $g(t)$ yields the discrete sequence $g[n]$, let $\mathbf{g}$ represent the sampled discrete sequence in vector form, that is $[\mathbf{g}]_n = g[n]$ for $1 \leq n \leq N$. Denoting the time-frequency shifts of $\mathbf{g}$ as $\mathbf{g}_{i,k}$, where

$$[\mathbf{g}_{i,k}]_n = \begin{cases} g[n-i]\, e^{j2\pi kn/M}, & 0 \leq i \leq n \leq N \\ 0, & else \end{cases},$$

the mismatched synthesis matrix $\tilde{\mathbf{S}}$ is defined as

$$\tilde{\mathbf{S}} = [\ \mathbf{g}_{0,0} \quad \mathbf{g}_{0,1} \quad \ldots \quad \mathbf{g}_{0,M} \quad \mathbf{g}_{1,0} \quad \ldots \quad \mathbf{g}_{1,M} \quad \ldots \quad \mathbf{g}_{N,M}\ ]. \tag{4.9}$$

As already mentioned, designing a mismatched dictionary with structure as in equation (4.9) simplifies dictionary design as well as analysis. This is due to the shift invariance property of the cross correlation between $\mathbf{g}_{m,n}$ and $\mathbf{s}_{i,k}$. Ignoring delay-Doppler edge effects, $\forall m, m+i \leq N$ and $\forall n, n+k \leq M$,

$$\begin{aligned} \langle \mathbf{g}_{m,n}, \mathbf{s}_{m+i,n+k} \rangle &= \sum_{l=1}^{N} (g[l-m]e^{j2\pi nl/M} \\ &\quad \times s^*[l-m-i]e^{-j2\pi(n+k)l/M}) \\ &= \sum_{l=1}^{N} g[l]s^*[l-i]e^{-j2\pi kl/M} \\ &= \langle \mathbf{g}_{0,0}, \mathbf{s}_{i,k} \rangle . \end{aligned} \tag{4.10}$$

As a result, the mismatched mutual coherence between $\mathbf{S}$ and $\tilde{\mathbf{S}}$ can be computed as

$$\begin{aligned} \mu\left(S, \tilde{S}\right) &= \max_{(i,j)\neq(0,0)} |\langle \mathbf{s}_{0,0}, \mathbf{g}_{i,j} \rangle| , \\ &= \max_{(i,j)\neq(0,0)} |\langle \mathbf{g}_{0,0}, \mathbf{s}_{i,j} \rangle| . \end{aligned}$$

In general, to reduce delay-Doppler edge effect, it is more suitable to calculate the mismatched mutual coherence using $N/2$ and $M/2$ for the location of the fixed point, that is $\mu\left(S, \tilde{S}\right) = \max_{(i,j)\neq(N/2,M/2)} \left|\left\langle \mathbf{g}_{N/2,M/2}, \mathbf{s}_{i,j} \right\rangle\right|$. In terms of matrix norm, the mismatched mutual coherence using any fixed point θ can be expressed as

$$\mu\left(S, \tilde{S}\right) = \left\|\mathbf{S}_{\theta}^{H} \mathbf{g}_{\theta}\right\|_{\infty} .$$

Hence, the mismatched filter design problem may be stated as the following optimization problem,

$$\hat{\mathbf{g}}_{\theta} = \arg\min_{\mathbf{g}} \left\|\mathbf{S}_{\bar{\theta}}^{H}\mathbf{g}\right\|_{\infty} \; s.t.\; \mathbf{s}_{\theta}^{H}\mathbf{g} = 1, \tag{4.11}$$

where the constraint is necessary to satisfy the assumptions in (4.3). Assuming there are P columns in the matrix $\mathbf{S}_{\bar{\theta}}$, this optimization problem can be solved using the linear program

$$\begin{aligned} \text{minimize} \quad & t \\ \text{subject to} \quad t \;\geq\; & \left[\left|\mathbf{S}_{\bar{\theta}}^{H}\mathbf{x}\right|\right]_{i}, \; \forall 1 \leq i \leq P \\ \mathbf{s}_{\theta}^{H}\mathbf{x} = \; & 1. \end{aligned}$$

with variables $\mathbf{x}$ and $t \in \mathbb{R}$. In [25,32], closed form expressions for mismatched filters are obtained by replacing the ℓ_{∞} norm in (4.11) with ℓ_2 norm. Let $\mathbf{s}_{\theta}$ be the k^{th} column of $\mathbf{S}$. The Lagrangian function for the new optimization problem can be expressed as

$$L\left(\mathbf{x}, \lambda\right) = \mathbf{x}^{H}\mathbf{S}\mathbf{F}\mathbf{S}^{H}\mathbf{x} + \lambda\left(\mathbf{x}^{H}\mathbf{s}_{\theta} - 1\right), \tag{4.12}$$

where $\mathbf{F}$ is an $(P+1)$ by $(P+1)$ diagonal matrix with diagonal values

$$[\mathbf{F}]_{i,i} = \begin{cases} 1, & i \neq k \\ 0, & i = k \end{cases}. \tag{4.13}$$

The optimization problem in (4.12) is equivalent to a constrained least squares problem and was first proposed in [25]. In terms of sidelobes, the optimization problem in (4.12) minimizes the energy in the sidelobes of the filter output. Taking derivative of $L\left(\mathbf{x}, \lambda\right)$ with respect to $\mathbf{x}$ and λ,

$$\begin{aligned} \frac{\partial L\left(\mathbf{x}, \lambda\right)}{\partial \mathbf{x}} &= 2\mathbf{S}\mathbf{F}\mathbf{S}^{H}\mathbf{x} + \lambda\mathbf{s}_{\theta} = 0, \\ \frac{\partial L\left(\mathbf{x}, \lambda\right)}{\partial \lambda} &= \mathbf{x}^{H}\mathbf{s}_{\theta} - 1 = 0. \end{aligned}$$

Combining both, the column of $\tilde{\mathbf{S}}$ corresponding to parameter θ that minimizes the energy in the sidelobes is given as

$$\mathbf{g}_{\theta} = \left(\mathbf{s}_{\theta}^{H}\left(\mathbf{S}\mathbf{F}\mathbf{S}^{H}\right)^{-1}\mathbf{s}_{\theta}\right)^{-1}\left(\mathbf{S}\mathbf{F}\mathbf{S}^{H}\right)^{-1}\mathbf{s}_{\theta} \tag{4.14}$$

Algorithm 4.2 Iterative re-weighted least squares approach to design of mismatched filters

1. Initialize $\mathbf{F}$ as in equation (4.13).
2. Generate mismatched filter using result in equation (4.14).
3. Update weight matrix $\mathbf{F}$ using equation (4.15).
4. Go to step 2 until convergence.

Although the mismatched filter designed using equation (4.14) minimizes the total energy in the sidelobes, it does not guarantee minimizing of the peak sidelobe level. As a result, there is no guarantee that the mismatched mutual coherence $\mu\left(S, \tilde{S}\right)$ would be reduced. To overcome this problem, a scheme that iteratively adapts $\mathbf{F}$ to reduce the peak sidelobe level is proposed in [32]. The basic idea behind this scheme is that after every iteration, the filter output is computed and is used to change the weights in the matrix $\mathbf{F}$. Hence, for larger filter output, a larger weight is assigned to the corresponding diagonal element in $\mathbf{F}$ so that the filter designed in the next iteration suppresses that sidelobe.

Let $\mathbf{g}_\theta^i$ be the mismatched filter obtained after i iterations. The filter output is then computed as $\mathbf{r} = \mathbf{S}^H\mathbf{g}_\theta^i$. The new matrix $\mathbf{F}^{i+1}$ is then computed as

$$\left[\mathbf{F}^{i+1}\right]_{j,j} = \begin{cases} \left[\mathbf{F}^i\right]_{j,j} \times \frac{\left|\mathbf{S}^H\mathbf{g}_\theta^i\right|}{P}, & j \neq k \\ 0, & j = k \end{cases}, \tag{4.15}$$

where k is the column number of $\mathbf{S}$ corresponding to $\mathbf{s}_\theta$ and $\mathbf{F}$ is a $(P+1)$ by $(P+1)$ diagonal matrix. Algorithm 4.2 summarizes the mismatched filter design approach.

It is important to point out that the iterative re-weighted least squares approach to mismatched filter design is not guaranteed to converge to the true minimum peak sidelobe filter. However, it has been shown to yield good filters in [32].

4.1.4 Sparse Spike Deconvolution

An important problem in signal processing is that of recovering a sparse spike train. The signal model can be written as

$$r[n] = (u * f)[n] + w[n], \quad n \in \{1, 2, \dots, N\} \tag{4.16}$$

where $*$ represents the convolution, u is the convolution kernel, w is additive noise and f is a linear combination of Dirac delta functions to be recovered. Denoting Dirac delta function as $\delta[n]$, f can be expressed as

$$f[n] = \sum_k a_k \delta[n-k], \quad n \in \{1, 2, \dots, N\} \tag{4.17}$$

This signal model is encountered in *seismic exploration* and in *target ranging radars*. In seismic exploration, r represents the reflected pressure waves and f is the underground reflectivity to be estimated. The convolution kernel u in this case is the seismic wavelet. In target ranging radars, f represents the point target environment with the position of each Dirac delta indicating the position of a target. The convolution kernel, u is the signal transmitted by the radar. In both of these applications, obtaining a good estimate of f is desired.

Let u_k denote an N dimensional vector defined as $u_k[l] = u[l-k],\ k, l \in \{1, \dots N\}$. Using (4.17) in (4.16), we can express the sparse spike signal model as [15]

$$r \;=\; \sum_k a_k u_k + w = Ua + w, \tag{4.18}$$

where the matrix $U = [\ u_1 \quad u_2 \quad \dots \quad u_N\ ]$. The model in (4.18) is analogous to (1.5) and by analogy, we can use the OMP algorithm with a dictionary $D = \{u_1, u_2, \dots, u_N\}$ to estimate a.

The dependence of the dictionary on the convolution kernel u shows that recovery of f using MP depends on u. Indeed, design of optimal transmit waveforms in radar has been a topic of extensive research. In seismic exploration, u depends on the transmitted pressure wave as well as other processing. Ideally, optimal recovery of f

requires u that satisfies $\langle u_k, u_l \rangle \approx \delta[k-l],\ \forall k, l \in \{1, 2, \ldots, N\}$. However, high energy, constant modulus and constrained bandwidth requirements on u in radar applications often make it difficult to satisfy this requirement. As a result, it becomes difficult to recover f if it has *closely* spaced Dirac functions in . In target ranging radar, the closely spaced Diracs case is particularly important for high resolution radars since it implies two targets nearby. In seismic exploration, closely spaced Diracs imply the presence of a thin geophysical layer which may be important in some applications.

To understand the difficulty in resolving closely spaced Diracs, consider a dictionary D with a convolution kernel u defined as

$$u[n] = (1 - \sigma^{-2}n^2)e^{-\sigma^{-2}n^2/2}, n \in \{1, ..., N\} \tag{4.19}$$

which is the second derivative of a Gaussian. Mallat used this kernel as an example to show the problems encountered when f has closely space Diracs. Figure (4.2a) shows a plot of the convolution kernel for $\sigma = 10$. Although there are a number of possibilities for the mismatched dictionary, $\tilde{D}$, we will define $\tilde{D}$ as

$$\begin{aligned} \tilde{D} &= \{\ \tilde{u}_1 \quad \tilde{u}_2 \quad \ldots \quad \tilde{u}_N\ \}, \\ \tilde{u}_k[n] &= u_k[n] \times h[n],\ n \in \{1, ..., N\} \end{aligned}$$

where $h[n]$ is the windowing function. For this example, we define the windowing function as

$$h[n] = \begin{cases} 1, & n < 12 \\ 0.2, & otherwise \end{cases}.$$

Figure (4.2b) shows a plot of the mismatched convolution kernel, $\tilde{u}$. The resulting ERCs for recovery of f composed of a linear combination of two Diracs using the OMP and MOMP algorithms is shown in figure (4.3). Suppose $f = a_1\delta[n-k_1] + a_2\delta[n-k_2]$. Assuming negligible noise, the results show that the MOMP algorithm can correctly recover f when $|k_2 - k_1| > 36$. The OMP algorithm, however, can only recover f accurately when $|k_2 - k_1| > 44$.

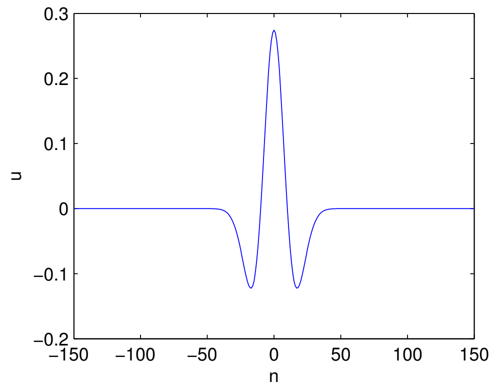

(a) Convolution kernel u

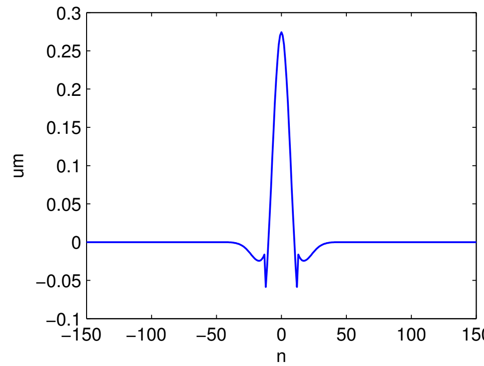

(b) Mismatch convolution kernel, $\tilde{u}$

Figure 4.2.: The convolution kernels, u and the mismatched convolution kernel $\tilde{u}$

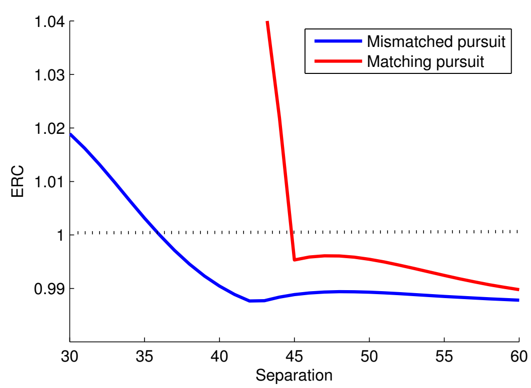

Figure 4.3.: ERC comparison for recovery of two Diracs using MP and MMP algorithm for u and $\tilde{u}$ shown in figure (4.2)

4.1.5 Simulation results

Figure (4.4) shows a comparison of the absolute recovery conditions of OMP (3.6.1) and MOMP (4.1.1) algorithms in a range radar for two targets with different separations. The extended barker code in equation (1.36) was used as the radar transmit signal. The mismatched dictionary was designed using Algorithm 4.2 and the resulting mismatched filter had a mismatching loss of 1.83dB. It can be seen in figure (4.4) that even though a target scene with two targets is resolvable using OMP algorithm for all target separations, the MOMP algorithm results in a smaller value of recovery condition. This suggests that for target scenes with recovery condition $\max_{\theta\in\overline{\Lambda}}\left\|\mathbf{S}_{\Lambda}^{\dagger}\mathbf{s}_{\theta}\right\|_{1} > 1$, it may be that the recovery condition for MOMP, $\max_{\theta\in\overline{\Lambda}}\left\|\left(\mathbf{S}_{\Lambda}^{H}\tilde{\mathbf{S}}_{\Lambda}\right)^{-1}\mathbf{S}_{\Lambda}^{H}\tilde{\mathbf{s}}_{\theta}\right\|_{1} < 1$. For example, consider a target scene $\Lambda = \{0, 2t_b, 4t_b, 6t_b, 11t_b\}$ consisting of 5 targets. For this target scene, $\max_{\theta\in\overline{\Lambda}}\left\|\mathbf{S}_{\Lambda}^{\dagger}\mathbf{s}_{\theta}\right\|_{1} = 1.053$ whereas $\max_{\theta\in\overline{\Lambda}}\left\|\left(\mathbf{S}_{\Lambda}^{H}\tilde{\mathbf{S}}_{\Lambda}\right)^{-1}\mathbf{S}_{\Lambda}^{H}\tilde{\mathbf{s}}_{\theta}\right\|_{1} = 0.1244$. Hence, this particular target scene is absolutely resolvable using MOMP algorithm but not using OMP algorithm.

In section (3.4), it was mentioned that mismatched filtering can improve resolution at the expense of probability of detection of a single target. This is true when detecting a single target with known parameters at the receiver. In a multiple target environment with unknown target parameters, the sidelobe structure of filter output can cause false alarm. The recovery condition (ERC) of the target scene indicates the peak sidelobe to mainlobe level of the filter output. For example, an ERC $= 0.5$ shows that it is possible to have a peak sidelobe to mainlobe level of 0.5. Such large sidelobe levels can make a big impact on the probability of false alarm. Hence, instead of using probability of detection to consider the resolution performance in noise, it is reasonable to consider the probability of resolution of the target scene in noise.

Figure (4.5) shows the probability of resolution of OMP and MOMP for three different target scenes. The threshold γ for each SNR was selected using equation (2.22) for a single deterministic target for a fixed probability of false alarm of 10^{-3}.

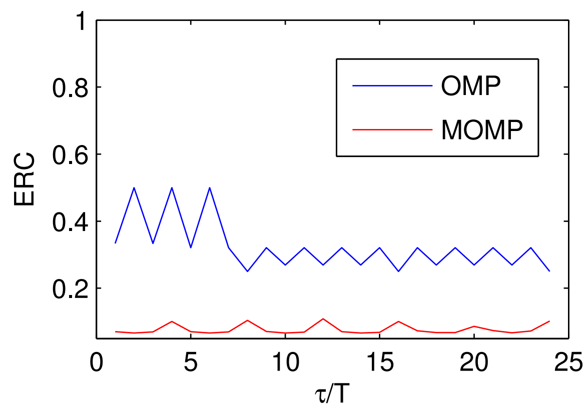

Figure 4.4.: Comparison of recovery condition (ERC) for OMP and MOMP algorithm in a range radar using combined barker code for different target separations τ.

The target amplitudes were also selected to achieve peak sidelobe to mainlobe ratio equal to the ERC. It can be seen from figure (4.5) that even though the use of mismatched filtering in MOMP can reduce SNR, the decrease in false alarm due to the decreased sidelobe levels can make up for it.

Unlike the range radar, the resolution of pulse-Doppler radar is restricted by the uncertainty principle. This manifests itself in the form of the volume constraint on the ambiguity function in equation (1.26). The uncertainty principle, in general, holds for all linear systems with a redundant dictionary. Because of this, the MOMP algorithm cannot be used to improve the resolution performance defined in (3.7) when all targets are equally likely. Figure 4.6 shows the resolution plot of pulse-Doppler radar using MOMP algorithm when the radar transmit signal is the combined barker sequence. The receive filter was designed using the iterative reweighted least squares technique proposed in [32] to minimize the peak sidelobe level. Comparing Figure 4.6 to Figure 3.7, it can be seen that there is no resolution improvement when using MOMP algorithm in a system with redundant dictionary. The next section discusses an algorithm which can be used in such cases.

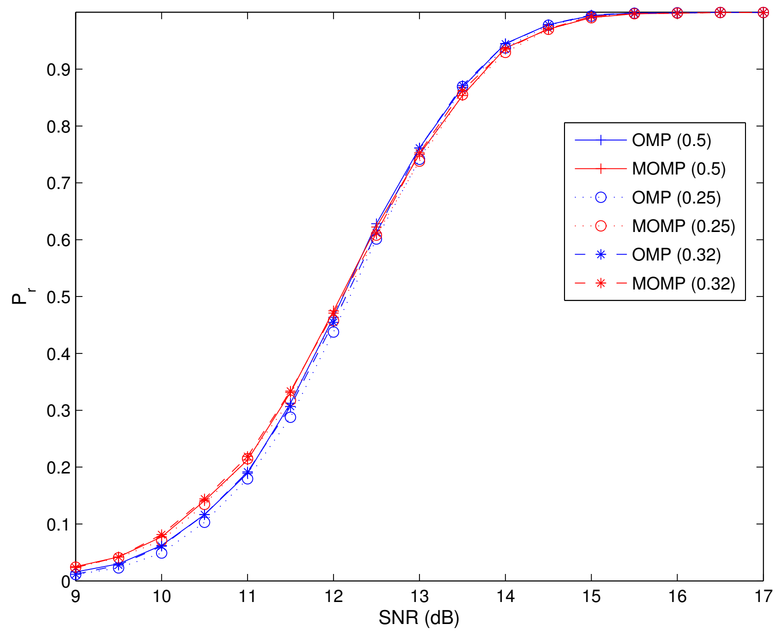

Figure 4.5.: Probability of resolution of target scenes with recovery condition values 0.5, 0.25 and 0.32 using OMP and MOMP. The mismatch loss for the filter in MOMP is 1.83dB.

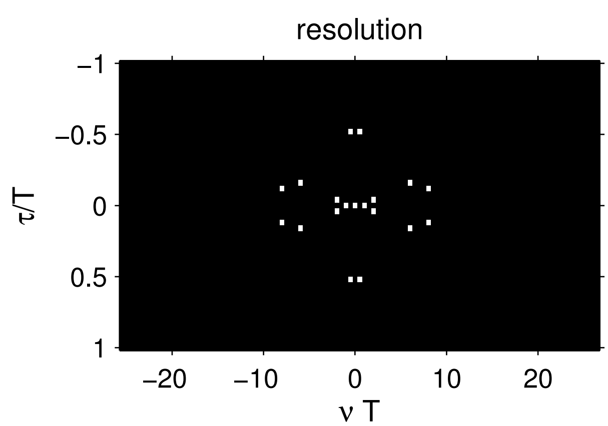

Figure 4.6.: Resolution of extended barker code in a pulse Doppler radar using MOMP algorithm.

Algorithm 4.3 Subspace mismatching pursuit solution for signal decomposition of $r = \sum_k a_k s_k + n$ in a redundant dictionary $\mathbf{S}$ with a subspace selection threshold η

- Initialize $\hat{\Lambda} = \emptyset$, $\bar{r} = r$, γ, $0 < \eta < 1$
- $\sigma = \max_\theta \left| s_\theta^H r \right|$
- while $\sigma > \gamma$
  - $\Psi = \left\{ \theta \mid \left| s_\theta^H \bar{r} \right| > \max\left(\eta\sigma, \gamma\right) \right\}$
  - Design $\tilde{S}_{\Psi \cup \hat{\Lambda}}$
  - $\hat{\theta} = \arg\max_{\theta \in \Psi} \left| \tilde{s}_\theta^H \bar{r} \right|$
  - $\hat{\Lambda} = \hat{\Lambda} \cup \hat{\theta}$
  - $\hat{\alpha} = \arg\min_\alpha \left\| r - S_{\hat{\Lambda}} \alpha \right\|^2$
  - $\bar{r} = r - S_{\hat{\Lambda}} \hat{\alpha}$
  - $\sigma = \max_\theta \left| s_\theta^H \bar{r} \right|$

4.2 Redundant Dictionaries

Although the mismatch pursuit algorithm proposed in section 4.1 works well for non redundant dictionaries, it is not suitable for redundant dictionaries constrained by the uncertainty principle. Consider, for example, the signal delay-Doppler dictionary of a pulse Doppler radar. Assume that the mismatch dictionary comprises of time delayed, and Doppler shifted versions of mismatched signal $g(t)$. Stutt's [2] invariant relation (1.26) shows that the total volume under the cross ambiguity function, $\chi_{sg}(\tau, \nu)$, remains constant if the energy of signal $g(t)$ is fixed. This means that although $g(t)$ could be designed to reduce the ambiguity in some delay Doppler region, the total volume of the cross ambiguity and hence the overall resolution, defined in (3.7), cannot be improved. To overcome this limitation, a mismatched pursuit algorithm based on a subspace of Col($\mathbf{S}$) is proposed in 4.3.

In each iteration, the *subspace mismatching* algorithm (SMOMP) obtains the matched filter output for the residue. Suppose the maximum value of the output is κ. The algorithm obtains a *peak set* consisting of all the atoms in the dictionary which satisfy

$$|\langle \bar{\mathbf{r}}, \mathbf{s}_\theta \rangle| \geq \eta\sigma,$$

where η is a user specified threshold parameter and $0 < \eta < 1$. The selection of this threshold depends on the transmit signal and the desired resolution. Assuming a sparse target scene environment, it is reasonable to assume that the cardinality of the peak set in each iteration satisfies

$$|\Psi| < N, \tag{4.20}$$

where N is the dimension of each atom $\mathbf{s}_\theta \in \mathbf{S}$. Under this assumption, it is possible to design a sub-dictionary mismatched to Ψ. The goal of the mismatched subdictionary is to satisfy

$$\left|\tilde{\Phi}^H \Phi_{\Upsilon_j}\right| \approx I. \tag{4.21}$$

The mismatched sub-dictionary is then used to select the atom to be removed in iteration j. Once the atom is selected, all other steps in each iteration are similar to the steps performed in the mismatched pursuit algorithm.

4.2.1 Mismatched sub-dictionary design

The synthesis matrix corresponding to the peak set, Φ_{Υ_j}, will usually have more rows than columns because of assumption (4.20). As a result, the least squares solution to the design problem in (4.21) is given by the Moore-Penrose pseudo inverse, that is

$$\tilde{\mathbf{S}}^H = \mathbf{S}^\dagger_{\Upsilon_j} = (\mathbf{S}^H_{\Upsilon_j}\mathbf{S}_{\Upsilon_j})^{-1}\mathbf{S}^H_{\Upsilon_j}. \tag{4.22}$$

4.2.2 Resolution

The resolution of the adaptive subspace algorithm in 4.3 depends on the mismatched subspace dictionary design in every iteration and the value of the constant η, where $0 < \eta < 1$. In this section, it will be assumed that $|\Upsilon| < N$ and that the designed mismatched synthesis matrix $\tilde{\mathbf{S}}_{\Psi \cup \hat{\Lambda}}$ approximately forms a bi-orthogonal pair to $\mathbf{S}_{\Psi \cup \hat{\Lambda}}$, that is, $\left|\tilde{\mathbf{S}}_{\Psi \cup \hat{\Lambda}}^H \mathbf{S}_{\Psi \cup \hat{\Lambda}}\right| \approx \mathbf{I}$. Furthermore, assuming a target set Λ, the SMOMP algorithm in 4.3 will fail to correctly recover Λ if, in any iteration, $\Psi \cap \Lambda = \emptyset$. Equation (3.11) shows that $\forall h \in \mathrm{Col}\left(\mathbf{S}_{\Lambda}\right)$,

$$\left\|\mathbf{S}_{\overline{\Lambda}}^H \mathbf{h}\right\|_\infty \leq \max_{\theta \in \overline{\Lambda}} \left\|\mathbf{S}_{\Lambda}^{\dagger} \mathbf{s}_\theta\right\|_1 \left\|\mathbf{S}_{\Lambda}^H \mathbf{h}\right\|_\infty .$$

Hence, in algorithm 4.3, the peak set Ψ is guaranteed to have at least one element $\ell \in \Psi$ such that $\ell \in \Lambda$ if

$$\eta < \min \left\{ \left(\max_{\theta \in \overline{\Lambda}} \left\|\mathbf{S}_{\Lambda}^{\dagger} \mathbf{s}_\theta\right\|_1 \right)^{-1}, 1 \right\}. \tag{4.23}$$

The condition on η in (4.23) is necessary for absolute resolvability of target set Λ and will be assumed to hold for the following analysis. Consider a target scene with L targets and target parameter set $\Lambda = \{\theta_1, \ldots, \theta_L\}$. Without loss of generality, assume after $j < L$ iterations of SMOMP, the estimated target set $\hat{\Lambda} = \{\theta_1, \theta_2, \ldots, \theta_j\}$. Define the set of remaining targets $\Lambda_r = \Lambda / \hat{\Lambda} = \{\theta_{j+1}, \ldots, \theta_L\}$. In general, the peak set Ψ in the $j+1$ iteration will be composed of some target elements $\xi \in \Lambda_r$ and some non target elements $\vartheta \in \overline{\Lambda}$. Let $\Psi = \Lambda_\Psi \cup \bar{\Lambda}_\Psi$, where $\Lambda_\Psi \subseteq \Lambda_r$ and $\overline{\Lambda}_\Psi \subset \overline{\Lambda}$. The residue vector in the $j+1$ iteration can be written as $\bar{\mathbf{r}} = \mathbf{S}_{\Lambda_\Psi} \alpha_{\Lambda_\Psi} + \mathbf{S}_{\hat{\Lambda}} \alpha_{\hat{\Lambda}} + \mathbf{S}_\Upsilon \alpha_\Upsilon$, where $\Upsilon = \Lambda_r / \Lambda_\Psi$. For $\eta \ll 1$, the effect of $\mathbf{S}_\Upsilon \alpha_\Upsilon$ on greedy target parameter selection can be ignored. This is due to the fact that for $\eta \ll 1$, $|\Upsilon| \ll |\Lambda_r|$ and $\left\|\mathbf{S}_\Upsilon^H \bar{\mathbf{r}}\right\|_\infty \ll \left\|\mathbf{S}_{\Lambda_\Psi}^H \bar{\mathbf{r}}\right\|_\infty$. Hence, the result of correlating the residue vector with the mismatched subspace atoms can be approximated as

$$\left|\tilde{\mathbf{s}}_\theta^H \bar{\mathbf{r}}\right| \approx \begin{cases} 0, & \theta \in \overline{\Lambda}_\Psi \\ \alpha_\theta, & \theta \in \Lambda_\Psi \end{cases} . \tag{4.24}$$

When the approximation in (4.24) holds, the SMOMP selects a correct target in the $j+1$ iteration. Furthermore, the result in equation (4.24) is exact when $\Upsilon = \emptyset$. Therefore, it is desirable to choose $\eta \ll 1$ so that $|\Upsilon| = 0$. However, depending on the transmit signal being used in the radar, a small η may result in a large peak set and the condition in (4.20) may not be met. Thus, the selection of η requires trade off between the ability to design a good mismatched subdictionary and the resolution of the algorithm. The following theorem summarizes these results.

Theorem 4.2.1 *Let $\Lambda = \{\theta_1, \ldots, \theta_L\}, \theta_i \in \mathcal{T}, \forall 1 \leq i \leq L$ denote a target scene with L targets. In any iteration of the SMOMP algorithm, the algorithm correctly selects a target in Λ if $\hat{\Lambda} \subseteq \Lambda$ and $\Lambda \subseteq \hat{\Lambda} \cup \Psi$.*

Proof Since $\mathbf{r} \in \mathrm{Col}(\mathbf{S}_\Lambda)$ and $\hat{\Lambda} \subseteq \Lambda$, the residue vector satisfies $\bar{\mathbf{r}} \in \mathrm{Col}(\mathbf{S}_\Lambda)$. Denote $\Lambda_\Psi \subseteq \Lambda$ such that $\Lambda_\Psi \subseteq \Psi$ and $\Lambda_\Psi \cap \hat{\Lambda} = \emptyset$. Then, the residue vector can be expressed as

$$\bar{\mathbf{r}} = \mathbf{S}_{\hat{\Lambda}}\alpha_{\hat{\Lambda}} + \mathbf{S}_{\Lambda_\Psi}\alpha_{\Lambda_\Psi}.$$

Then, because of the bi-orthogonality property of the mismatched subspace, $\forall\theta \in \Psi$, $\theta \notin \Lambda$,

$$\begin{aligned} \left|\tilde{\mathbf{s}}_\theta^H \bar{\mathbf{r}}\right| &= \left|\tilde{\mathbf{s}}_\theta^H \mathbf{S}_{\hat{\Lambda}}\alpha_{\hat{\Lambda}} + \tilde{\mathbf{s}}_\theta^H \mathbf{S}_{\Lambda_\Psi}\alpha_{\Lambda_\Psi}\right| \\ &= 0. \end{aligned}$$

Furthermore, $\forall\theta \in \Psi$, $\theta \in \Lambda$,

$$\begin{aligned} \left|\tilde{\mathbf{s}}_\theta^H \bar{\mathbf{r}}\right| &= \left|\tilde{\mathbf{s}}_\theta^H \tilde{\mathbf{s}}_\theta \alpha_\theta\right| \\ &\geq 0. \end{aligned}$$

Hence, the selected target is guaranteed to be in Λ. ■

4.3 Simulation results

Figure 4.7 shows a target scene containing 8 total targets. In this particular scene, the targets are assumed to have the same magnitude and phase. The radar transmit

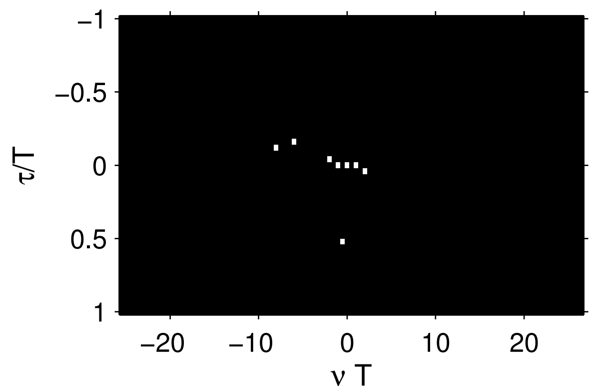

Figure 4.7.: Target scene with $\max_{\theta \in \overline{\Lambda}} \left\| \mathbf{S}_{\Lambda}^{\dagger} \mathbf{s}_{\theta} \right\|_1 = 3.07$.

signal is assumed to be the combined barker sequence. The OMP recovery condition of Theorem 3.6.1 for the target scene is 3.07. The matched filter bank output for the signal received from the target scene is shown in Figure 4.8a. It can be seen that since the signal dictionary does not satisfy the incoherence property, estimation of the actual target scene from the matched filter output is hard. Furthermore, since $\max_{\theta \in \overline{\Lambda}} \left\| \mathbf{S}_{\Lambda}^{\dagger} \mathbf{s}_{\theta} \right\|_1 = 3.07$, this particular scene is not absolutely resolvable using OMP algorithm. Figure 4.8b shows the target scene estimate obtained using OMP. Finally, Figure 4.8 shows that the SMOMP algorithm correctly estimates the target scene. All results in Figure 4.8 were obtained by assuming no noise in the received signal.

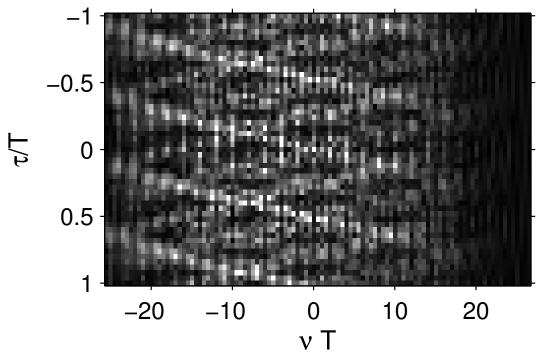

(a) Matched filter output

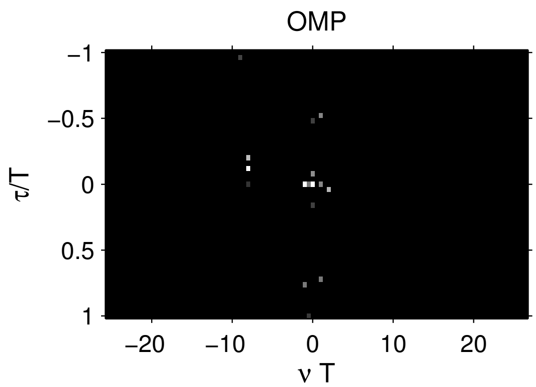

(b) Target scene estimate using OMP

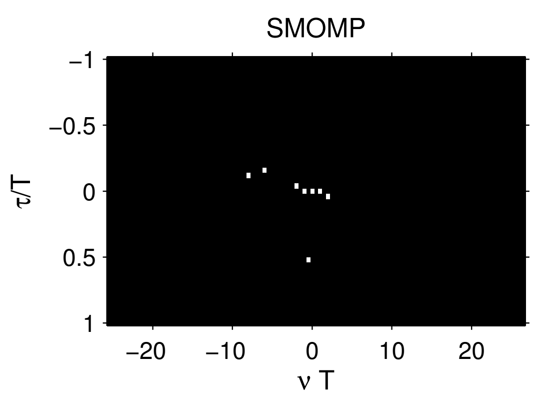

(c) Target scene estimate using SMOMP

Figure 4.8.: Comparison of radar recovery algorithms for target scene in Figure 4.7 assuming ∞ SNR.

5. PURSUIT USING MULTIPLE CHANNELS

Radars using multiple transmit signals and multiple receive antennas have received increasing interest in recent years. Because they borrow concepts from multiple input multiple output (MIMO) communications, these radars are commonly referred to as MIMO radars. It has been shown that they can result in improved resolution [33, 34], detection [34, 35], parameter identifiability [36] and estimation, target tracking, jamming and clutter suppression [35]. Even though the term MIMO is relatively new in radar literature, the concept has existed for a few decades. For example, multistatic radars are a type of MIMO radar which have been studied for some time. However, the recent explosion in MIMO communications research has given added impetus to the MIMO radar research.

MIMO radars can be classified into two broad categories: *coherent MIMO* radar and the *statistical MIMO* radar [34]. In statistical MIMO radar, antennas transmitting different waveforms are widely separated resulting in independent target scattering response. As a result, this type of radar can yield improved detection performance compared to the traditional radars. In coherent MIMO radar, all transmit antennas are closely spaced so that the target scattering response is same for each transmit-receive pair. This type of radar can provide improved resolution and parameter estimation. In this chapter, we focus exclusively on the coherent MIMO radar from a resolution perspective. In particular, we show that suitable chosen transmit waveforms can result in improved resolution even in the presence of cross correlation terms.

The rest of the chapter is organized as follows: In section (5.1), we present the signal model of a coherent MIMO radar. Section 5.2 studies the resolution performance of greedy pursuit algorithms applied to radar system using linear channel combining. It is shown that significant resolution improvement can be obtained by using multiple transmit waveforms. Nonlinear channel combining is analyzed in section 5.3. It is shown that combining nonlinear channel combining can help in mitigating the problems associated with nonlinear channel combining. Finally, sections 5.4 and 5.5 present simulation results comparing the recovery performance and the performance in noise of the MIMO radar systems using greedy algorithms.

5.1 Signal model

Consider a coherent MIMO radar system with K transmit waveforms $s_1(t)$, $s_2(t)$,..., $s_K(t)$. Assume all K transmit signals have the same bandwidth and the receive time frequency dictionary corresponding to each waveform is $\mathbf{S}_1, \mathbf{S}_2, \ldots, \mathbf{S}_K$ respectively. Each dictionary, $\mathbf{S}_i$, is assumed to be formulated as in section 1.2.4.1. The baseband received signal from a single point target can be written as

$$r(t) = \sum_{i=1}^{K} \alpha s_i(t-\tau) e^{j2\pi v t} + w(t), \tag{5.1}$$

where α is the complex amplitude of the target return and τ, ν are the time delay and Doppler corresponding to the target. Since the MIMO radar is assumed to be coherent with colocated antennas and all the transmit signals have the same bandwidth, carrier frequency and are transmitted simultaneously, the target parameters α, τ, ν are same for all the waveforms. The multiple target extension of the signal model in (5.1) can be expressed as

$$r(t) = \sum_{j=1}^{K} \sum_{i=1}^{L} \alpha_i s_j(t-\tau_i) e^{j2\pi v_i t} + w(t), \tag{5.2}$$

where the target scene is assumed to consist of L point targets. Furthermore, in this chapter, it is assumed that for a sampling period T_s, the discrete time signal corresponding to (5.2) can be written as

$$r[n] = \sum_{j=1}^{K} \sum_{i=1}^{L} \alpha_i s_j \left[n - k_i\right] e^{j2\pi \omega_i n/M} + w\left[n\right], \; 1 \leq n \leq N,$$

where $k_i = \tau_i/T_s$, $k_i \in \mathbb{Z}$ is the delay and $\omega_i/M = \nu_i T_s$, $\omega_i \in \mathbb{Z}$ is the Doppler corresponding to the i^{th} target. The receive signal model in (5.2) can be written in a vector form similar to (1.18) as

$$\begin{aligned} \mathbf{r} &= \sum_{j=1}^{K} \mathbf{S}_j \alpha + \mathbf{w} \\ &= \mathbf{S}\alpha + \mathbf{w}, \end{aligned} \tag{5.3}$$

where $\mathbf{S} = \sum_{j=1}^{K} \mathbf{S}_j$ is the new signal dictionary and α is the target scene vector as in (1.18). The model in (5.3) can be seen to similar to the received signal model for a radar using one transmit signal (1.18). Hence, the OMP algorithm with a *normalized* receive signal dictionary $\bar{\mathbf{S}} = \frac{1}{K}\sum_{j=1}^{K} \mathbf{S}_j$ may be used to recover the target scene from (5.3).

5.1.1 Signal pairs

In [22], a MIMO radar system with two different LFM waveforms has been studied. The LFM waveform was previously introduced in section 1.5. In particular, Rasool [22] showed significant improvement in the composite ambiguity function of a MIMO system using an LFM upchirp and an LFM downchirp with the same time-bandwidth product. For some simulations in this chapter, a MIMO radar system using an LFM upchirp and an LFM downchirp with a time-bandwidth product of 40 will be used.

Another signal pair that will be used frequently in this chapter is based on the combined barker codes which were also introduced in section 1.5. The signal pair used in this chapter is defined as

$$\begin{aligned} \mathbf{s}_1 &= b_m^{13} \otimes b_m^4, \\ \mathbf{s}_2 &= b_m^4 \otimes b_m^{13}, \end{aligned}$$

where $\otimes$ denotes the Kronecker product, and b_m^{13} and b_m^4 represent the length 13 and length 4 Barker sequences respectively.

5.2 Linear Channel combining

The received signal model in (5.3) shows that the MIMO radar is equivalent to a radar with a single transmit waveform when the transmit signal is given as $s(t) = \sum_{i=1}^{K} s_i(t)$. Since practical radar signals must have constant amplitude to overcome the constraints of high power amplifiers, the set of achievable ambiguity functions in pulse-Doppler radars is severely constrained. With a MIMO radar, this constraint can be overcome since the individual signals, $s_i(t)$ are required to be constant amplitude but their linear sum can effectively form a signal with varying amplitude. Hence, as long as a desired radar transmit signal can be expressed as a linear sum of constant amplitude signals, it can be implemented in practice using the MIMO radar approach. Denoting the normalized composite signal dictionary $\bar{\mathbf{S}} = \frac{1}{K}\sum_{j=1}^{K} \mathbf{S}_j$, the matched filter estimate of the target scene is given as

$$\hat{\alpha} = \bar{\mathbf{S}}^H \mathbf{r} = \frac{1}{K}\left(\mathbf{S}^H \mathbf{S}\alpha + \mathbf{S}^H \mathbf{w}\right). \tag{5.4}$$

Furthermore, similar to the definition of discrete ambiguity function in (1.28), the discrete *composite ambiguity function* is defined as

$$\chi^C[\tau, \nu] = \left[\mathbf{S}^H \mathbf{s}_{0,0}\right]_{\tau M+\nu}.$$

Hence, using the shift invariance property of the signal dictionary $\mathbf{S}$, the target scene estimate at the output of the matched filter can be expressed as a linear sum of shifted composite ambiguity functions

$$[\tilde{\alpha}]_{\tau M+\nu} = \frac{1}{K}\sum_{(i,j)\in\Lambda} [\alpha]_{iM+j}\, \chi^C[\tau - i, \nu - j],$$

which is similar to equation (1.29) for radar systems with single transmit waveform. The composite ambiguity function itself is related to the ambiguity function of each of the K radar transmit signals as

$$\begin{aligned}
\chi^{C}[\tau,\nu] &= \left[\mathbf{S}^{H}\mathbf{s}_{0,0}\right]_{\tau M+\nu} \\
&= \left[\left(\sum_{i=1}^{K}\mathbf{S}_{i}^{H}\right)\left(\sum_{j=1}^{K}\mathbf{s}_{0,0}^{j}\right)\right]_{\tau M+\nu} \\
&= \left[\sum_{i=1}^{K}\sum_{j=1}^{K}\mathbf{S}_{i}^{H}\mathbf{s}_{0,0}^{j}\right]_{\tau M+\nu} \\
&= \left[\sum_{i=1}^{K}\mathbf{S}_{i}^{H}\mathbf{s}_{0,0}^{i}\right]_{\tau M+\nu} + \left[\sum_{\substack{m=1\\ m\neq n}}^{K}\sum_{n=1}^{K}\mathbf{S}_{m}^{H}\mathbf{s}_{0,0}^{n}\right]_{\tau M+\nu} \\
&= \sum_{i=1}^{K}\chi_{i,i}[\tau,\nu] + \sum_{\substack{m=1\\ m\neq n}}^{K}\sum_{n=1}^{K}\chi_{m,n}[\tau,\nu],
\end{aligned} \tag{5.5}$$

where $\chi_{m,n}[\tau,\nu]$ represents the discrete cross ambiguity function between m^{th} and n^{th} radar transmit signals. Assuming the effect of cross ambiguity function $\chi_{m,n}[\tau,\nu]$ is negligible in (5.5), it can be seen that $\forall\,[\tau,\nu] \neq [0,0]$ the composite ambiguity function satisfies

$$\begin{aligned}
\chi^{C}[\tau,\nu] &\approx \sum_{i=1}^{K}\chi_{i,i}[\tau,\nu] \\
&\leq \sum_{i=1}^{K}\mu\left(\mathbf{S}_{i}\right),
\end{aligned} \tag{5.6}$$

where $\mu(\mathbf{S}_i)$ is the mutual coherence of the dictionary $\mathbf{S}_i$ as defined in equation (1.30). Additionally, when the cross ambiguity functions are negligible, $\chi^{C}[0,0] \approx K$. Hence, using (5.6), the mutual coherence of the normalized composite signal dictionary $\bar{\mathbf{S}} = \frac{1}{K}\sum_{j=1}^{K}\mathbf{S}_j$ can be bounded as

$$\mu(\bar{\mathbf{S}}) \leq \frac{\sum_{i=1}^{K}\mu(\mathbf{S}_i)}{K}. \tag{5.7}$$

Define the set $\mathrm{T}_i = \{[\tau, \nu] \,|\, |\chi_{i,i}[x, y]| \approx \mu(\mathbf{S}_i)\}$. In general, if the set of radar transmit signals is carefully chosen in such a way that $\forall 1 \leq i, j \leq K$ and $i \neq j$,

$$\forall [\tau, \nu] \in \mathrm{T}_i, \; |\chi_{jj}[\tau, \nu]| \approx 0, \tag{5.8}$$

the bound in (5.7) is very loose and $\mu(\bar{\mathbf{S}}) \ll \left(\sum_{i=1}^{K} \mu(\mathbf{S}_i)\right)/K$. In chapter 3 it was shown that for high resolution using OMP algorithm, it is desirable to have a signal dictionary with small mutual coherence (3.12). Hence, for a set of radar signals satisfying the condition in (5.8), the MIMO radar using OMP algorithm with a *normalized* composite signal dictionary $\bar{\mathbf{S}} = \frac{1}{K}\sum_{j=1}^{K} \mathbf{S}_j$ can result in considerable improvement in target resolution. Furthermore, the condition in (5.8) also provides suitable constraints for designing the set of radar signals.

5.2.1 Resolution

Comparing the MIMO received signal model in equation (5.3) with the radar model presented in section 1.2, the equivalence is readily apparent. As a result, the sparse recovery performance using OMP algorithm on the MIMO radar signal model in equation (5.3) is also applicable to MIMO radar. The following theorem restates the conditions under which a target scene is resolvable in noiseless conditions when OMP algorithm is used.

Theorem 5.2.1 *Consider a MIMO radar with receive signal dictionaries corresponding to each transmit signal denoted as* $\mathbf{S}_1, \ldots, \mathbf{S}_K$*. Let* $\Lambda = \{\theta_1, \ldots, \theta_L\}, \theta_i \in \mathcal{T}, \forall 1 \leq i \leq L$ *denote the set of target parameters in the target scene with associated target amplitudes . Then, the target scene is absolutely resolvable using the OMP algorithm at the radar receiver with a receive dictionary* $\mathbf{S} = \mathbf{S}_1 + \ldots + \mathbf{S}_K$*, if and only if*

$$\max_{\theta \in \overline{\Lambda}} \left\| \mathbf{S}_{\Lambda}^{\dagger} \mathbf{s}_{\theta} \right\|_1 < 1.$$

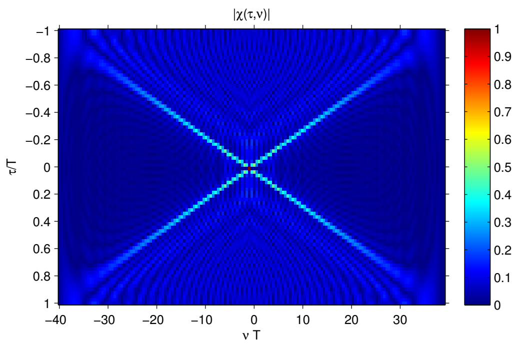

(a) Composite ambiguity function for linear channel combining.

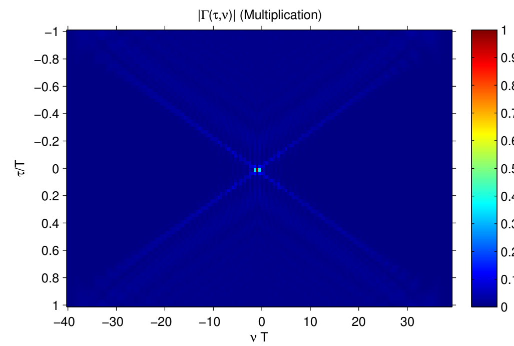

(b) Channel combining by multiplying the ambiguity functions.

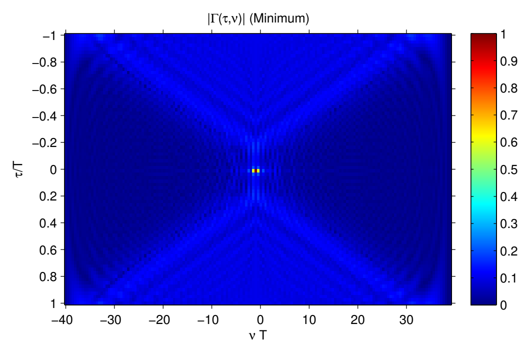

(c) Channel combining using minimum of the two ambiguity functions.

Figure 5.1.: Comparison of different MIMO channel combining techniques for a single target located at $(\tau, \nu) = (0, 0)$ using two transmit signals: An LFM upchirp and an LFM downchirp.

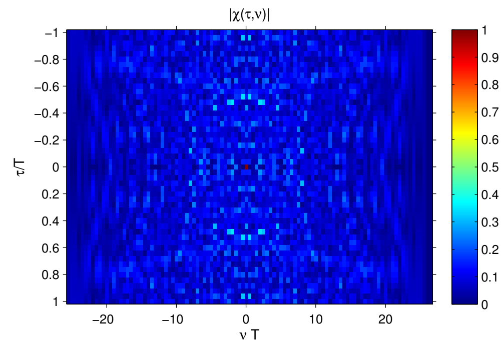

(a) Composite ambiguity function for linear channel combining.

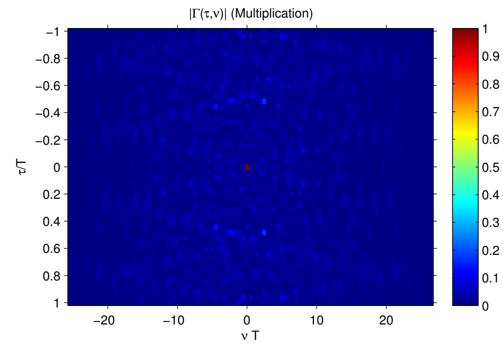

(b) Channel combining by multiplying the ambiguity functions.

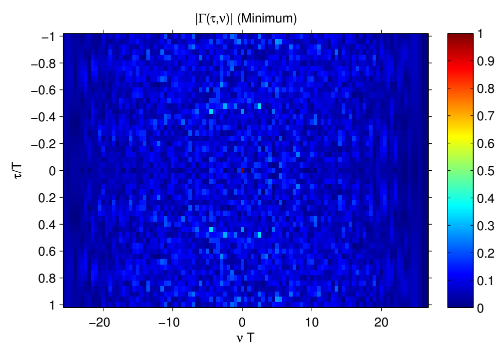

(c) Channel combining using minimum of the two ambiguity functions.

Figure 5.2.: Comparison of different MIMO channel combining techniques for a single target located at $(\tau, \nu) = (0, 0)$ using two transmit signals: Combined 13 by 4 barker code and combined 4 by 13 barker code.

5.2.2 Simulation results

Consider a coherent MIMO radar system utilizing two transmit waveforms, $s_1(t)$ and $s_2(t)$. Both transmit signals are chosen to be LFM chirps with different chirp rate, that is

$$s_i(t) = \frac{1}{\sqrt{T}} rect\left(\frac{t}{T}\right) e^{j\pi k_i t^2}.$$

For this particular example, we use $k_1 = -k_2$. Figure 5.1a shows the composite ambiguity function of the radar system when matched filters are used at the receiver. Figure 5.3b shows the corresponding resolution diagram for the MIMO system. Compared to the resolution plot of an individual LFM chirp shown earlier in Chapter 3, it can be seen that transmitting more than one waveform yields considerable improvement in resolution.

Figure 5.3a presents the resolution plot of a radar system using the pair of combined Barker codes. Once again, the improvement compared to transmitting a single combined Barker code is apparent.

5.3 Nonlinear channel combining

The matched filter output $\hat{\alpha}$ in the previous section is equivalent to filtering the received signal with a bank of matched filters matched to each of the K signals $s_i(t)$, $1 \leq i \leq K$ and then linearly combining the result. Ignoring noise, this can be seen by using the definition $\bar{\mathbf{S}} = \frac{1}{K}\left(\sum_{i=1}^{K} \mathbf{S}_i\right)$ to rewrite the equation (5.4) as

$$\hat{\alpha} = \frac{1}{K} \sum_{i=1}^{K} \mathbf{S}_i^H \mathbf{S} \alpha. \tag{5.9}$$

Nonlinear channel combining techniques have been proposed recently in radar literature [22] to improve the resolution of MIMO radar. Let $f(\mathbf{x})$, $\mathbf{x} \in \mathbb{R}^K$ denote a nonlinear function. In this dissertation, it will be assumed that $f(\mathbf{x})$ is a *monotonic function* over $\mathbb{R}_+^K = [0, \infty]$. Hence, $\forall \mathbf{x}, \mathbf{y} \in \mathbb{R}^K$ such that $[\mathbf{x}]_i \leq [\mathbf{y}]_i$, $\forall 1 \leq i \leq K$, the function satisfies $f(\mathbf{x}) \leq f(\mathbf{y})$.

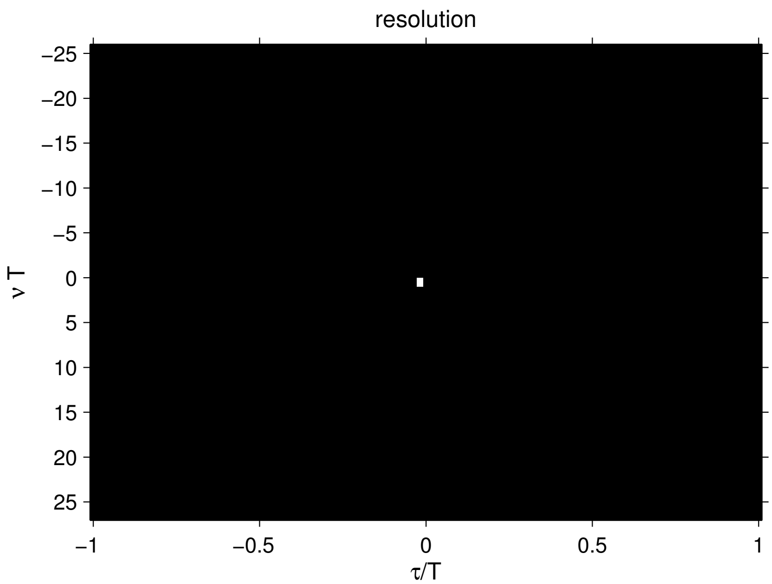

(a) Resolution diagram for the two waveform coherent MIMO radar system using combined 13 by 4 and 4 by 13 barker sequences.

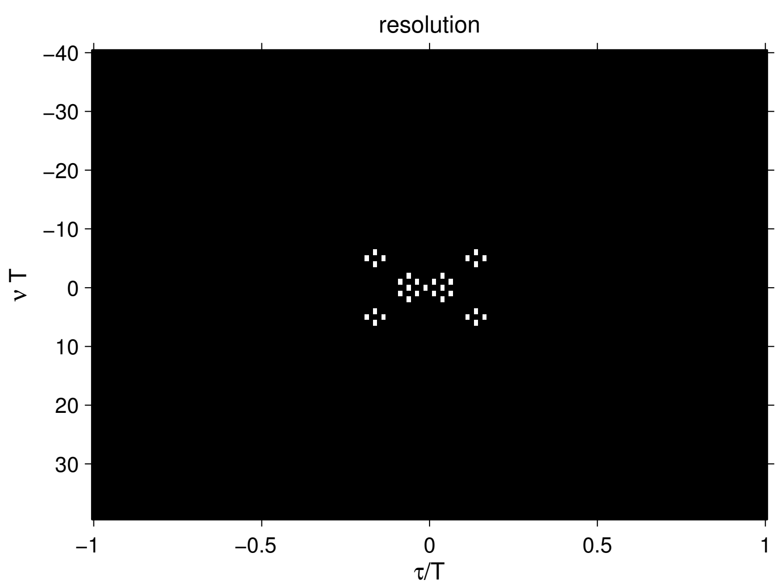

(b) Resolution diagram for the two waveform coherent MIMO radar system using an up-chirp and a down-chirp with $BT = 40$

Figure 5.3.: Resolution plots of coherent MIMO radar systems.

Assuming $f(\cdot)$ as the nonlinear channel combining function, the matched filter estimate of the target scene using nonlinear channel combining techniques proposed in [22] can be expressed as

$$[\hat{\alpha}]_i = \frac{1}{K} f\left(\left[\left|\mathbf{S}_1^H \mathbf{S}\alpha\right|\right]_i, \left[\left|\mathbf{S}_2^H \mathbf{S}\alpha\right|\right]_i, \ldots, \left[\left|\mathbf{S}_K^H \mathbf{S}\alpha\right|\right]_i\right). \tag{5.10}$$

Denoting the vector element wise nonlinear operator $\diamondsuit$, the matched filter estimate in (5.10) can be expressed in vector form as

$$\hat{\alpha} = \frac{1}{K}\left(\left|\mathbf{S}_1^H \mathbf{S}\alpha\right| \diamondsuit \left|\mathbf{S}_2^H \mathbf{S}\alpha\right| \diamondsuit \ldots \diamondsuit \left|\mathbf{S}_K^H \mathbf{S}\alpha\right|\right). \tag{5.11}$$

Using the notation $\Gamma[\tau,\nu] = [\hat{\alpha}]_{\tau M+\nu}$ for the delay Doppler image of $\hat{\alpha}$. Then, for a single target located at $[\tau,\nu] = [0,0]$, the delay Doppler image using (5.11) can be expressed as

$$\begin{aligned}\Gamma[\tau,\nu] &= \frac{1}{K}\Big(\left[\left|\mathbf{S}_1^H \mathbf{s}_{0,0}\right|\right]_{\tau M+\nu} \left|[\alpha]_0\right| \diamondsuit \ldots \diamondsuit \left[\left|\mathbf{S}_K^H \mathbf{s}_{0,0}\right|\right]_{\tau M+\nu} \left|[\alpha]_0\right|\Big), \\ &= \frac{1}{K}\left(\left|\chi_1^C[\tau,\nu]\right| \left|[\alpha]_0\right| \diamondsuit \ldots \diamondsuit \left|\chi_K^C[\tau,\nu]\right| \left|[\alpha]_0\right|\right),\end{aligned} \tag{5.12}$$

where $\chi_i^C[\tau,\nu] = \mathbf{S}_i^H \mathbf{s}_{0,0}$, $\forall 1 \leq i \leq K$. Figures 5.2 and 5.1 compare the delay Doppler image obtained after channel combining for a single target located at $[\tau,\nu] = [0,0]$ with the composite ambiguity function. In general, it can be seen that in a single target environment, nonlinear combining techniques result in considerably reduced sidelobes compared to the linear combining of channels. In a multi-target environment, however, it has been shown that nonlinear channel combining can cause the creation of *virtual targets* [22]. These are false targets created due to the nonlinear interaction of the off diagonal elements in the matrices $\mathbf{S}_i^H \mathbf{S}$. To overcome this problem, the authors in [22] have suggested using a larger number of diverse radar signals to reduce the affect of virtual targets. In this section, however, we combine the nonlinear channel combining idea (5.11) with the OMP algorithm to propose an algorithm that can improve resolution without suffering from some problems with the nonlinear technique. Algorithm 5.1 shows the new algorithm which will be called *Nonlinear MIMO matching pursuit* (NLMMP) from now on. Like the MOMP algorithm presented in chapter 4, the NLMMP differs from OMP algorithm only in the

Algorithm 5.1 Nonlinear MIMO pursuit solution for signal decomposition of $r = \sum_k a_k s_k + w$. The nonlinear channel combining operator is denoted $\diamondsuit$ and $\tilde{\mathbf{S}}$ represents the normalized version of the composite signal dictionary $\mathbf{S} = \left(\sum_{i=1}^{K} \mathbf{S}_i\right)$. All columns of $\tilde{\mathbf{S}}$ are assumed to be unit norm.

- Initialize $\hat{\Lambda} = \emptyset$, $\bar{\mathbf{r}} = \mathbf{r}$, γ
- $\sigma = \max_\theta \left|\tilde{\mathbf{s}}_\theta^H \mathbf{r}\right|$
- while $\sigma > \gamma$
  - $\mathbf{z}_i = \left|\tilde{\mathbf{S}}_i^H \bar{\mathbf{r}}\right|$, $\forall 1 \leq i \leq K$
  - $\mathbf{z} = \mathbf{z}_1 \diamondsuit \mathbf{z}_2 \diamondsuit \ldots \diamondsuit \mathbf{z}_K$
  - $\hat{\theta} = \arg\max_\theta \left[\mathbf{z}\right]_\theta$
  - $\hat{\Lambda} = \hat{\Lambda} \cup \hat{\theta}$
  - $\hat{\alpha} = \arg\min_\alpha \left\|\mathbf{r} - \tilde{\mathbf{S}}_{\hat{\Lambda}} \alpha\right\|^2$
  - $\bar{\mathbf{r}} = \mathbf{r} - \tilde{\mathbf{S}}_{\hat{\Lambda}} \hat{\alpha}$
  - $\sigma = \max_\theta \left|\tilde{\mathbf{s}}_\theta^H \bar{\mathbf{r}}\right|$

greedy target selection step. Intuitively, since the nonlinear combining step in (5.11) reduces the sidelobes, it results in decreased mutual coherence and hence improved resolution.

Consider a target scene with target parameter set Λ. The received signal, $\mathbf{r}$, from such a target scene is then in the column space of $\bar{\mathbf{S}}_\Lambda$. Hence if the first i iterations of the NLMMP algorithm select targets in Λ, that is $\hat{\Lambda} \subseteq \Lambda$, then by definition the residue vector in $i+1$ iteration is also in the column space of $\bar{\mathbf{S}}_\Lambda$. As a result, to be able to absolutely resolve a target scene with target parameters Λ, it is necessary to satisfy

$$\sup_{\mathbf{h} \in \mathrm{Col}\left(\bar{\mathbf{S}}_\Lambda\right)} \frac{\left\|\left|\mathbf{S}_{1,\bar{\Lambda}}^H \mathbf{h}\right| \diamondsuit \ldots \diamondsuit \left|\mathbf{S}_{K,\bar{\Lambda}}^H \mathbf{h}\right|\right\|_\infty}{\left\|\left|\mathbf{S}_{1,\Lambda}^H \mathbf{h}\right| \diamondsuit \ldots \diamondsuit \left|\mathbf{S}_{K,\Lambda}^H \mathbf{h}\right|\right\|_\infty} < 1, \tag{5.13}$$

where $\mathbf{S}_{i,\Lambda}$ and $\mathbf{S}_{1,\overline{\Lambda}}^H$ denote the subdictionaries of $\mathbf{S}_i$ consisting only of columns indexed by the set Λ and $\overline{\Lambda}$, respectively. The exact recovery condition in (5.13) is, in general, difficult to compute. Instead, it may be useful to find an upperbound to the exact recovery condition. Using the notation from algorithm 5.1, in any iteration of the NLMMP algorithm, a correct target is selected if

$$\forall j \in \overline{\Lambda},\ \exists i \in \Lambda\ s.t.\ [\mathbf{z}]_i > [\mathbf{z}]_j\,.$$

Since $\bar{\mathbf{r}} \in \mathrm{Col}\left(\mathbf{S}_\Lambda\right)$, let $\bar{\mathbf{r}} = \mathbf{S}_\Lambda \alpha$. Then, $\forall i \in \overline{\Lambda}$,

$$\begin{aligned} [\mathbf{z}]_i &= \left|\mathbf{s}_{1,i}^H \mathbf{S}_\Lambda \alpha\right| \diamondsuit \ldots \diamondsuit \left|\mathbf{s}_{K,i}^H \mathbf{S}_\Lambda \alpha\right|, \\ &\leq \left\{\left\|\mathbf{s}_{1,i}^H \mathbf{S}_\Lambda\right\|_1 \|\alpha\|_\infty\right\} \diamondsuit \ldots \diamondsuit \left\{\left\|\mathbf{s}_{K,i}^H \mathbf{S}_\Lambda\right\|_1 \|\alpha\|_\infty\right\}, \end{aligned} \tag{5.14}$$

where $\mathbf{s}_{l,i}$ represents the i^{th} column in the synthesis matrix $\mathbf{S}_l$ of the l^{th} transmit signal. Similarly, $\forall i \in \Lambda$ and $1 \leq l \leq K$,

$$\begin{aligned} [\mathbf{z}_l]_i &= \left|\mathbf{s}_{l,i}^H \mathbf{S}_\Lambda \alpha\right| \\ &= \left|\mathbf{s}_{l,i}^H \mathbf{s}_i \alpha_i + \sum_{j \in \Lambda, j \neq i} \mathbf{s}_{l,j}^H \mathbf{s}_j \alpha_j\right| \\ &\geq \left|\mathbf{s}_{l,i}^H \mathbf{s}_i \alpha_i\right| - \left|\sum_{j \in \Lambda, j \neq i} \mathbf{s}_{l,j}^H \mathbf{s}_j \alpha_j\right|, \end{aligned} \tag{5.15}$$

where α_i denotes the target amplitude corresponding to target with parameters $i \in \Lambda$. Define

$$\eta_l = \min_{i \in \Lambda} \left|\mathbf{s}_{l,i}^H \mathbf{s}_i\right|, \tag{5.16}$$

and

$$\mu_\Lambda^l = \max_{i,j \in \Lambda, i \neq j} \left|\mathbf{s}_{l,i}^H \mathbf{s}_j\right|. \tag{5.17}$$

Using (5.16) and (5.17) in (5.15), $\forall i \in \Lambda$, $[\mathbf{z}_l]_i$ can be bounded as

$$[\mathbf{z}_l]_i \geq \eta_l \left|\alpha_i\right| - \left(\|\alpha\|_1 - |\alpha_i|\right) \mu_\Lambda^l.$$

Furthermore, since the nonlinear channel combining is assumed to be monotonic, $\forall i \in \Lambda$, the elements of vector $\mathbf{z}$ in algorithm 5.1 can be bounded as

$$[\mathbf{z}]_i \geq \left\{\eta_1 |\alpha_i| - \left(\|\alpha\|_1 - |\alpha_i|\right) \mu_\Lambda^1\right\} \diamondsuit \ldots \diamondsuit \left\{\eta_K |\alpha_i| - \left(\|\alpha\|_1 - |\alpha_i|\right) \mu_\Lambda^K\right\}.$$

Hence, the maximum absolute value at a target position after nonlinear channel combining can be bounded as

$$\max_{i\in\Lambda}[\mathbf{z}]_i \geq \left\{\eta_1 \|\alpha\|_\infty - \left(\|\alpha\|_1 - \|\alpha\|_\infty\right)\mu_\Lambda^1\right\} \diamondsuit \ldots \diamondsuit \left\{\eta_K \|\alpha\|_\infty - \left(\|\alpha\|_1 - \|\alpha\|_\infty\right)\mu_\Lambda^K\right\}.$$

The NLMMP algorithm will select a target $\theta \in \Lambda$ in this iteration if

$$\frac{\max_{i\in\overline{\Lambda}}[\mathbf{z}]_i}{\max_{i\in\Lambda}[\mathbf{z}]_i} < 1.$$

As a result if received signal noise is negligible, for any residue vector $\bar{\mathbf{r}} = \mathbf{S}_\Lambda\alpha$, the greedy target selection step chooses a correct target if

$$\frac{\max_{i\in\overline{\Lambda}}\left\{\left\|\mathbf{s}_{1,i}^H\mathbf{S}_\Lambda\right\|_1\|\alpha\|_\infty\right\}\diamondsuit\ldots\diamondsuit\left\{\left\|\mathbf{s}_{K,i}^H\mathbf{S}_\Lambda\right\|_1\|\alpha\|_\infty\right\}}{\left\{\eta_1 \|\alpha\|_\infty - \left(\|\alpha\|_1 - \|\alpha\|_\infty\right)\mu_\Lambda^1\right\} \diamondsuit \ldots \diamondsuit \left\{\eta_K \|\alpha\|_\infty - \left(\|\alpha\|_1 - \|\alpha\|_\infty\right)\mu_\Lambda^K\right\}} < 1. \tag{5.18}$$

The recovery condition in (5.18) requires knowledge of the target amplitudes α in the residue vector. In the following sections, the recovery performance of two nonlinear operations proposed in [22] is further analyzed and conditions for absolute resolution are derived.

5.3.1 Point-wise Multiplication

Consider a MIMO radar using the NLMMP algorithm with a nonlinear function $f(\mathbf{x}) = [\mathbf{x}]_0[\mathbf{x}]_1\ldots[\mathbf{x}]_{K-1}$. It can be easily verified that $f(\mathbf{x})$ is a monotonic function and hence satisfies the necessary requirements for a valid channel combining function. For any two vectors $\mathbf{x},\mathbf{y} \in \mathbb{R}^L$, the nonlinear operator $\diamondsuit$ corresponding to $f(\cdot)$ is

$$\begin{bmatrix}[\mathbf{x}]_0\\ \vdots\\ [\mathbf{x}]_{L-1}\end{bmatrix} \diamondsuit \begin{bmatrix}[\mathbf{y}]_0\\ \vdots\\ [\mathbf{y}]_{L-1}\end{bmatrix} = \begin{bmatrix}[\mathbf{x}]_0[\mathbf{y}]_0\\ \vdots\\ [\mathbf{x}]_{L-1}[\mathbf{y}]_{L-1}\end{bmatrix}.$$

As a result, the nonlinear operator $\diamondsuit$ in this section will be called the *pointwise multiplication* operator. To understand why using this operator makes sense, it is useful to compare the composite ambiguity function with the output of pointwise

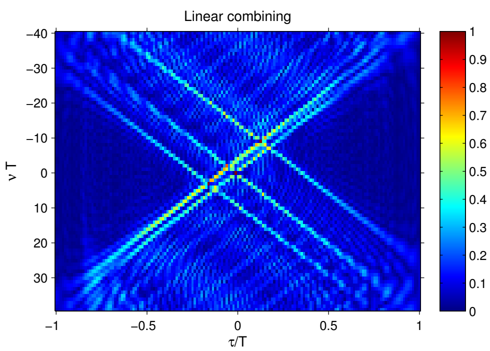

(a) Linearly combining the channels

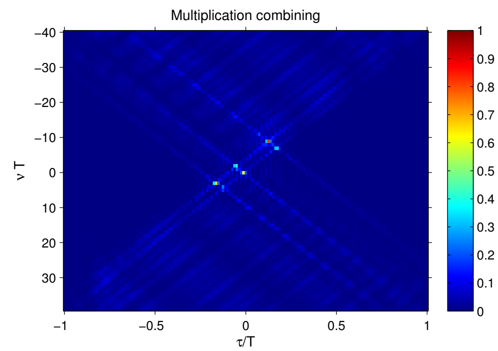

(b) Point-wise multiplication combining

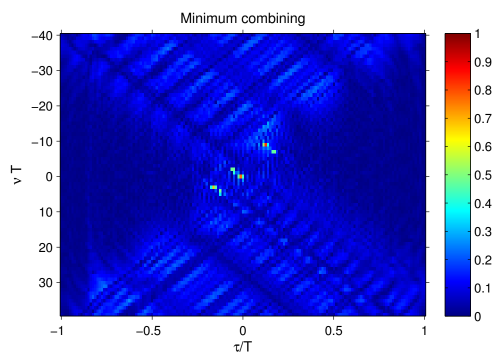

(c) Point-wise minimum combining

Figure 5.4.: Comparison of linear channel combining and nonlinear channel combining in a multi-target environment using LFM upchirp and downchirp. The target scene consists of three targets at $(\tau_1, \nu_1) = (0, 0)$, $(\tau_1, \nu_1) = (0.15T, 3/T)$ and $(\tau_1, \nu_1) = (0.1375T, -9/T)$.

multiplication combining for a single target located at $[\tau, \nu] = [0, 0]$. Figures (5.2b) and (5.1b) show that the sidelobes at the output of NLMMP algorithm, when pointwise multiplication is used, are much smaller than the sidelobes in the corresponding composite ambiguity functions in (5.2a) and (5.1a) respectively. Since the recovery condition of pursuit algorithms is, in general, related to the peak sidelobe to peak mainlobe ratio, smaller sidelobes indicate better recovery performance. However, it is important to point out that unlike the linear channel combining approach, the output of nonlinear channel combining can no longer be related to an imaging system (1.24) where the ambiguity function acts as the point spread function. Consequently, in a target scene with multiple targets, the nonlinearly combined output can no longer be expressed as a linear combination of shifted versions of the function $\Gamma[\tau, \nu]$ shown in figures (5.2b) and (5.1b). Instead, the nonlinear interaction between the channels can sometimes cause significant sidelobes in a multi-target environment. These undesirable sidelobes have been termed virtual targets in [22]. Figure 5.4b shows the result of channel combining using pointwise multiplication in a target environment with 3 targets. It can be seen that it is difficult to differentiate between actual targets and virtual targets. In this section, it will be shown that the NLMMP algorithm can remove these sidelobes in certain conditions.

Theorem 5.3.1 *Consider a MIMO radar with receive signal dictionaries corresponding to each transmit signal denoted as* $\mathbf{S}_1, \ldots, \mathbf{S}_K$. *Let* $\Lambda = \{\theta_1, \ldots, \theta_L\}, \theta_i \in \mathcal{T}, \forall 1 \leq i \leq L$ *denote the set of target parameters in the target scene. Then, the target scene is guaranteed to be absolutely resolvable using NLMMP algorithm with pointwise multiplication if*

$$\frac{\kappa_\Lambda}{\{\eta_1 + (1 - |\Lambda|)\,\mu_\Lambda^1\} \times \ldots \times \{\eta_K + (1 - |\Lambda|)\,\mu_\Lambda^K\}} < 1, \tag{5.19}$$

where $\kappa_\Lambda = \max_{i \in \overline{\Lambda}} \left[\left\{ \left\| \mathbf{s}_{1,i}^H \mathbf{S}_\Lambda \right\|_1 \right\} \times \ldots \times \left\{ \left\| \mathbf{s}_{K,i}^H \mathbf{S}_\Lambda \right\|_1 \right\} \right]$ *and* η_i *and* μ_Λ^i *are defined in (5.16) and (5.17), respectively. Furthermore, if the condition in (5.19) is not satisfied, the target scene may or may not be absolutely resolvable.*

Proof From equation (5.18), the condition for correct recovery when pointwise multiplication operator is used can be written as

$$\frac{\max_{i\in\overline{\Lambda}}\left[\left\{\left\|\mathbf{s}_{1,i}^{H}\mathbf{S}_{\Lambda}\right\|_1\|\alpha\|_\infty\right\}\times\ldots\times\left\{\left\|\mathbf{s}_{K,i}^{H}\mathbf{S}_{\Lambda}\right\|_1\|\alpha\|_\infty\right\}\right]}{\{\eta_1\|\alpha\|_\infty-(\|\alpha\|_1-\|\alpha\|_\infty)\,\mu_\Lambda^1\}\times\ldots\times\{\eta_K\|\alpha\|_\infty-(\|\alpha\|_1-\|\alpha\|_\infty)\,\mu_\Lambda^K\}}<1.$$

Dividing both numerator and denominator by $\|\alpha\|_\infty$, the recovery condition can be expressed as

$$\frac{\max_{i\in\overline{\Lambda}}\left[\left\{\left\|\mathbf{s}_{1,i}^{H}\mathbf{S}_{\Lambda}\right\|_1\right\}\times\ldots\times\left\{\left\|\mathbf{s}_{K,i}^{H}\mathbf{S}_{\Lambda}\right\|_1\right\}\right]}{\{\eta_1-(\|\alpha\|_1/\|\alpha\|_\infty-1)\,\mu_\Lambda^1\}\times\ldots\times\{\eta_K-(\|\alpha\|_1/\|\alpha\|_\infty-1)\,\mu_\Lambda^K\}}<1.$$

Also, since $\|\alpha\|_1/\|\alpha\|_\infty\leq|\Lambda|$, if

$$\frac{\max_{i\in\overline{\Lambda}}\left[\left\{\left\|\mathbf{s}_{1,i}^{H}\mathbf{S}_{\Lambda}\right\|_1\right\}\times\ldots\times\left\{\left\|\mathbf{s}_{K,i}^{H}\mathbf{S}_{\Lambda}\right\|_1\right\}\right]}{\{\eta_1-(|\Lambda|-1)\,\mu_\Lambda^1\}\times\ldots\times\{\eta_K-(|\Lambda|-1)\,\mu_\Lambda^K\}}<1,$$

then correct recovery of Λ is guaranteed irrespective of the target amplitude vector α. ■

Figure 5.5 shows the resolution plot obtained using Theorem 5.3.1 for the LFM and combined Barker code pairs. Compared to the resolution plots obtained for linear channel combining technique, the NLMMP algorithm seems to have poor resolution. However, it should be kept in mind that these plots were obtained using a loose bound. In section 5.5, it will be shown that the actual recovery performance of NLMMP algorithm using multiplication is much better than that suggested by these plots.

The recovery condition in (5.19) can sometimes be too loose to be useful. Furthermore, it is difficult to relate the condition in (5.19) to the recovery conditions of each of the K individual radar transmit signals.

Consider the recovery condition in (5.13) for the NLMMP algorithm. For pointwise multiplication operator, the left side of the condition in (5.13) can be restated as

$$\begin{aligned}\sup_{\mathbf{h}\in\mathrm{Col}(\bar{\mathbf{S}}_\Lambda)}\frac{\left\|\left|\mathbf{S}_{1,\overline{\Lambda}}^{H}\mathbf{h}\right|\times\ldots\times\left|\mathbf{S}_{K,\overline{\Lambda}}^{H}\mathbf{h}\right|\right\|_\infty}{\left\|\left|\mathbf{S}_{1,\Lambda}^{H}\mathbf{h}\right|\times\ldots\times\left|\mathbf{S}_{K,\Lambda}^{H}\mathbf{h}\right|\right\|_\infty} &\leq \sup_{\mathbf{h}\in\mathrm{Col}(\bar{\mathbf{S}}_\Lambda)}\frac{\left\|\mathbf{S}_{1,\overline{\Lambda}}^{H}\mathbf{h}\right\|_\infty\times\ldots\times\left\|\mathbf{S}_{K,\overline{\Lambda}}^{H}\mathbf{h}\right\|_\infty}{\left\|\left|\mathbf{S}_{1,\Lambda}^{H}\mathbf{h}\right|\times\ldots\times\left|\mathbf{S}_{K,\Lambda}^{H}\mathbf{h}\right|\right\|_\infty}\\ &\leq r_1(\Lambda)\,r_2(\Lambda)\ldots r_K(\Lambda)\,\rho(\Lambda)\end{aligned}\tag{5.20}$$

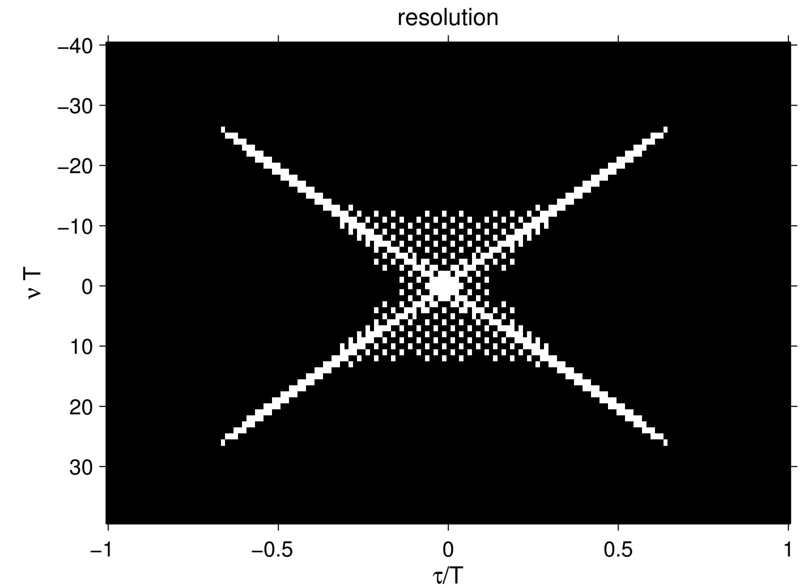

(a) Resolution plot of NLMMP algorithm for LFM upchirp and downchirp.

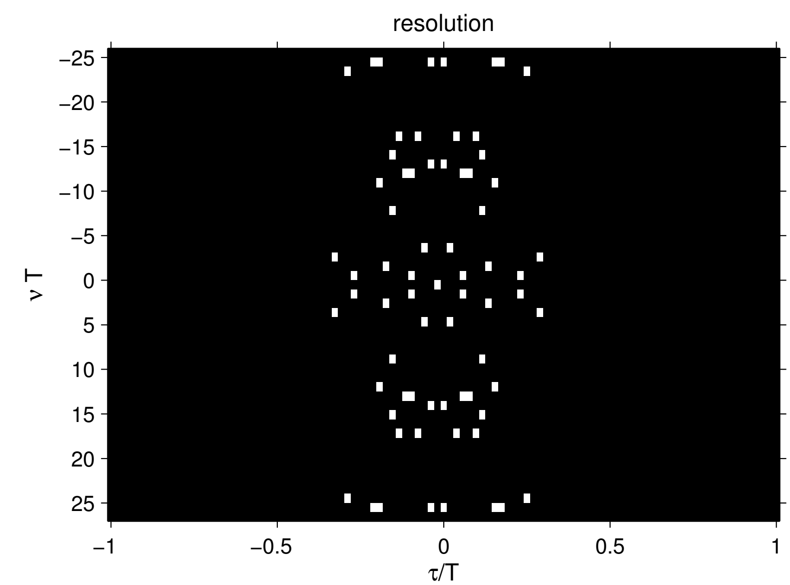

(b) Resolution plot of NLMMP algorithm for the two combined barker codes.

Figure 5.5.: Resolution bound of NLMMP algorithm using pointwise multiplication for channel combining.

where $r_i(\Lambda)$ denotes the recovery condition of the received signal $\mathbf{r} = \mathbf{S}_\Lambda \alpha$ using the mismatched dictionary $\mathbf{S}_i$ (theorem 4.1.1) and

$$\rho(\Lambda) = \sup_{\mathbf{h} \in \mathrm{Col}(\bar{\mathbf{S}}_\Lambda)} \frac{\left\|\mathbf{S}_{1,\Lambda}^H \mathbf{h}\right\|_\infty \times \ldots \times \left\|\mathbf{S}_{K,\Lambda}^H \mathbf{h}\right\|_\infty}{\left\|\left|\mathbf{S}_{1,\Lambda}^H \mathbf{h}\right| \times \ldots \times \left|\mathbf{S}_{K,\Lambda}^H \mathbf{h}\right|\right\|_\infty}. \tag{5.21}$$

In general, when the targets in the target scene have significantly different radar cross sections, the maximum magnitude in the mismatched filter output will occur at the same target for all K banks of mismatched filters. This implies that $\forall 1 \le j \le K$, the index $\hat{i} = \arg\max_i \left[\left|\mathbf{S}_{j,\Lambda}^H \mathbf{h}\right|\right]_i$ will be same. Similarly, when multiple targets in the target scene have radar cross sections approximately equal to the maximum radar cross section in the target scene, $\left\|\mathbf{S}_{1,\Lambda}^H \mathbf{h}\right\|_\infty \times \ldots \times \left\|\mathbf{S}_{K,\Lambda}^H \mathbf{h}\right\|_\infty \approx \left\|\left|\mathbf{S}_{1,\Lambda}^H \mathbf{h}\right| \times \ldots \times \left|\mathbf{S}_{K,\Lambda}^H \mathbf{h}\right|\right\|$. Hence, in general, $\rho(\Lambda) \approx 1$ and a rough test for resolvability of a target scene is $r_1(\Lambda) \times \ldots \times r_K(\Lambda) < 1$.

Equation (5.20) also shows that to obtain high resolution using channel multiplication in NLMMP, it is important to select a set of waveforms with diverse resolution plots. For example, in a MIMO radar with two transmit signals, it is important to select a transmit signal pair that have resolution plots with no common non-resolvable points. Consider a target scene Λ that is resolvable using signal 1 but not using signal 2. This means that $r_1(\Lambda) < 1$ and $r_2(\Lambda) > 1$. Then, for resolution of this target scene using pointwise multiplication, it is desirable to have $r_1(\Lambda) \times r_2(\Lambda) < 1$. Hence, when designing a set of radar transmit signals for use with NLMMP algorithm utilizing pointwise multiplication, a rough rule of thumb is to ensure that the product of individual recovery factors is less than 1.

5.3.2 Point-wise Minimum

Another nonlinear channel combining operator proposed in [22] is the pointwise minimum operator which is equivalent to the nonlinear function $f(\mathbf{x}) = \min_i [\mathbf{x}]_i$. Since $f(\mathbf{x})$ is monotonic, it is a valid function for use in NLMMP algorithm. For any two vectors $\mathbf{x}, \mathbf{y} \in \mathbb{R}^L$, the nonlinear operator $\diamondsuit$ corresponding to pointwise minimum operation can be expressed as

$$\begin{bmatrix} [\mathbf{x}]_0 \\ \vdots \\ [\mathbf{x}]_{L-1} \end{bmatrix} \diamondsuit \begin{bmatrix} [\mathbf{y}]_0 \\ \vdots \\ [\mathbf{y}]_{L-1} \end{bmatrix} = \begin{bmatrix} \min\left([\mathbf{x}]_0, [\mathbf{y}]_0\right) \\ \vdots \\ \min\left([\mathbf{x}]_{L-1} [\mathbf{y}]_{L-1}\right) \end{bmatrix}.$$

Intuitively, it is easy to see why channel combining using minimum operator can improve the resolution of a radar. Although all the sidelobes in a pulse Doppler radar cannot be made zero due to the uncertainty principle, it is possible to design a set of K radar signals with non overlapping sidelobes. This means that if a transmit signal has a significant sidelobe at $[\tau_1, \nu_1]$, there is at least one waveform in the set of transmitted signals which has negligible sidelobe at $[\tau_1, \nu_1]$. Figures 5.2c and 5.1c show the output of NLMMP algorithm using pointwise minimum for a target located at $[\tau, \nu] = [0, 0]$. Compared to the composite ambiguity functions in figures 5.2a and 5.1a, it can be seen that the pointwise minimum combining reduces the sidelobes in the output. However, as was discussed in section 5.3.1, nonlinear channel combining techniques suffer from virtual targets when a target scene consists of multiple targets. Figure 5.4c shows the effect of pointwise minimum channel combining of the matched filter outputs of all channels. Compared to linear channel combining output in figure 5.4a, it is apparent that pointwise minimum combining decreases the sidelobes. However, the presence of virtual targets in figure 5.4c can increase the false alarm rate of the radar system.

Theorem 5.3.2 *Consider a MIMO radar with receive signal dictionaries corresponding to each transmit signal denoted as* $\mathbf{S}_1, \ldots, \mathbf{S}_K$*. Let* $\Lambda = \{\theta_1, \ldots, \theta_L\}, \theta_i \in \mathcal{T}, \forall 1 \leq i \leq L$ *denote the set of target parameters in the target scene. Then, the target scene is guaranteed to be absolutely resolvable using NLMMP algorithm with pointwise minimum* combining *if*

$$\frac{\kappa_\Lambda}{\min_{1 \leq j \leq K} \left\{\eta_j + (1 - |\Lambda|)\, \mu_\Lambda^j\right\}} < 1, \tag{5.22}$$

where $\kappa_\Lambda = \max_{i\in\overline{\Lambda}}\left[\min_{1\le j\le K}\left\{\left\|\mathbf{s}_{j,i}^H\mathbf{S}_\Lambda\right\|_1\right\}\right]$ *and* η_i *and* μ_Λ^i *are defined in (5.16) and (5.17), respectively. Furthermore, if the condition in (5.22) is not satisfied, the target scene may or may not be absolutely resolvable.*

Proof From equation (5.18), the condition for correct recovery when pointwise multiplication operator is used can be written as

$$\frac{\max_{i\in\overline{\Lambda}}\left[\min_{1\le j\le K}\left\{\left\|\mathbf{s}_{j,i}^H\mathbf{S}_\Lambda\right\|_1\|\alpha\|_\infty\right\}\right]}{\min_{1\le j\le K}\left\{\eta_j\|\alpha\|_\infty-\left(\|\alpha\|_1-\|\alpha\|_\infty\right)\mu_\Lambda^j\right\}}<1.$$

Dividing both numerator and denominator by $\|\alpha\|_\infty$, the recovery condition can be expressed as

$$\frac{\max_{i\in\overline{\Lambda}}\left[\min_{1\le j\le K}\left\{\left\|\mathbf{s}_{j,i}^H\mathbf{S}_\Lambda\right\|_1\right\}\right]}{\min_{1\le j\le K}\left\{\eta_j-\left(\|\alpha\|_1/\|\alpha\|_\infty-1\right)\mu_\Lambda^j\right\}}<1.$$

Also, since $\|\alpha\|_1/\|\alpha\|_\infty\le|\Lambda|$, if

$$\frac{\max_{i\in\overline{\Lambda}}\left[\min_{1\le j\le K}\left\{\left\|\mathbf{s}_{j,i}^H\mathbf{S}_\Lambda\right\|_1\right\}\right]}{\min_{1\le j\le K}\left\{\eta_j-\left(|\Lambda|-1\right)\mu_\Lambda^j\right\}}<1,$$

then correct recovery of Λ is guaranteed irrespective of the target amplitude vector α. ■

Theorem 5.3.3 *Suppose a MIMO radar with receive signal dictionaries* $\mathbf{S}_1,\ldots,\mathbf{S}_K$ *is used to estimate a target scene with target parameters* $\Lambda=\{\theta_1,\ldots,\theta_L\}$*. Assume that the targets selected in the first* j *iterations of the NLMMP algorithm using pointwise minimum combining are in* Λ*. If the residue vector in the* $j+1$ *iteration of the NLMMP algorithm is* $\bar{\mathbf{r}}=\mathbf{S}_\Lambda\alpha_\Lambda$*, then the selected target in* $j+1$ *iteration is also in* Λ *if*

$$r_i(\Lambda)=\max_{\theta\in\overline{\Lambda}}\left\|\left(\mathbf{S}_\Lambda^H\mathbf{S}_{i,\Lambda}\right)^{-1}\mathbf{S}_\Lambda^H\mathbf{s}_{i,\theta}\right\|_1<1,$$

where $i=\arg\min_i\left\|\mathbf{S}_{i,\Lambda}^H\bar{\mathbf{r}}\right\|_\infty$.

Proof Let $i=\arg\min_i\left\|\mathbf{S}_{i,\Lambda}^H\bar{\mathbf{r}}\right\|_\infty$. Then the recovery condition in equation (5.13) for $\mathbf{h}=\bar{\mathbf{r}}$ can be written as

$$\frac{\min_{1\le j\le K}\left\|\mathbf{S}_{j,\overline{\Lambda}}^H\bar{\mathbf{r}}\right\|_\infty}{\left\|\mathbf{S}_{i,\Lambda}^H\bar{\mathbf{r}}\right\|_\infty}<1. \tag{5.23}$$

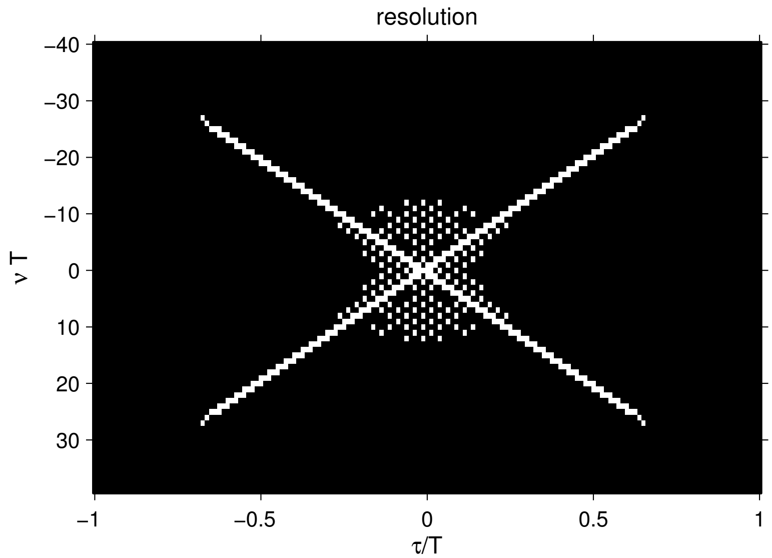

(a) Resolution plot of NLMMP algorithm for LFM upchirp and downchirp.

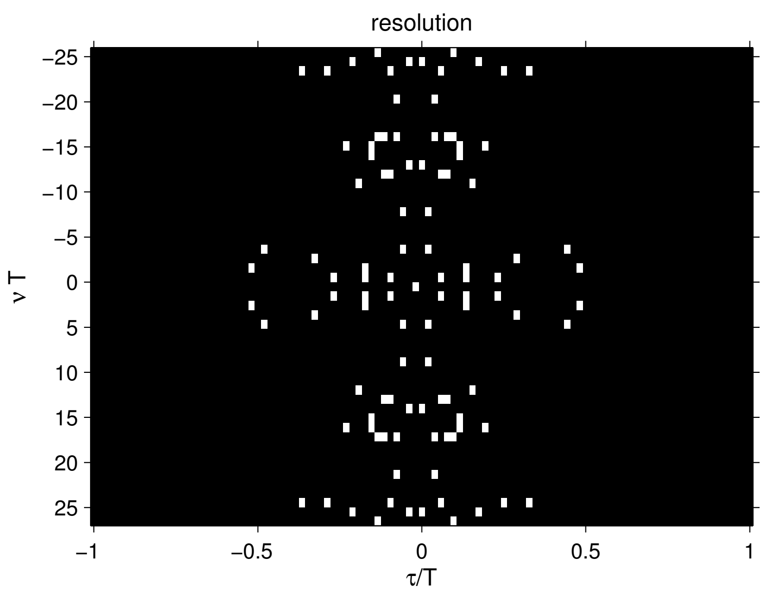

(b) Resolution plot of NLMMP algorithm for the two combined barker codes.

Figure 5.6.: Resolution bound of NLMMP algorithm using pointwise minimum for channel combining.

However, since $\min_{1\leq j\leq K}\left\|\mathbf{S}_{j,\overline{\Lambda}}^{H}\bar{\mathbf{r}}\right\|_{\infty}\leq\left\|\mathbf{S}_{i,\overline{\Lambda}}^{H}\bar{\mathbf{r}}\right\|_{\infty}$, the left term in equation (5.23) can be bounded as

$$\begin{aligned}\frac{\left\|\mathbf{S}_{i,\overline{\Lambda}}^{H}\bar{\mathbf{r}}\right\|_{\infty}}{\left\|\mathbf{S}_{i,\Lambda}^{H}\bar{\mathbf{r}}\right\|_{\infty}} &\leq \sup_{\bar{\mathbf{r}}\in\mathrm{Col}(\mathbf{S}_{\Lambda})}\frac{\left\|\mathbf{S}_{i,\overline{\Lambda}}^{H}\bar{\mathbf{r}}\right\|_{\infty}}{\left\|\mathbf{S}_{i,\Lambda}^{H}\bar{\mathbf{r}}\right\|_{\infty}},\\ &= r_i\left(\Lambda\right).\end{aligned}$$

Hence, correct recovery of the target scene in noiseless conditions is guaranteed when $r_i\left(\Lambda\right)<1$. ■

Since theorem 5.3.3 holds for all $\bar{\mathbf{r}}\in\mathrm{Col}\left(\mathbf{S}_{\Lambda}\right)$, a direct consequence is that a target scene with target parameters given by the set Λ is absolutely resolvable using NLMMP with minimum channel combining if

$$\max_{1\leq i\leq K} r_i\left(\Lambda\right)<1.$$

This shows that if a target scene is resolvable using MOMP algorithm with each of the K signal dictionaries $\mathbf{S}_1,\ldots,\mathbf{S}_K$, then it is also resolvable using NLMMP with pointwise minimum combining. However, it should be kept in mind that both theorems 5.3.2 and 5.3.3 give a lower bound on the resolution performance. Hence, the resolution plots in Figure 5.6 should be considered with a grain of salt. Simulation results later in this chapter will show that NLMMP with minimum channel combining provides improved resolution performance compared to the OMP or MOMP algorithm.

5.4 Resolution in noise

Detection performance of a single target using nonlinear channel combining techniques was analyzed by Rasool in [22]. In comparison to the matched filter, it was shown that the channel combining using multiplication and minimum operation require approximately 1dB and 2dB more SNR to achieve the same probability of detection. It was argued that the decrease in sidelobes merits the relatively small loss in detection performance.

The detection performance of NLMMP algorithm is, however, different from the results derived in [22]. This is because the NLMMP algorithm uses matched filtering in every iteration to decide if a target is present or not. This was discussed earlier in section 4.1.2. As a result, irrespective of the channel combining operation used, the threshold γ in NLMMP algorithm is the same as matched filter threshold derived in section 2.4.

Figure (5.7) shows the probability of resolution of NLMMP algorithm in comparison with the OMP algorithm. Three different target scenes with peak sidelobe to peak mainlobe ratio of 0.53, 0.65 and 0.71 were used. In all three cases, figure (5.7) shows that NLMMP algorithm using pointwise multiplication has resolution performance similar to the OMP algorithm using composite signal dictionary. At lower SNR however, NLMMP algorithm using pointwise minimum operator requires about 0.5dB more SNR to achieve the same resolution performance in all three cases. This can be attributed to the loss in SNR associated with channel combining using the minimum operation as compared to the linear channel combining.

5.5 Target scene recovery examples

Although the resolution plots in section 5.3 using loose recovery bounds leave much to be desired, our simulations show that the actual performance of NLMMP algorithm is much better. In this section, a radar system using the combined Barker code pair in section 5.1 is assumed.

Figure 5.8 shows three different target scenes with all targets having same phase and amplitude. Matched filter output using linear channel combining and two nonlinear channel combining techniques is shown in Figure 5.9. It can be seen that although the nonlinear channel combining can reduce the total sidelobe energy, the presence of virtual targets still makes target resolution difficult.

The recovery of target scenes A, B and C is shown in Figures 5.10, 5.11 and 5.12 respectively. It can be seen that there may be scenarios where the linear channel

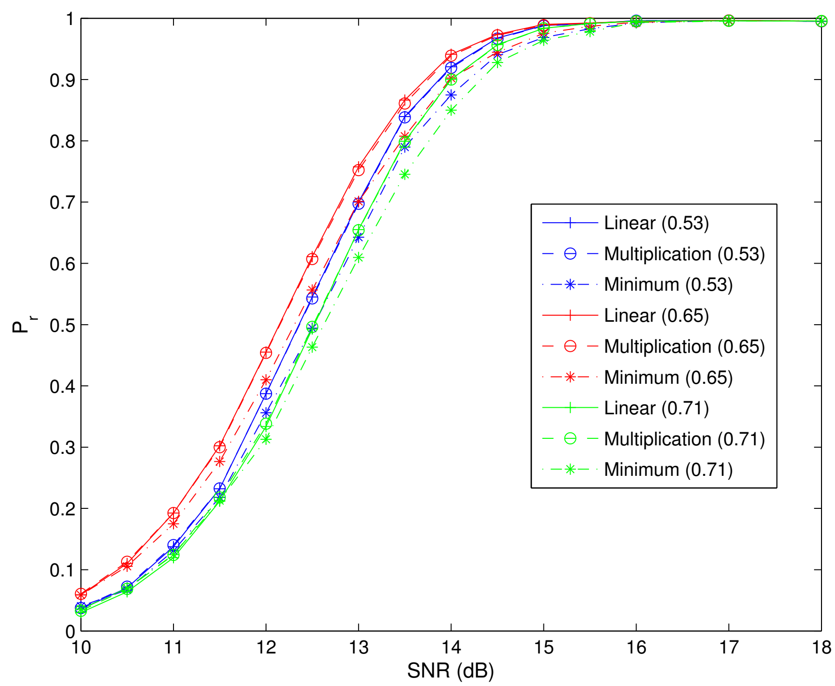

Figure 5.7.: Probability of resolution of target scenes consisting of two targets with equal amplitude for a fixed $P_{FA} = 10^{-3}$.

combining fails to recover correctly even though the NLMMP algorithm works fine. In general, however, the NLMMP algorithm seems to perform much better than the resolution plots in section 5.3 suggest.

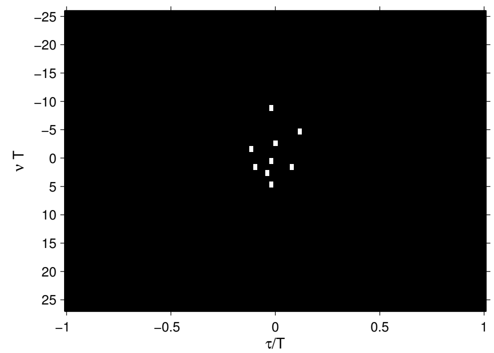

(a) Target scene A

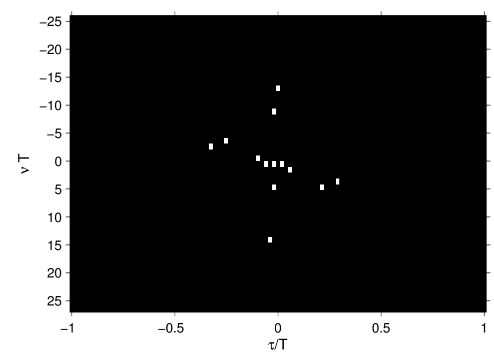

(b) Target scene B

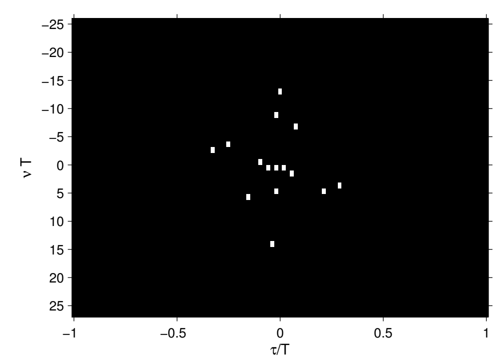

(c) Target scene C

Figure 5.8.: Three different target scenes used for comparing recovery performance.

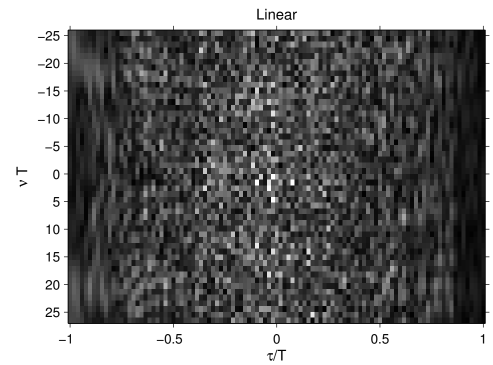

(a) Target scene A recovery using matched filtering and linear channel combining

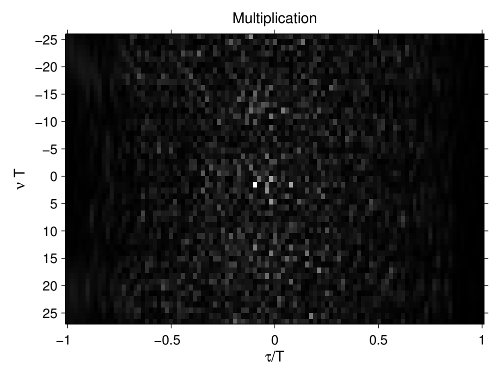

(b) Target scene A recovery using matched filtering and channel combining using multiplication.

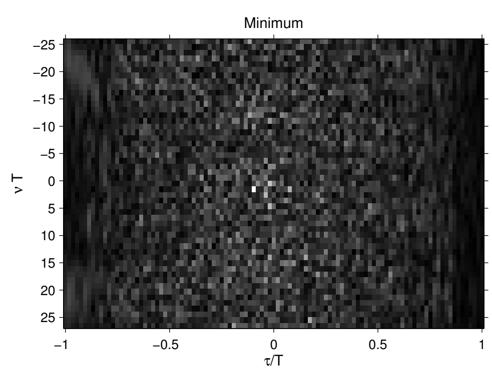

(c) Target scene A recovery using matched filtering and minimum channel combining

Figure 5.9.: Recovery of target scene A using matched filtering.

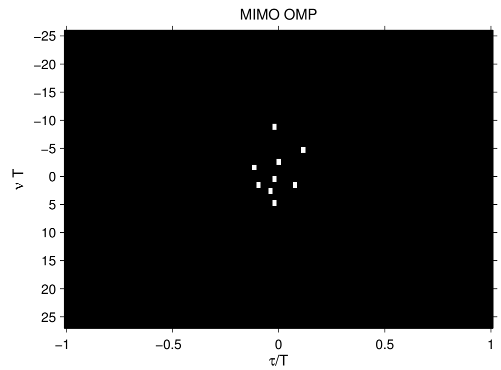

(a) Target scene A recovery using OMP algorithm.

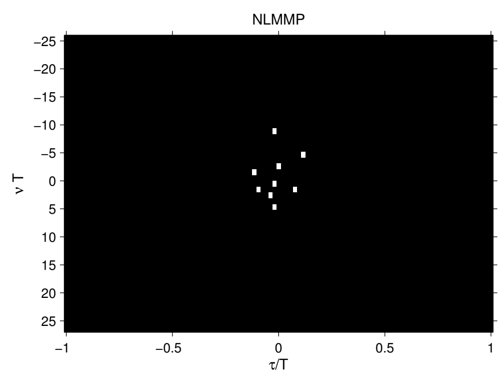

(b) Target scene A recovery using NLMMP with channel combining using multiplication.

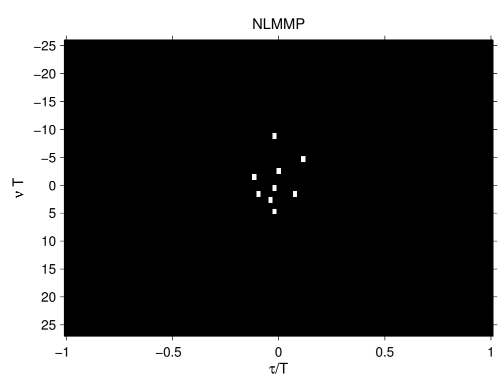

(c) Target scene A recovery using NLMMP with minimum channel combining.

Figure 5.10.: Recovery of target scene A using greedy pursuit algorithms.

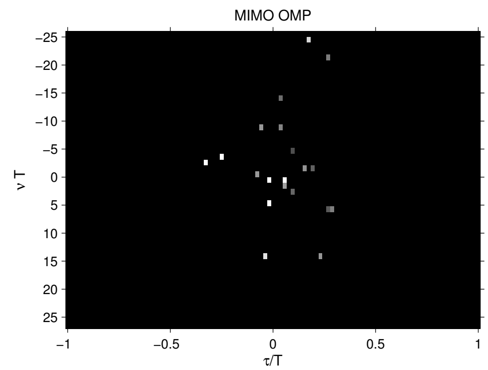

(a) Target scene B recovery using OMP algorithm.

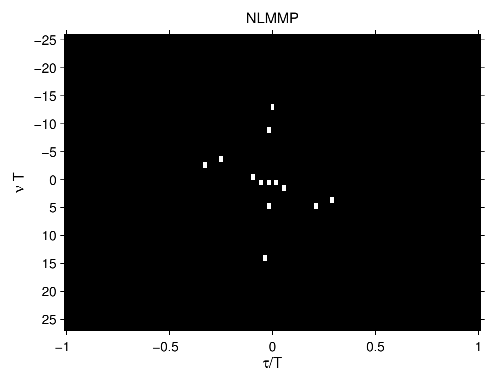

(b) Target scene B recovery using NLMMP with channel combining using multiplication.

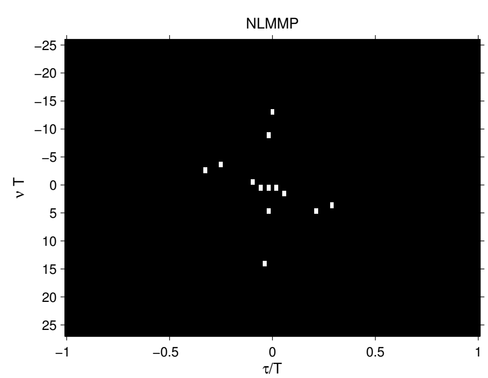

(c) Target scene B recovery using NLMMP with minimum channel combining.

Figure 5.11.: Recovery of target scene B using greedy pursuit algorithms.

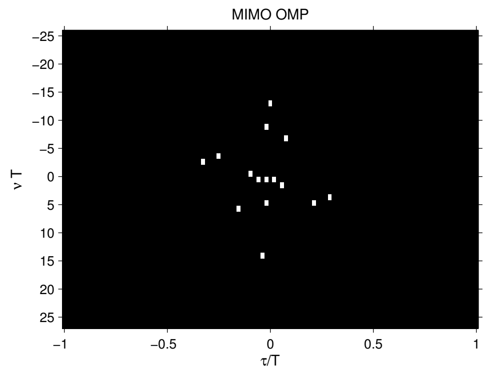

(a) Target scene C recovery using OMP algorithm.

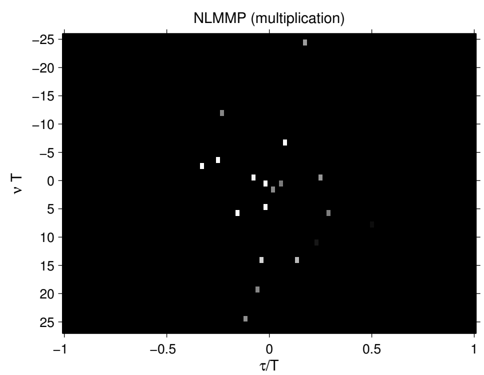

(b) Target scene C recovery using NLMMP with channel combining using multiplication.

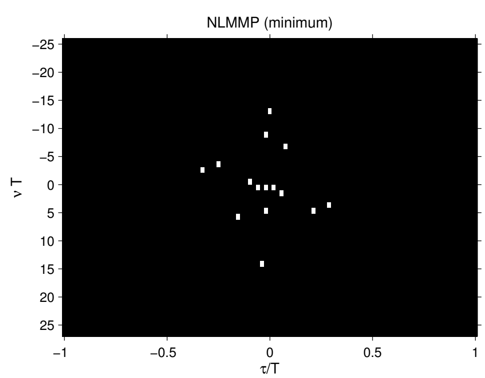

(c) Target scene C recovery using NLMMP with minimum channel combining.

Figure 5.12.: Recovery of target scene C using greedy pursuit algorithms.

6. RECOVERY OF EXTENDED TARGETS

All of the target scene recovery algorithms presented previously in Chapters 2 through 5 assumed a sparse point target model. While this assumption holds for low resolution search radar systems, targets in a high resolution radar with target identification capability can typically span multiple delay-Doppler bins. As a result, the point target assumption is no longer valid. Such targets are often called *extended targets*.

Under certain conditions, a radar system operating in a target environment consisting of extended targets can be modeled as

$$\mathbf{r} = \mathbf{S}\boldsymbol{\alpha} + \mathbf{w}, \tag{6.1}$$

where $\boldsymbol{\alpha}$ is now assumed to be *block sparse* [37]. Block sparsity will be formally defined in section 6.1. The signal model in equation (6.1) can be seen to be similar to the signal model in (1.18) for point target environment. Hence, using the likelihood ratio test to obtain suitable detection algorithms for the extended target model will still result in the same algorithms discussed previously. Therefore, it may seem pointless to consider algorithms specifically designed for recovering extended targets. However, a close inspection of the resolution plots in Chapters 3-5 shows that most recovery algorithms are more likely to fail when two targets are close in range and/or Doppler. This is because the sidelobes and mainlobes of nearby targets can interfere with each other creating spurious peaks and suppressing actual peaks which can throw off the greedy algorithms. The recovered vector $\hat{\boldsymbol{\alpha}}$ is then no longer the optimal sparse solution as the greedy algorithm tries to reduce the energy in the residue signal $\bar{\mathbf{r}}$.

Extended targets can be modeled as contiguous clusters of point targets in discrete time. As a result, the OMP algorithm and its variants discussed earlier are unlikely to perform well in such target environments. This problem is also experienced in other applications of compressed sensing and sparse recovery. For example, block sparsity has been shown to occur in multiple measurement vector (MMV) [38] problem and the measurement of gene expression levels [39]. They have also been shown to arise in sampling of signals that lie in a union of subspaces [37, 40]. As a result, the recovery of sparse blocks has received considerable recent interest [37, 41–43].

Most of the existing work in recovering block sparse signals is focused towards utilizing a known structure in the data. For example, in [37], variants of OMP and MP algorithm called Block OMP (BOMP) and Block MP (BMP) are studied. The key difference between OMP and BOMP algorithms is in the target selection step. Recall, in each iteration of the OMP algorithm, the selected atom is the one most correlated with the residue vector $\bar{\mathbf{r}}$, that is,

$$\hat{\theta} = \arg\max_{\theta} \left| \mathbf{s}_{\theta}^{H} \bar{\mathbf{r}} \right| .$$

In BOMP, however, it is assumed that all the possible clusters are known a priori. Then, rather than matching to each individual atom, the BOMP algorithm matches the residue to the sub-dictionaries corresponding to the permissible clusters. This has the effect of reducing the dictionary size at the receiver. Now assuming the target scene vector α has the form

$$\boldsymbol{\alpha} = \left[\begin{array}{cccc} \boldsymbol{\alpha}^{(1)} & \boldsymbol{\alpha}^{(2)} & \ldots & \boldsymbol{\alpha}^{(L)} \end{array} \right]^{T},$$

where $\boldsymbol{\alpha}^{(i)}$ denotes the i^{th} target cluster $\forall i \in \{1, 2, \ldots, L\}$. Assuming the sub-dictionary corresponding to the i^{th} target cluster is denoted as $\mathbf{S}^{(i)}$, the BOMP algorithm selects cluster $\hat{i}$ such that

$$\hat{i} = \arg\max_{i} \left\| \left(\mathbf{S}^{(i)}\right)^{H} \bar{\mathbf{r}} \right\|_{2} .$$

Similar modifications have also been proposed to the basis pursuit algorithm [9] for recovery of sparse clusters. In [41], Yuan et al. propose the *group lasso* algorithm which is based on the optimization

$$\hat{\boldsymbol{\alpha}} = \min_{\boldsymbol{\alpha}} \left\{ \frac{1}{2} \left\| \mathbf{r} - \mathbf{S}\boldsymbol{\alpha} \right\|_2^2 + \lambda \sum_{i=1}^{L} \sqrt{\rho_i} \left\| \boldsymbol{\alpha}^{(i)} \right\|_2 \right\},$$

where ρ_i is the length of cluster i, that is, $\rho_i = \left\|\boldsymbol{\alpha}^{(i)}\right\|_0$. When each cluster has size 1, the group lasso algorithm simplifies to the basis pursuit algorithm. For applications where the groups/ clusters themselves are sparse, Simon et al. [42] proposed the *sparse-group lasso* which can be formulated as the optimization problem

$$\hat{\boldsymbol{\alpha}} = \min_{\boldsymbol{\alpha}} \left\{ \frac{1}{2} \left\|\mathbf{r} - \mathbf{S}\boldsymbol{\alpha}\right\|_2^2 + (1-\eta)\,\lambda \sum_{i=1}^{L} \sqrt{\rho_i} \left\|\boldsymbol{\alpha}^{(i)}\right\|_2 + \eta\lambda \left\|\alpha\right\|_1 \right\},$$

where $\eta \in [0, 1]$. The parameter η can be used to select between the basis pursuit on one extreme and the group lasso on the other.

Similar enhancements have been made to other sparse recovery algorithms for recovering block sparse signals [37, 44]. However, all of these algorithms assume that the block structure of the sparse signal is known a priori. In radar application, this implies that the location and extent of the targets should be known beforehand. Since this is not true, most of these existing algorithms are not valid for use in radar applications.

Radar specific block sparse recovery algorithms have been studied by R. Bose in [45,46]. In Sequence CLEAN [45], a tree search algorithm is presented that chooses the m largest peaks in each iteration. The tree nodes corresponding to the minimum energy or “mass” at the end of the algorithm then specify the target positions. Another variation of the CLEAN algorithm called LEAN CLEAN [46] uses post processing after the CLEAN algorithm to “cluster” the contiguous targets. However, the LEAN CLEAN algorithm uses some parameters that require making assumptions about the output of the CLEAN algorithm in the first stage. In any case, the key idea behind these algorithms is to utilize the block nature of the sparse vector $\boldsymbol{\alpha}$ to improve recovery performance.

In this chapter, we present a forward-backward greedy algorithm designed for block targets. In the forward stage, the algorithm selects a target location and starts clustering the neighboring target points. In the backward step, the algorithm goes through the selected target locations to make sure they are all contributing towards reducing the energy in the residue vector $\bar{\mathbf{r}}$. The resulting algorithm will be shown to perform well compared to the OMP algorithm in the presence of block targets.

Rest of this chapter is organized as follows: Section 6.1 formally defines extended targets and block sparsity. The problems associated with using OMP algorithm are discussed in Section 6.2. Section 6.3 presents the forward-backward algorithm for block targets. Finally, Section 6.4 shows simulation results comparing the recovery performance of OMP algorithm and forward-backward algorithm for block targets.

6.1 Extended target model and Block sparsity

The radar signal model in Chapter 1 was derived assuming point targets. As a result, each delay-Doppler bin at the radar output was assumed to be composed of independent targets scattered around. In a high resolution radar, however, many real life targets are contiguous. Hence, single targets may span multiple delay-Doppler bins. Furthermore, since these nearby delay-Doppler bins correspond to the same target, the radar output can no longer be assumed to be composed of independent targets in each delay-Doppler bin. In this Chapter, any target that spans multiple delay-Doppler bins at the radar output will be called an *extended target*. It should be noted that, by definition, an extended target for one radar may be a point target for another. Therefore, it is important to know the radar resolution when talking about an extended target.

In general, the receive signal for a range radar can be modeled as

$$\begin{aligned} r(t) &= \alpha(t) * s(t) + w(t), \\ &= \int_{-\infty}^{\infty} \alpha(\tau)\, s(t-\tau)\, d\tau + w(t), \end{aligned}$$

where $*$ denotes continuous time convolution. For a point target environment, $\alpha(t) = \sum_{i=1}^{L} \alpha_i \delta(t-\tau_i)$, which leads to the point target model in equation (1.18). Figure 6.1 shows simple examples of extended targets and point targets in a range radar. In this chapter, support of the extended targets in time will be assumed to be much smaller than the total signal duration. This assumption is necessary to ensure that

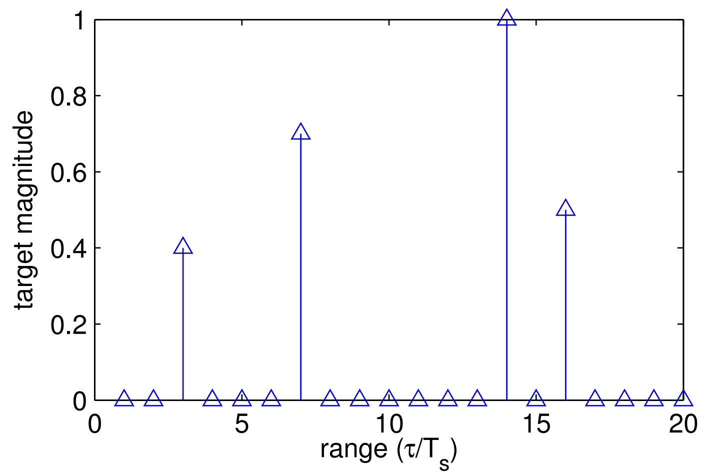

(a) Point targets

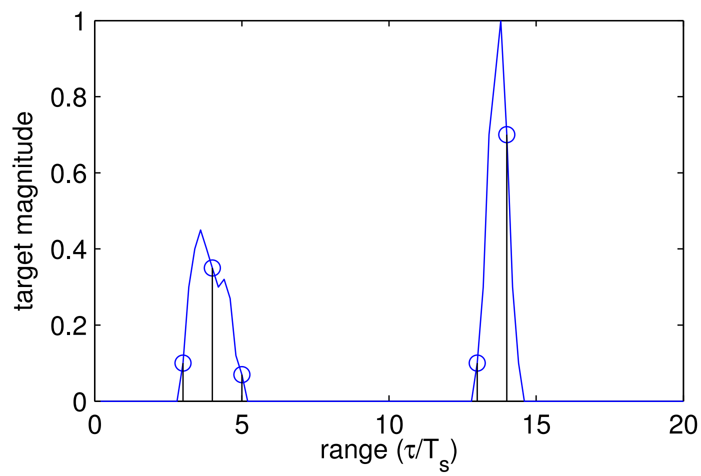

(b) Extended targets

Figure 6.1.: Comparison of Extended target and Point targets in range. T_s denotes sampling period.

the discrete sampled target vector is sparse. Assuming both signal $s(t)$ and the target scene function $\alpha(t)$ are band limited in frequency domain, the sampled discrete time received sequence can be written as [47]

$$\begin{aligned} r[n] &= \alpha[n] \star s[n] + w[n], \\ &= \sum_{i=1}^{N} \alpha[i]\, s[n-i] + w[n], \end{aligned} \tag{6.2}$$

where $\star$ denotes the discrete time convolution and N is the length of the sampled sequence. It can be seen that the discrete time receive signal model in equation (6.2) is similar to the model presented in equation 1.13 for point targets. Define vectors $\mathbf{r} = [\ r[1]\ \ r[2]\ \ \ldots\ \ r[N]\ ]^T$ and $\mathbf{w} = [\ w[1]\ \ w[2]\ \ \ldots\ \ w[N]\ ]^T$, (6.2) can be written as

$$\mathbf{r} = \sum_{i=1}^{N} \alpha[i]\, \mathbf{s}_i + \mathbf{w},$$

where

$$[\mathbf{s}_i]_n = \begin{cases} s[n-i-1], & 1 \le i \le n \le N, \\ 0 & else \end{cases}.$$

Define the receive signal dictionary as $\mathbf{S} = [\mathbf{s}_1, \ldots, \mathbf{s}_N]$, the receive signal model can be written as

$$\mathbf{r} = \mathbf{S}\boldsymbol{\alpha} + \mathbf{w}, \tag{6.3}$$

where $\boldsymbol{\alpha} \in \mathbb{R}^N$ is the vector of target amplitudes. The vector model of the received signal in equation (6.3) can be seen to be similar to the vector model of point targets presented in equation (1.14). However, the two models differ in the structure of the target vector $\boldsymbol{\alpha}$. For example, for the two target scenes in Figure 6.1, the sampled target amplitude vectors are equal to

$$\begin{aligned} \boldsymbol{\alpha}_p &= [\ldots, 0, 0.4, 0, 0, 0, 0.7, 0, \ldots, 0, 1, 0, 0.5, 0, \ldots], \\ \boldsymbol{\alpha}_e &= [\ldots, 0, 0.1, 0.35, 0.07, 0, \ldots, 0, 0.1, 0.7, 0, \ldots], \end{aligned}$$

where $\boldsymbol{\alpha}_p$ and $\boldsymbol{\alpha}_e$ represent target vectors for point target scene and extended target scene, respectively. It can be seen that while both target vectors are sparse, the nonzero elements of $\boldsymbol{\alpha}_e$ tend to occur in groups or clusters. Such sparse signal vectors where the nonzero values are clustered together are known as *block sparse* signals. In a radar system, the groups or clusters in a block sparse signal represent extended targets.

Similarly, for a range-Doppler radar, the sampled received signal in vector form can be expressed as

$$\mathbf{r} = \mathbf{S}\boldsymbol{\alpha} + \mathbf{w}, \tag{6.4}$$

where the target amplitude vector $\boldsymbol{\alpha}$ and the synthesis matrix $\mathbf{S}$ are given as

$$\begin{aligned} \mathbf{S} &= [\ \mathbf{s}_{0,0} \quad \mathbf{s}_{0,1} \quad \ldots \quad \mathbf{s}_{0,M-1} \quad \mathbf{s}_{1,0} \quad \ldots \quad \mathbf{s}_{1,M-1} \quad \ldots \quad \mathbf{s}_{N-1,M-1}\ ], \\ \boldsymbol{\alpha} &= [\ \alpha_{0,0} \quad \alpha_{0,1} \quad \ldots \quad \alpha_{0,M-1} \quad \alpha_{1,0} \quad \ldots \quad \alpha_{1,M-1} \quad \ldots \quad \alpha_{N-1,M-1}\ ], \end{aligned} \tag{6.5}$$

and

$$[s_{i,k}]_n = \begin{cases} s[n-i]e^{j2\pi kn/M}, & 0 \le i \le n \le N, \\ 0 & else \end{cases}.$$

The receive signal model in equation (6.4) is once again similar to the receive signal model in a point target environment (1.18). However, unlike the target amplitude vector in a point target environment, the target amplitude vector $\boldsymbol{\alpha}$ is block sparse in extended target environment.

It should be mentioned here that block sparsity does not always imply that the indices of the nonzero values in $\boldsymbol{\alpha}$ are consecutive integers. For example, using the notation in (6.5), an extended target in Doppler may form a target vector with nonzero values separated by M. Hence, when talking about block sparsity of extended target model, the term block will imply clustering in terms of radar target parameters rather than in the target amplitude vector $\boldsymbol{\alpha}$.

Figures 6.2 and 6.3 show two extended targets in range and Doppler together with the matched filter estimate. It was assumed that the radar transmit waveform in use is the combined Barker sequence. It can be seen that the high sidelobe structure of the transmit waveform makes target resolution difficult. The result of using OMP

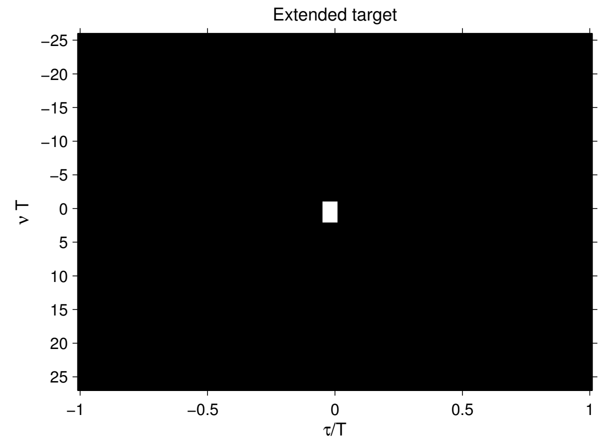

(a) Extended target scene 1.

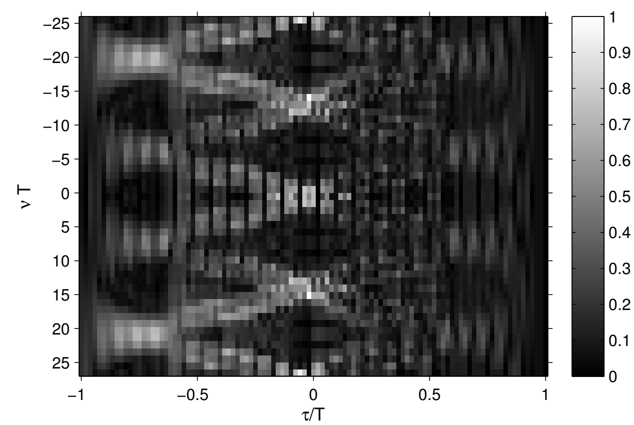

(b) Matched filter output for extended target 1.

Figure 6.2.: Extended target 1 and its matched filter estimate.

algorithm to recover the extended targets is shown in Figure 6.4. For both extended targets, the sidelobe behavior can be seen to throw the OMP algorithm off track.

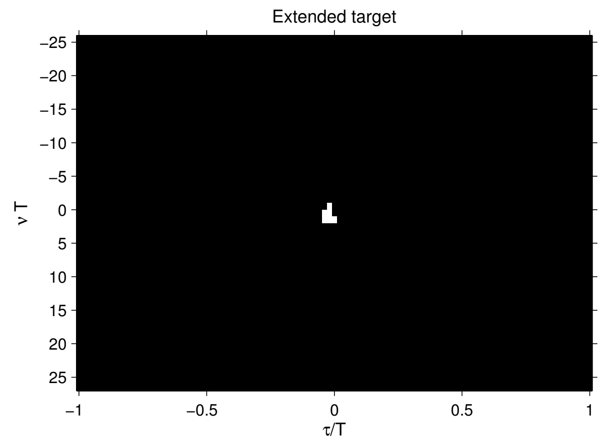

(a) Extended target scene 2.

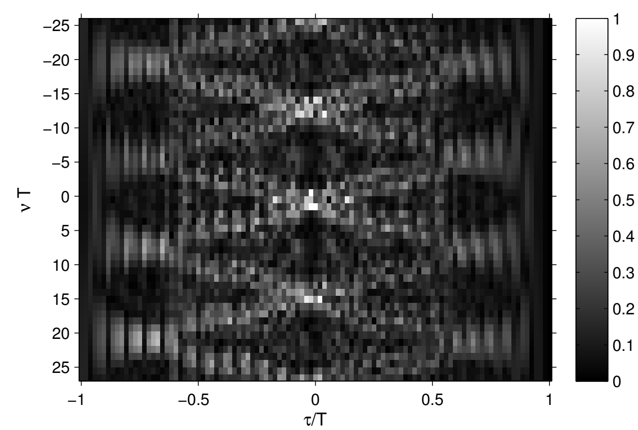

(b) Matched filter output for extended target 2.

Figure 6.3.: Extended target 2 and its matched filter estimate.

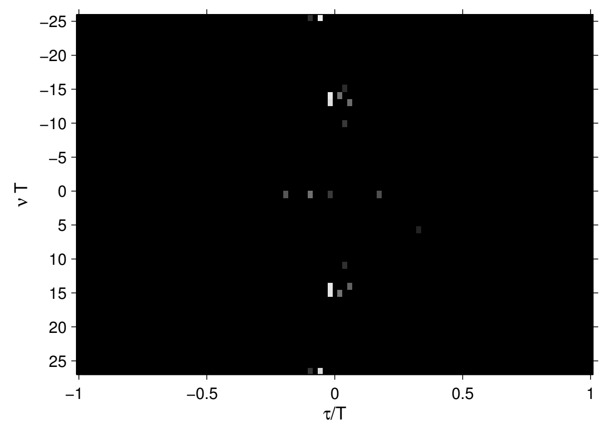

(a) OMP recovery of extended target scene 1.

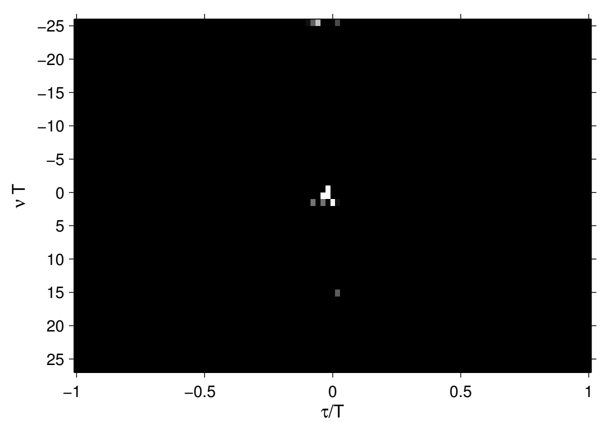

(b) OMP recovery of extended target 2.

Figure 6.4.: Recovery of extended target scene 1 and 2 using OMP algorithm.

6.2 Extended targets and OMP algorithm

Considering extended targets as clusters of point targets, it is clear that correct recovery requires a transmit waveform with an incoherent receive signal dictionary. When this is not true, Figure 6.4 shows that the OMP algorithm is completely unsuitable for recovering extended targets. A close inspection of the OMP output for extended targets shows that there are three major problems with OMP which limit its performance.

Firstly, the OMP algorithm performs poorly when the first few iterations select the wrong target. The subsequent iterations of the OMP algorithm are then used to mitigate the effect of earlier mistakes and, as a result, the output is no longer sparse. This problem can be seen in the recovery of extended target 1 in Figure 6.2. The matched filter output in this case has two peaks at $(\tau, \nu) = (0, -15\nu T)$ and $(\tau, \nu) = (0, 15\nu T)$. Since both of these peaks do not correspond to an actual target, the first few iterations of the OMP algorithm select wrong target locations. This can be seen in the OMP output in Figure 6.4. The subsequent iterations of the algorithm are then spent trying to cancel out the newly created sidelobes.

Secondly, the recovery performance of the OMP algorithm is limited by the fact that there is no way to correct for mistakes in previous iterations. For example, consider the output of OMP algorithm for the extended target 2 in Figure 6.4. Although the first few iterations of the algorithm select correct targets, a wrong selection in subsequent iteration again causes the algorithm to get off track.

Thirdly, due to the complex interaction between the mainlobes and sidelobes in an extended target, the target amplitudes at the output of matched filter can vary greatly. Consequently, even when the OMP algorithm selects a correct target location, the maximum likelihood estimate of the amplitude may be very different from the actual target amplitude. Suppose, for example, that the amplitude of a target constructively interferes with the sidelobes of neighboring range-Doppler bins. The maximum likelihood estimate of the target amplitude in this case may be much greater than the actual amplitude. As a result, the following iterations of the greedy algorithm may be spent trying to compensate for excessive target cancellation. This problem can be seen during the recovery of extended target 2.

The first problem can be mitigated in a number of different ways. One approach to overcome this obstacle may be to use an approach similar to the SMOMP algorithm together with a tree algorithm. In this Chapter, a simpler approach utilizing the weighted volume of the neighborhood will be used. The intuition behind this approach can be seen in Figure 6.2. While the peaks in the matched filter output do not correspond to any target, volume is still maximum in the neighborhood of the actual target. Hence, instead of selecting a target based on the peak of the matched filter output alone, the selected target location is one that maximizes the weighted volume in the neighborhood. Consider the received signal model in equation (6.4) with amplitude vector as defined in equation (6.5). Assume that for any length MN vector $\mathbf{g}$,

$$\mathbf{g} = [\ g_{0,0} \quad g_{0,1} \quad \cdots \quad g_{0,M-1} \quad g_{1,0} \quad \cdots \quad g_{1,M-1} \quad \cdots \quad g_{N-1,M-1}\ ],$$

the *image matrix* $\mathbf{G}$ can be written as

$$\mathbf{G} = \begin{bmatrix} g_{0,0} & g_{0,1} & \cdots & g_{0,M-1} \\ g_{1,0} & g_{1,1} & \cdots & g_{1,M-1} \\ \vdots & \vdots & & \vdots \\ g_{N-1,0} & g_{n-1,1} & \cdots & g_{N-1,M-1} \end{bmatrix}.$$

Denoting the image matrix of any vector $\mathbf{g}$ as $(\mathbf{g})_{im}$, The selected target location θ satisfies

$$\theta = \arg\max_{\theta} \left[\mathbf{W} \otimes \left(\mathbf{S}^H \mathbf{r}\right)_{im}\right]_{\theta},$$

where $\mathbf{W}$ represents the weighting matrix and $\otimes$ denotes 2 dimensional autocorrelation. For example, one simple weighting matrix $\mathbf{W}$ that uses the immediate neighbors only is given as

$$\mathbf{W} = \begin{bmatrix} 0.2 & 0.5 & 0.2 \\ 0.5 & 1 & 0.5 \\ 0.2 & 0.5 & 0.2 \end{bmatrix}.$$

The simulation results presented in section (6.4) will use this weighting matrix. In practice, the weighting matrix should be designed taking into account the types of targets expected in the environment. Hence, if the targets are expected to be extended in range, a higher weight should be assigned to range than Doppler.

Solution to the second problem was recently proposed by T. Zhang in [48]. The key idea behind the proposed forward backward algorithm is that the contribution of the wrongly selected atoms to the cost function decreases as number of iterations increase. Thus, in every backward step, the algorithm in [48] goes through all the selected atoms in the forward steps to make sure they are all contributing towards minimizing some cost function. Algorithm 6.1 shows the backward step proposed in [48]. In each iteration of the greedy algorithm, after the forward step, the backward algorithm is called with the recovered sets in current and previous iterations $\hat{\Lambda}^k$ and $\hat{\Lambda}^{k-1}$ as inputs. Since the goal of the recovery algorithm is to minimize cost function

$$f(\Lambda) = \left\| r - \mathbf{S}_\Lambda \mathbf{S}_\Lambda^\dagger \mathbf{r} \right\|^2 + \lambda \left\| \mathbf{S}_\Lambda^\dagger \mathbf{r} \right\|_p,$$

using a sparse set Λ, the backward step searches for an element in $j \in \Lambda$ with least contribution towards minimizing $f(\cdot)$. Then, if the increase in cost function is much less than the improvement in cost in the previous forward step, j is removed from Λ. The intuition behind this algorithm is that if the greedy algorithm selects the correct atoms in every iteration, the cost function should continue to decrease with each successive iteration yielding a smaller improvement. The backward step ensures such a progression is being made.

Finally, the third problem in recovering extended targets can be mitigated to some extent by limiting the algorithm to one extended target until it is fully recovered.

Algorithm 6.1 Backward step.

- Input: $\hat{\Lambda}^k, \hat{\Lambda}^{k-1}$.
- Initialize $\eta \in [0, 1]$
- do
  - $j = \arg\min_{j \in \hat{\Lambda}^k} \left\{ f\left(\hat{\Lambda}^k / j\right) \right\}$.
  - if $\left[f\left(\hat{\Lambda}^k / j\right) - f\left(\hat{\Lambda}^k\right) \right] \leq \eta \left[f\left(\hat{\Lambda}^{k-1}\right) - f\left(\hat{\Lambda}^k\right) \right]$
    * $\hat{\Lambda}^k = \hat{\Lambda}^k / j$
  - else break
- while true
- return $\hat{\Lambda}^k$

Intuitively, this is because the maximum likelihood estimate of the amplitude of the extended target will be more accurate when the target location is completely known. As a result, the algorithm is less likely to create large sidelobes that can cause interference in subsequent iterations. More formally, suppose Λ is a set of target parameters. Denote the set of contiguous neighbors of all the elements in Λ as C_Λ. Then, a suitable algorithm for extended targets would first select some target θ, and then search for suitable targets in C_θ. In this Chapter, for any target location $\theta = (\tau, \nu)$, the neighborhood will be defined as

$$C_\theta = \left\{ (\tau - 1, \nu), (\tau + 1, \nu), (\tau, \nu - 1), (\tau, \nu + 1) \right\}.$$

6.3 Forward-Backward algorithm for extended targets

An algorithm incorporating all the ideas discussed in the previous section is presented as Algorithm 6.2. For rest of this Chapter, the algorithm will be referred to as forward backward algorithm for extended targets (FBE). The algorithm uses nested loop structure for target selection. The main loop uses the weighted volume to select the location $\hat{\theta}$ of an extended target. Then, the inner loop searches for suitable target locations in the neighborhood of $\hat{\theta}$. The set of target locations in the current extended target is denoted as Λ_g. Every time the set Λ_g is expanded by searching over the neighborhood, the algorithm calls the backtracking algorithm 6.1 to correct for any wrong selections. The search over the neighborhood continues until no more suitable locations are found. The algorithm then moves on to the outer loop where the location of next extended target is computed.

Although the algorithm was designed to improve the recovery performance of extended targets, it still performs well for point targets. In particular, when the weighting matrix is selected as [1], and using an empty set for the neighborhood, the algorithm simplifies to the adaptive forward backward greedy algorithm proposed in [48].

Algorithm 6.2 Forward backward algorithm for recovery of extended targets in received signal $\mathbf{r}$.

- Initialize $\hat{\Lambda} = \emptyset$, $\bar{\mathbf{r}} = \mathbf{r}$, $\mathbf{W}$,η, λ, γ.
- $\sigma = \max_\theta \left[\mathbf{W} \otimes \left(\mathbf{S}^H \mathbf{r}\right)_{im}\right]_\theta$
- while $\sigma > \gamma$
  - $\hat{\theta} = \arg\max_\theta \left|\mathbf{s}_\theta^H \bar{\mathbf{r}}\right|$
  - $\hat{\Lambda} = \hat{\Lambda} \cup \hat{\theta}$
  - $\hat{\alpha} = \arg\min_\alpha \|\mathbf{r} - \mathbf{S}_{\hat{\Lambda}} \alpha\|^2$
  - $\bar{\mathbf{r}} = \mathbf{r} - \mathbf{S}_{\hat{\Lambda}} \hat{\alpha}$
  - Initialize $\Lambda_g = \left\{\hat{\theta}\right\}$
  - Repeat
    * Find the set C_{Λ_g} of neighbors of Λ_g.
    * $\mathcal{N} = \left\{i \in C_{\Lambda_g} \mid \left|\mathbf{s}_i^H \bar{\mathbf{r}}\right| \geq \gamma\right\}$
    * if ($\mathcal{N} = \emptyset$), break.
    * $\Lambda_g = \Lambda_g \cup \mathcal{N}$
    * Call backward step with $\hat{\Lambda}^k = \Lambda_g \cup \hat{\Lambda}$, $\hat{\Lambda}^{k-1} = \hat{\Lambda}$.
    * Set returned set from backward step as$\hat{\Lambda}$
    * $\hat{\alpha} = \arg\min_\alpha \|\mathbf{r} - \mathbf{S}_{\hat{\Lambda}} \alpha\|^2$
    * $\bar{\mathbf{r}} = \mathbf{r} - \mathbf{S}_{\hat{\Lambda}} \hat{\alpha}$
  - $\sigma = \max_\theta \left[\mathbf{W} \otimes \left(\mathbf{S}^H \bar{\mathbf{r}}\right)_{im}\right]_\theta$

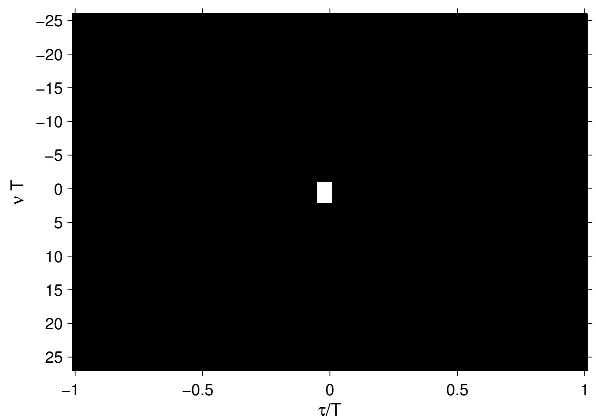

Figure 6.5.: Extended target 1 recovery using FBE.

6.4 Simulation results

Figures 6.5 and 6.6 show the result of using FBE to recover extended target 1 and 2. The radar transmit waveform was assumed to be the combined Barker code. It can be seen that the FBE seems to mitigate the three problems discussed in section 6.2 and correctly recovers the extended targets.

Figure 6.7 shows a target scene with two extended targets and two point targets. Once again, the target scene is correctly recovered using FBE as shown in Figure 6.8.

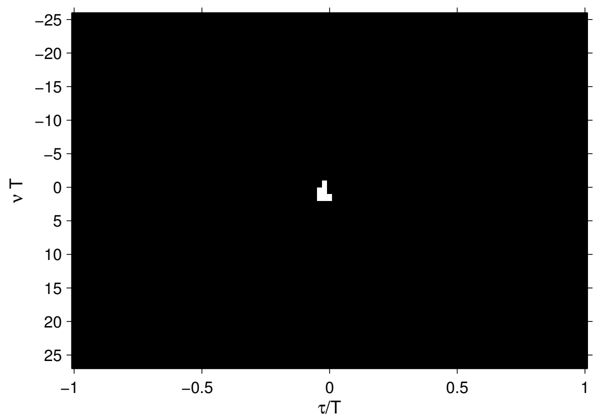

Figure 6.6.: Extended target 2 recovery using FBE.

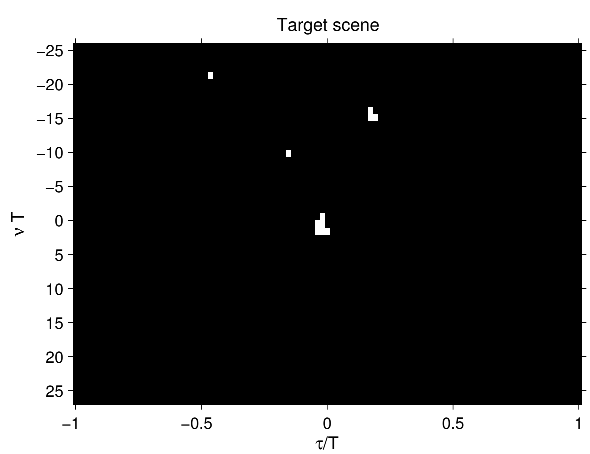

Figure 6.7.: Target scene with multiple targets.

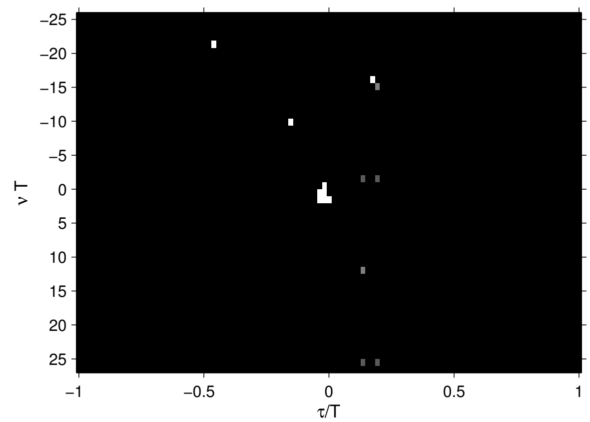

(a) Recovery of target scene in Figure 6.7 using OMP.

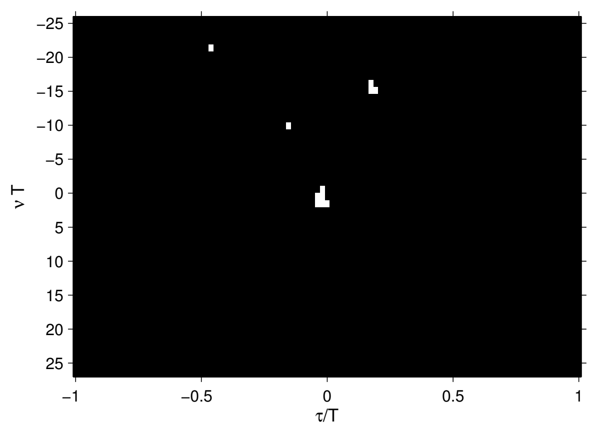

(b) Recovery of target scene in Figure 6.7 using FBE.

Figure 6.8.: Recovery of Multi-target scene in Figure 6.7.

7. SUMMARY AND FUTURE WORK

This thesis began with the goal of achieving improved multi-target resolution in range and delay Doppler radar. Towards this goal, Chapter 1 formulated multi-target recovery problem as a sparse solution to an under determined linear system. While this model can be readily obtained for both range and pulse Doppler radar, it has only recently been applied to radar systems [10, 49]. Additionally, mutual coherence of the receive signal dictionary is an important parameter often used in sparse recovery literature to analyze the recovery performance of a system. Radar engineers, on the other hand, typically use autocorrelation and ambiguity functions to compare the resolution of a radar system. It was shown in Chapter 1 that the two are closely related and improving one entails improving the other.

Chapter 2 applied the likelihood ratio test to the sparse multi-target signal model presented in Chapter 1. In particular, it was shown that the optimal detector is computationally infeasible. As a result, a greedy solution was presented. Furthermore, it was shown that the optimal detector simplifies to the matched filter only when the received signal dictionary is orthogonal. In addition, single target detection performance of the matched filter and the proposed greedy algorithm were shown to be equal.

In radar literature, the ambiguity function is often used to graphically compare the resolution of a radar in noiseless conditions. In additive noise, single target probability of detection and false alarm are used for analyzing performance. In chapter 3, we show that these performance metrics do not always scale naturally to a multi-target scene. As a result, we formally define radar resolution and propose a quantitative measure to compare it. The proposed quantitative measure was used to analyze the resolution performance of the greedy algorithm. This allowed us to show that iterative greedy algorithms may work in some target environments even when the coherence condition is not satisfied.

In chapter 4, we used the similarity between matched filters and the matching pursuit algorithms to propose a pursuit algorithm using mismatched dictionaries. Resolution performance was analyzed and the algorithm was found to be suitable for non-redundant dictionaries. In particular, it was shown that combining mismatched filters with greedy algorithms allow improved resolution without always losing detection performance. An extension of the mismatched pursuit algorithm was then proposed for redundant dictionaries which was based on adaptive signal processing. Simulation results were presented to show the efficacy of the proposed algorithms.

In chapter 5, we presented multiple channel pursuit algorithms in radar. It was shown that the receive signal model is similar to the sparse linear model presented in Chapter 1 when the channels are combined linearly. As a result, the greedy target recovery algorithm can be applied directly using a composite signal dictionary. Furthermore, target recovery performance of the greedy algorithm was used to analyze the performance of multiple transmit signals. Simulation results further confirmed the improvement in resolution obtained using multiple channels.

Radar systems with multiple transmit waveforms using nonlinear channel combining techniques have been proposed recently [22] to improve resolution. These combining schemes suffer from ghost targets and reduced detection probability due to loss in SNR. In Chapter 5, we showed that the nonlinear combining schemes can be used with greedy algorithms to eliminate ghost targets. Furthermore, it was shown that these algorithms also have a better detection performance.

While all the previous algorithms assumed point target environment, targets in high resolution radars can often be modeled as extended targets. Chapter 6 analyzed radar signal model for extended targets and it was shown that the target scene vector in this case has additional structure in the form of block sparsity. A forward backward greedy algorithm for recovering extended targets was then presented. It was shown using simulations that the proposed algorithm works well in target scenes comprised of a mixture of point and extended targets.

In future, there are a number of ways the work in this thesis can be expanded on. For example, all of the algorithms in this thesis were derived assuming narrowband radar waveforms. When this assumption is not valid, the received signal is time delayed, frequency shifted and time scaled version of the transmitted signal. In this case, the receive signal dictionary needs to be expanded to take into account the time scaling effect of Doppler on broadband signals. Similarly, the radar system in this thesis was assumed to have one pulse in each coherent pulse interval. In practice, radar systems typically utilize much longer coherent pulse intervals. This results in the well known "bed of nails" ambiguity function. It would be interesting to see the resolution performance and also to see if there is a way the range ambiguity in pulsed systems can be avoided using greedy algorithms.

Another key assumption in this thesis was the absence of *straddle losses*. Recall the receive signal model in vector form, the target delay and Doppler were assumed to be integer multiples of sampling periods in time and frequency. In an actual radar system, there is no way to ensure this. When this assumption is not true, there is a loss in SNR which is known as straddle loss. While for sufficiently high sampling period, the straddle losses may be negligible, its effect on greedy algorithms remains a topic of interest for the future.

Another interesting problem for future is that of the MIMO waveform design. In Chapter 5, two pairs of radar waveforms were used to simulate the performance of MIMO radar systems. However, design of optimal set of transmit waveforms is an important problem for future radar systems. In this direction, we believe that the analysis of MIMO radar recovery performance may prove to be useful.

The advantage of using backward steps to correct for the greedy nature of the recovery algorithms in this thesis was discussed in Chapter 6. Conditions under which such an algorithm correctly recovers the targets may be another way this thesis can be extended. Furthermore, although the backward algorithm was only discussed for extended targets, it may prove to be useful for recovering point target scenes also.

Finally, the ultimate goal of this thesis has always been to study the possibility of using pursuit algorithms on real radar data. While actual data is not available at this time, it is known that real radar data suffers from clutter which makes greedy algorithms unsuitable. In [50], it was shown that application of clutter cancellation before using iterative algorithms yields suitable results. For future, the possibility of applying iterative greedy algorithms on radar data with clutter by incorporating prior information in the signal dictionary remains another topic of research.

LIST OF REFERENCES

LIST OF REFERENCES

[1] L. Brown, *A Radar History of World War II: Technical and Military Imperatives.* Institute of Physics Publishing, 1999.

[2] C. Stutt, "A note on invariant relations for ambiguity and distance functions," *IEEE Transactions on Information Theory*, vol. 5, pp. 164–167, Dec. 1959.

[3] P. M. Woodward, "RADAR AMBIGUITY ANALYSIS," *RRE Technical note*, vol. 731, Feb. 1967.

[4] G. Davis, S. Mallat, and M. Avellaneda, "Adaptive greedy approximations," *Constructive Approximation*, vol. 13, no. 1, pp. 57–98, 1997.

[5] S. Mallat, "Matching pursuits with time-frequency dictionaries," *IEEE Transactions on Signal Processing*, vol. 41, no. 12, pp. 3397–3415, 1993.

[6] Y. C. Pati, R. Rezaiifar, and P. S. Krishnaprasad, "Orthogonal matching pursuit: recursive function approximation with applications to wavelet decomposition," *Proceedings of 27th Asilomar Conference on Signals Systems and Computers*, vol. 1, pp. 40–44, 1993.

[7] Z. Z. Geoffrey Davis, Stéphane Mallat, "Adaptive Time-Frequency Decompositions with Matching Pursuits,"

[8] R. A. DeVore and V. N. Temlyakov, "Some remarks on greedy algorithms," *Advances in Computational Mathematics*, vol. 5, pp. 173–187, Dec. 1996.

[9] M. A. S. Scott Shaobing Chen, David L. Donoho, "Atomic decomposition by basis pursuit,"

[10] T. Strohmer and B. Friedlander, "Compressed sensing for MIMO radar - algorithms and performance," in *2009 Conference Record of the Forty-Third Asilomar Conference on Signals, Systems and Computers*, pp. 464–468, IEEE, 2009.

[11] P. P. Vaidyanathan, "Compressed sensing in MIMO radar," in *2008 42nd Asilomar Conference on Signals, Systems and Computers*, pp. 41–44, IEEE, Oct. 2008.

[12] W. Alltop, "Complex sequences with low periodic correlations (Corresp.)," *IEEE Transactions on Information Theory*, vol. 26, pp. 350–354, May 1980.

[13] R. Baraniuk and P. Steeghs, "Compressive Radar Imaging," in *2007 IEEE Radar Conference*, pp. 128–133, IEEE, Apr. 2007.

[14] M. Tello Alonso, P. Lopez-Dekker, and J. J. Mallorqui, "A Novel Strategy for Radar Imaging Based on Compressive Sensing," *IEEE Transactions on Geoscience and Remote Sensing*, vol. 48, pp. 4285–4295, Dec. 2010.

[15] S. Mallat, *A Wavelet Tour of Signal Processing, Third Edition: The Sparse Way.* Academic Press, 2008.

[16] J. Tropp, "Greed is Good: Algorithmic Results for Sparse Approximation," *IEEE Transactions on Information Theory*, vol. 50, pp. 2231–2242, Oct. 2004.

[17] X. H. David L. Donoho, "Uncertainty principles and ideal atomic decomposition,"

[18] N. Levanon and E. Mozeson, *Radar Signals.* J. Wiley, 2004.

[19] N. Levanon, *Radar Principles.* Wiley-Interscience, 1988.

[20] D. Farden and L. Scharf, "A unified framework for the Sussman, Moyal, and Janssen formulas," *IEEE Signal Processing Magazine*, vol. 23, pp. 124–125, May 2006.

[21] E. E. Hollis, "Comparison of Combined Barker Codes for Coded Radar Use," *IEEE Transactions on Aerospace and Electronic Systems*, vol. AES-3, no. 1, 1967.

[22] S. B. Rasool and M. R. Bell, "Biologically Inspired Processing of Radar Waveforms for Enhanced Delay-Doppler Resolution," *IEEE Transactions on Signal Processing*, vol. 59, pp. 2698–2709, June 2011.

[23] S. M. Kay, *Fundamentals of Statistical Signal Processing, Volume 2: Detection Theory*, vol. II of *Prentice Hall Signal Processing Series.* Prentice Hall, 1998.

[24] S. M. Kay, *Fundamentals of Statistical Signal Processing, Volume I: Estimation Theory*, vol. 37 of *Prentice Hall Signal Processing Series.* Prentice Hall, 1993.

[25] M. Ackroyd and F. Ghani, "Optimum Mismatched Filters for Sidelobe Suppression," *IEEE Transactions on Aerospace and Electronic Systems*, vol. AES-9, no. 2, 1973.

[26] A. Rihaczek and R. Golden, "Range Sidelobe Suppression for Barker Codes," *IEEE Transactions on Aerospace and Electronic Systems*, vol. AES-7, no. 6, 1971.

[27] S. Zoraster, "Minimum Peak Range Sidelobe Filters for Binary Phase-Coded Waveforms," *IEEE Transactions on Aerospace and Electronic Systems*, vol. AES-16, pp. 112–115, Jan. 1980.

[28] J. A. Högbom, "Aperture Synthesis with a Non-Regular Distribution of Interferometer Baselines," *Astronomy and Astrophysics Supplement Series*, vol. 15, p. 417, June 1974.

[29] J. G. Proakis and D. K. Manolakis, *Digital Signal Processing (4th Edition).* Prentice Hall, 2006.

[30] L. Rebollo-Neira, "Oblique Matching Pursuit," *IEEE Signal Processing Letters*, vol. 14, pp. 703–706, Oct. 2007.

[31] K. Lee, Y. Bresler, and M. Junge, "Oblique pursuits for compressed sensing," *Information Theory, IEEE . . .*, 2013.

[32] J. Baden and M. Cohen, “Optimal peak sidelobe filters for biphase pulse compression,” *IEEE International Conference on Radar*, 1990.

[33] D. Bliss and K. Forsythe, “Multiple-input multiple-output (MIMO) radar and imaging: degrees of freedom and resolution,” in *The Thrity-Seventh Asilomar Conference on Signals, Systems & Computers, 2003*, vol. 1, pp. 54–59, IEEE, 2003.

[34] A. Haimovich, R. Blum, and L. Cimini, “MIMO Radar with Widely Separated Antennas,” *IEEE Signal Processing Magazine*, vol. 25, no. 1, pp. 116–129, 2008.

[35] P. Stoica, “Target detection and parameter estimation for MIMO radar systems,” *IEEE Transactions on Aerospace and Electronic Systems*, vol. 44, pp. 927–939, July 2008.

[36] P. Stoica and W. Roberts, “On Parameter Identifiability of MIMO Radar,” *IEEE Signal Processing Letters*, vol. 14, pp. 968–971, Dec. 2007.

[37] Y. C. Eldar, P. Kuppinger, and H. Bolcskei, “Block-Sparse Signals: Uncertainty Relations and Efficient Recovery,” *IEEE Transactions on Signal Processing*, vol. 58, pp. 3042–3054, June 2010.

[38] S. Cotter, B. Rao, and K. Kreutz-Delgado, “Sparse solutions to linear inverse problems with multiple measurement vectors,” *IEEE Transactions on Signal Processing*, vol. 53, pp. 2477–2488, July 2005.

[39] F. Parvaresh, H. Vikalo, S. Misra, and B. Hassibi, “Recovering Sparse Signals Using Sparse Measurement Matrices in Compressed DNA Microarrays,” *IEEE Journal of Selected Topics in Signal Processing*, vol. 2, pp. 275–285, June 2008.

[40] R. G. B. Volkan Cevher, “Recovery of clustered sparse signals from compressive measurements,” in *Int. Conf. on Sampling Theory and Applications (SAMPTA)*, 2009.

[41] M. Yuan and Y. Lin, “Model selection and estimation in regression with grouped variables,” *Journal of the Royal Statistical Society: Series B (Statistical Methodology)*, vol. 68, pp. 49–67, Feb. 2006.

[42] R. T. Noah Simon, “A sparse-group lasso,” *Journal of Computational and Graphical Statistics*, 2013.

[43] M. Mishali and Y. Eldar, “Blind Multiband Signal Reconstruction: Compressed Sensing for Analog Signals,” *IEEE Transactions on Signal Processing*, vol. 57, pp. 993–1009, Mar. 2009.

[44] R. G. Baraniuk, V. Cevher, M. F. Duarte, and C. Hegde, “Model-Based Compressive Sensing,” *IEEE Transactions on Information Theory*, vol. 56, pp. 1982–2001, Apr. 2010.

[45] R. Bose, A. Freedman, and B. Steinberg, “Sequence CLEAN: a modified deconvolution technique for microwave images of contiguous targets,” *IEEE Transactions on Aerospace and Electronic Systems*, vol. 38, no. 1, pp. 89–97, 2002.

[46] R. Bose, “Lean CLEAN: Deconvolution Algorithm for Radar Imaging of Contiguous Targets,” *IEEE Transactions on Aerospace and Electronic Systems*, vol. 47, pp. 2190–2199, July 2011.

[47] R. van denBoomgaard and R. van derWeij, "Gaussian Convolutions Numerical Approximations Based on Interpolation," *Scale-Space and Morphology in Computer Vision*, vol. 2106, pp. 205–214, 2001.

[48] T. Zhang, "Adaptive Forward-Backward Greedy Algorithm for Learning Sparse Representations," *IEEE Transactions on Information Theory*, vol. 57, pp. 4689–4708, July 2011.

[49] M. Herman and T. Strohmer, "High-Resolution Radar via Compressed Sensing," *IEEE Transactions on Signal Processing*, vol. 57, pp. 2275–2284, June 2009.

[50] J. H. Ender, "On compressive sensing applied to radar," *Signal Processing*, vol. 90, pp. 1402–1414, May 2010.

[51] S. D. Blunt, A. K. Shackelford, K. Gerlach, and K. J. Smith, "Doppler compensation & single pulse imaging using adaptive pulse compression," *IEEE Transactions on Aerospace and Electronic Systems*, vol. 45, no. 2, pp. 647–659, 2009.

[52] T. L. Foreman, "Adapting the CLEAN Deconvolver and CLEAN Detector to Doppler Uncertainty," in *IEEE National Radar Conference - Proceedings*, pp. 325–330, 2007.

[53] R. Gribonval, P. Depalle, X. Rodet, E. Bacry, and S. Mallat, "Sound Signals Decomposition Using a High Resolution Matching Pursuit," in *Proc. Int. Computer Music Conf. (ICMC'96)*, pp. 293–296, 1996.

[54] K. Gröchenig, "Foundations of Time-Frequency Analysis. 2001," *Birkhäuser, Boston*.

[55] S. Jaggi, W. C. Karl, S. Mallat, and A. S. Willsky, "High Resolution Pursuit for Feature Extraction," *Applied and Computational Harmonic Analysis*, vol. 5, pp. 428–449, Oct. 1998.

[56] Mark A. Richards, *Fundamentals of Radar Signal Processing.* McGraw-Hill Professional, 2 ed., 2014.

[57] A. Maud and M. Bell, "Sparse recovery and resolution of pulse-Doppler radar," *Radar Conference, 2014 IEEE*, 2014.

[58] N. S. Subotic, B. Thelen, K. Cooper, W. Buller, J. Parker, J. Browning, and H. Beyer, "Distributed RADAR waveform design based on compressive sensing considerations," in *2008 IEEE Radar Conference*, pp. 1–6, IEEE, May 2008.

[59] B. P. Wakker and U. J. Schwarz, "The Multi-Resolution CLEAN and its application to the short-spacing problem in interferometry," *Astronomy and Astrophysics*, vol. 200, pp. 312–322, July 1988.

[60] Y. Yu, A. P. Petropulu, and H. V. Poor, "Compressive Sensing for MIMO Radar," July 2009.

APPENDICES

A. MOYAL'S IDENTITY

Define

$$\begin{aligned}\psi_{fg}(\tau,t) &= g(t)\overset{*}{f}(t+\tau)\\ \tilde{\psi}_{fg}(\tau,t) &= \overset{*}{g}(-t)f(\tau-t)\end{aligned}$$

then it can be shown that the following identity holds

$$(\psi_{fg} * \tilde{\psi}_{yx})(t,\tau) = (\psi_{fy} * \tilde{\psi}_{gx})(\tau,t) \tag{A.1}$$

where $*$ represents one dimensional convolution with respect to the first variable. Using $F_{\nu,t}$ to represent Fourier transform from t domain to ν domain, we can write the ambiguity function as

$$\begin{aligned}\chi_{gf}(\tau,\nu) &= F_{\nu,t}\psi_{fg}(\tau,t)\\ &= \int g(t)\overset{*}{f}(t+\tau)e^{j2\pi\nu t}dt\end{aligned}$$

We also define

$$\begin{aligned}\chi_{gf}(f,t) &= F_{f,\tau}\psi_{gf}(\tau,t)\\ &= \int g(\tau)\overset{*}{f}(t+\tau)e^{j2\pi f\tau}d\tau\end{aligned}$$

Now taking Fourier transform of equation (A.1),

$$\begin{aligned}F_{\nu,t}(\psi_{fg} * \tilde{\psi}_{yx})(t,\tau) &= F_{\nu,t}F^{-1}_{f,\tau}F_{f,\tau}(\psi_{fy} * \tilde{\psi}_{gx})(\tau,t)\\ \chi_{gf}\overset{*}{\chi}_{xy}(\tau,\nu) &= F_{\nu,t}F^{-1}_{f,\tau}\chi_{yf}\overset{*}{\chi}_{xg}(f,t)\end{aligned}$$

which is known as the Sussman's identity. Moving the Fourier transforms to the left side results in

$$\begin{aligned}F^{-1}_{\nu,t}F_{f,\tau}\chi_{gf}\overset{*}{\chi}_{xy}(\tau,\nu) &= \chi_{yf}\overset{*}{\chi}_{xg}(f,t)\\ \int\int \chi_{gf}\overset{*}{\chi}_{xy}(\tau,\nu)e^{-j2\pi\nu t}e^{j2\pi f\tau}d\tau d\nu &= \chi_{yf}\overset{*}{\chi}_{xg}(f,t)\end{aligned}$$

In particular, for $f = t = 0$, $\chi_{yf}(0,0) = \int y(\tau)\overset{*}{f}(\tau)d\tau$ and $\chi_{xg}(0,0) = \int x(\tau)\overset{*}{g}(\tau)d\tau$, so

$$\int\int \chi_{gf}\overset{*}{\chi}_{xy}(\tau,\nu)d\tau d\nu = \int y(\tau)\overset{*}{f}(\tau)d\tau \int \overset{*}{x}(\tau)g(\tau)d\tau$$

which is the Moyal's identity.

B. EQUIVALENCE OF ALGORITHMS

Consider a target scene with K targets. Then, to recover the target scene correctly, the optimal sparse problem (1.2), results in

$$\left\|\mathbf{r}-\Phi\mathbf{a}_K\right\|^2+\lambda\left\|\mathbf{a}_K\right\|_0 \;\; < \;\; \left\|\mathbf{r}-\Phi\mathbf{a}_{K+1}\right\|^2+\lambda\left\|\mathbf{a}_{K+1}\right\|_0, \tag{B.1}$$

where $a_i = \arg\min_{\mathbf{a}\in V_i}\left\|\mathbf{r}-\Phi\mathbf{a}\right\|^2$ represents target coefficient vector with i targets. Using this in (B.1),

$$\left\|\mathbf{r}-\Phi\mathbf{a}_K\right\|^2-\left\|\mathbf{r}-\Phi\mathbf{a}_{K+1}\right\|^2<\lambda,$$

which is equivalent to (2.9).

C. GLRT FOR ORTHONORMAL DICTIONARY

From equation (2.11), the GLRT for multiple target environment can be written as

$$\min_{\mathcal{L}\in\Lambda_K} \left\|\mathbf{r} - \mathbf{S}_{\mathcal{L}}\mathbf{S}_{\mathcal{L}}^{\dagger}\mathbf{r}\right\|^2 - \min_{\mathcal{L}\in\Lambda_{K+1}} \left\|\mathbf{r} - \mathbf{S}_{\mathcal{L}}\mathbf{S}_{\mathcal{L}}^{\dagger}\mathbf{r}\right\|^2 \underset{\mathcal{H}_0}{\overset{\mathcal{H}_1}{\gtrless}} \gamma,$$

where $\mathbf{r}$ denotes received signal and $\mathbf{S}$ denotes the signal dictionary. Define $\sigma = \min_{\mathcal{L}\in\Lambda_{K+1}} \left\|\mathbf{r} - \mathbf{S}_{\mathcal{L}}\mathbf{S}_{\mathcal{L}}^{\dagger}\mathbf{r}\right\|^2$. Assuming all the atoms in $\mathbf{S}$ are orthonormal, for any subdictionary $\mathbf{S}_{\mathcal{L}}$, $\mathbf{S}_{\mathcal{L}}^H\mathbf{S}_{\mathcal{L}} = \mathbf{I}$ and hence, $\mathbf{S}_{\mathcal{L}}\mathbf{S}_{\mathcal{L}}^{\dagger} = \mathbf{S}_{\mathcal{L}}\mathbf{S}_{\mathcal{L}}^H$. The second term in (2.11) can then be written as

$$\begin{aligned}
\sigma &= \min_{\mathcal{L}\in\Lambda_{K+1}} \left\|\mathbf{r} - \mathbf{S}_{\mathcal{L}}\mathbf{S}_{\mathcal{L}}^H\mathbf{r}\right\|^2 \\
&= \min_{\mathcal{L}\in\Lambda_K,\theta\in\Lambda_1/\mathcal{L}} \left\|\mathbf{r} - \mathbf{S}_{\mathcal{L}}\mathbf{S}_{\mathcal{L}}^H\mathbf{r} - \mathbf{s}_\theta\mathbf{s}_\theta^H\mathbf{r}\right\|^2 \\
&= \min_{\mathcal{L}\in\Lambda_K,\theta\in\Lambda_1/\mathcal{L}} \left[\left\|\mathbf{r} - \mathbf{S}_{\mathcal{L}}\mathbf{S}_{\mathcal{L}}^H\mathbf{r}\right\|^2 - \left\|\mathbf{s}_\theta^H\mathbf{r}\right\|^2\right] \\
&= \min_{\mathcal{L}\in\Lambda_K} \left\|\mathbf{r} - \mathbf{S}_{\mathcal{L}}\mathbf{S}_{\mathcal{L}}^H\mathbf{r}\right\|^2 - \max_{\theta\in\Lambda_1/\hat{\mathcal{L}}} \left\|\mathbf{s}_\theta^H\mathbf{r}\right\|^2,
\end{aligned} \tag{C.1}$$

where $\hat{\mathcal{L}} = \arg\min_{\mathcal{L}\in\Lambda_K} \left\|\mathbf{r} - \mathbf{S}_{\mathcal{L}}\mathbf{S}_{\mathcal{L}}^H\mathbf{r}\right\|^2$. Using (C.1) in (2.11), for an orthonormal dictionary the test can be written as

$$\max_{\theta\in\Lambda_1/\hat{\mathcal{L}}} \left\|\mathbf{s}_\theta^H\mathbf{r}\right\|^2 \underset{\mathcal{H}_0}{\overset{\mathcal{H}_1}{\gtrless}} \gamma.$$

VITA

VITA

Abdur Rahman M. Maud received his B.S. degree in Electrical Engineering from University of Engineering and Technology, Lahore, Pakistan in 2008, and the MS in Electrical and Computer Engineering from Purdue University, West Lafayette, IN, in 2012. His research interests are in array signal processing, beamforming, radar waveform design, MIMO radar and sparse signal processing.